HIGH TEMPERATURE CREEP DEFORMATION IN SOLID SOLUTION ALLOYS OF LEAD

by

MALCOLM A. CLARK
B.A.Sc., University of Toronto, 1966

A THESIS SUBMITTED IN PARTIAL FULFILMENT OF
THE REQUIREMENTS FOR THE DEGREE OF
DOCTOR OF PHILOSOPHY

in the Department
of
METALLURGY

We accept this thesis as conforming to the
required standard

THE UNIVERSITY OF BRITISH COLUMBIA

August, 1975

In presenting this thesis in partial fulfilment of the requirements for an advanced degree at the University of British Columbia, I agree that the Library shall make it freely available for reference and study. I further agree that permission for extensive copying of this thesis for scholarly purposes may be granted by the Head of my Department or by his representatives. It is understood that copying or publication of this thesis for financial gain shall not be allowed without my written permission.

Department of METALLURGY

The University of British Columbia
2075 Wesbrook Place
Vancouver, Canada
V6T 1W5

Date OCT. 7/1975

ABSTRACT

Some high temperature creep properties of two alloy systems, Pb-Bi and Pb-In, have been studied. Three compositions in each system were used with all alloys being solid solutions at the deformation temperature.

Solid solutions are usually divided into two groups, Class I and Class II, because of differences in certain creep properties. Attempts were made to classify the six alloys on the basis of the stress dependence of the steady state strain rate. Emphasis was also placed on the transient strain rate behaviour. Both initial transients from application of the load to attainment of steady state and transients in response to small increases or decreases in stress were studied as functions of stress, temperature and solute content. Significant differences were found in the shapes of the transients between the two alloy systems at some stresses and temperatures. These differences did not always coincide with the classification based on the steady state strain rate results.

In Class I alloys, the glide of dislocations is usually considered as controlling the deformation, whereas in Class II dislocation climb is the recognized controlling mechanism. Two commonly accepted glide and recovery theories were evaluated for the present alloys but were found inadequate for some of the results. Two more recent theories of creep, the combined glide-recovery theory and the rearrangement theory, provided better theoretical characterizations for the two classes of alloy.

TABLE OF CONTENTS

LIST OF TABLES

LIST OF FIGURES

ACKNOWLEDGMENTS

I would like to express my gratitude for the advice of my research supervisor Dr. T.H. Alden. Thanks are also due to other members of the department and fellow graduate students with special appreciation to J. Brezden for his expert artistic work, to officemates, S.R. Bala and A.S. Rao, for support during comprehensive and thesis preparation and to M. Fraser and I. Wilkomirsky for their extinguishing efforts during the Great Fire of '74. I would especially like to thank Kathie for her patience and understanding during this seemingly never-ending process.

Financial assistance of an Alcan Fellowship, 1973, and NRC Grant No. A-4991 is gratefully acknowledged.

Chapter 1

INTRODUCTION

Time-dependent deformation in pure metals has been extensively researched but, by comparison, the creep of simple metallic solid solutions is not well understood. Recently, attempts have been made (Cannon and Sherby, 1970; Mohamed and Langdon, 1974) to divide solid solution alloys into two classes on the basis of certain creep characteristics: Class I alloys in which some deformation phenomena are *different from* pure metals, and Class II alloys which possess creep properties *similar to* pure metals.

Class II alloys, in common with pure metals, usually have:[1]

1) A power law dependence of steady-state creep rate on stress;

$$\dot{\varepsilon}_{ss} \propto \sigma^n$$

with a stress exponent n of about 4.5,

2) An "instantaneous" or loading strain upon initial application of the load,

3) An extensive primary creep region with a continually decreasing strain rate,

4) A creep rate influenced by changes in stacking fault energy and subgrain size.

Class I alloys have these characteristics different from pure metals:[2]

1) A stress exponent close to 3, i.e. $\dot{\varepsilon}_{ss} \propto \sigma^3$,

2) Little or no "instantaneous" strain,

3) Restricted primary creep with, in some cases, complex variations in creep rate,

4) A creep rate not influenced by stacking fault energy or subgrain size.

Some attempts have been made to distinguish which material properties are important in determining the class of a particular alloy. In one such correlation (Cannon and Sherby, 1970), a large size difference between the solute and solvent atom, coupled with low elastic modulus of the solvent appeared to promote Class I type behaviour (Figure 1.1).

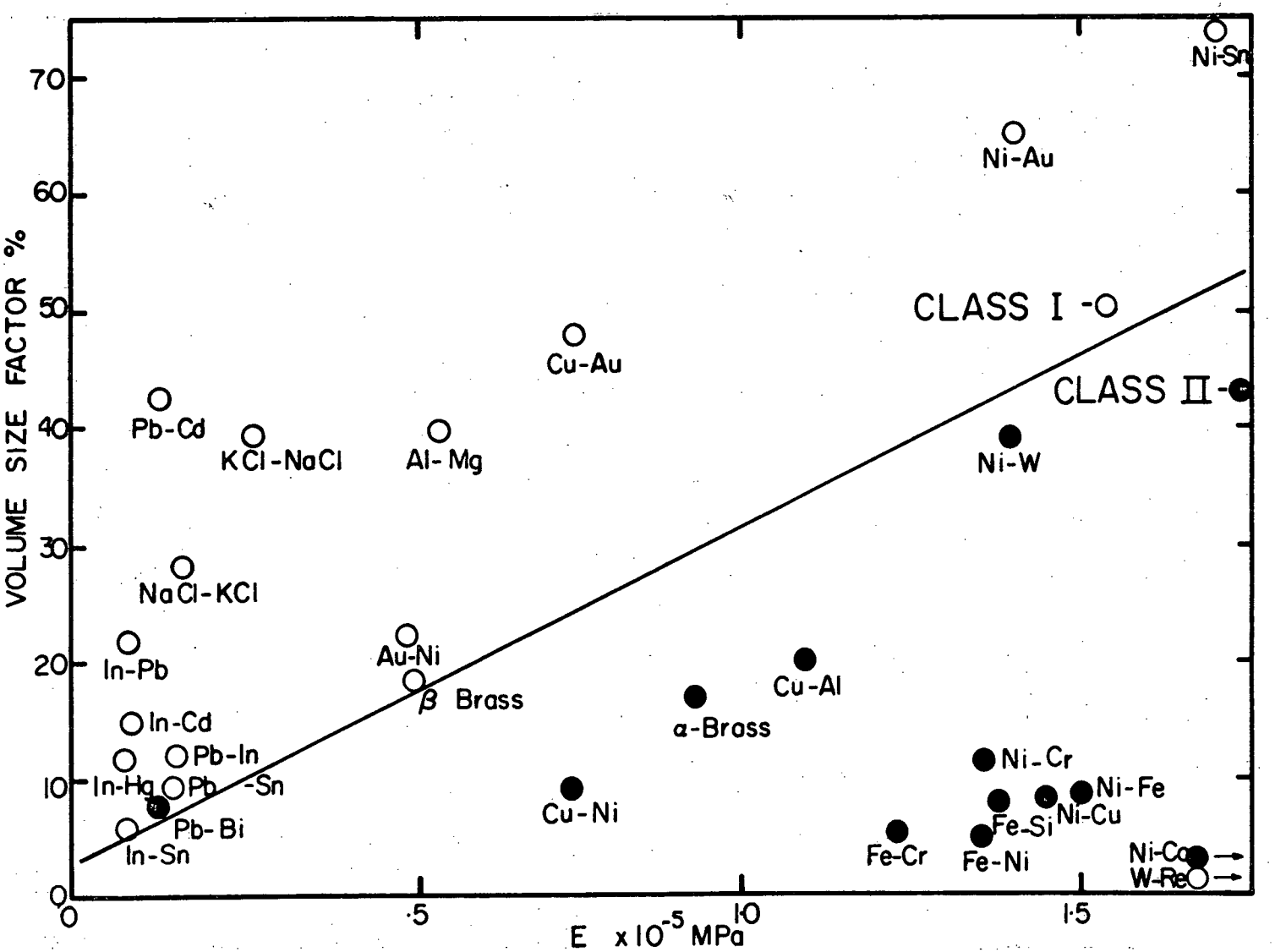

Figure 1.1. Influence of volume size factor and Young's modulus (E) of pure solvent in determining class of solid solution alloys.

SIMPLE THEORIES

From comparisons of some creep properties with predictions of two theories (Weertman, 1955, 1957a, 1957b, 1968), it has been postulated that the steady state creep rate is controlled by dislocation glide in Class I alloys and by dislocation climb in Class II.

The models, upon which the theories are based, are similar in nature. Dislocations are emitted from sources and glide across the slip plane until they encounter the stress field of dislocations on adjacent planes (Figure 1.2). If the dislocation is stopped by the stress field, pile-ups of dislocations will begin to form and exert a back stress on the source eventually stopping its operation. *Steady state* creep, requires that dislocations continually climb out of the slip plane to allow fresh dislocations to be generated. The model then involves two sequential processes, dislocation glide followed by dislocation climb, and the rate of strain is controlled by the slower of the two.

If glide is very fast and the climb rate is slow, climb is rate controlling (Class II). The steady state strain rate $\dot{\varepsilon}_s$ will then vary as the climb rate which, in turn, will depend upon the diffusion of vacancies away from or towards the dislocation.

The concentrated stress at the head of the pile-up will assist this vacancy flux. The strain rate will therefore

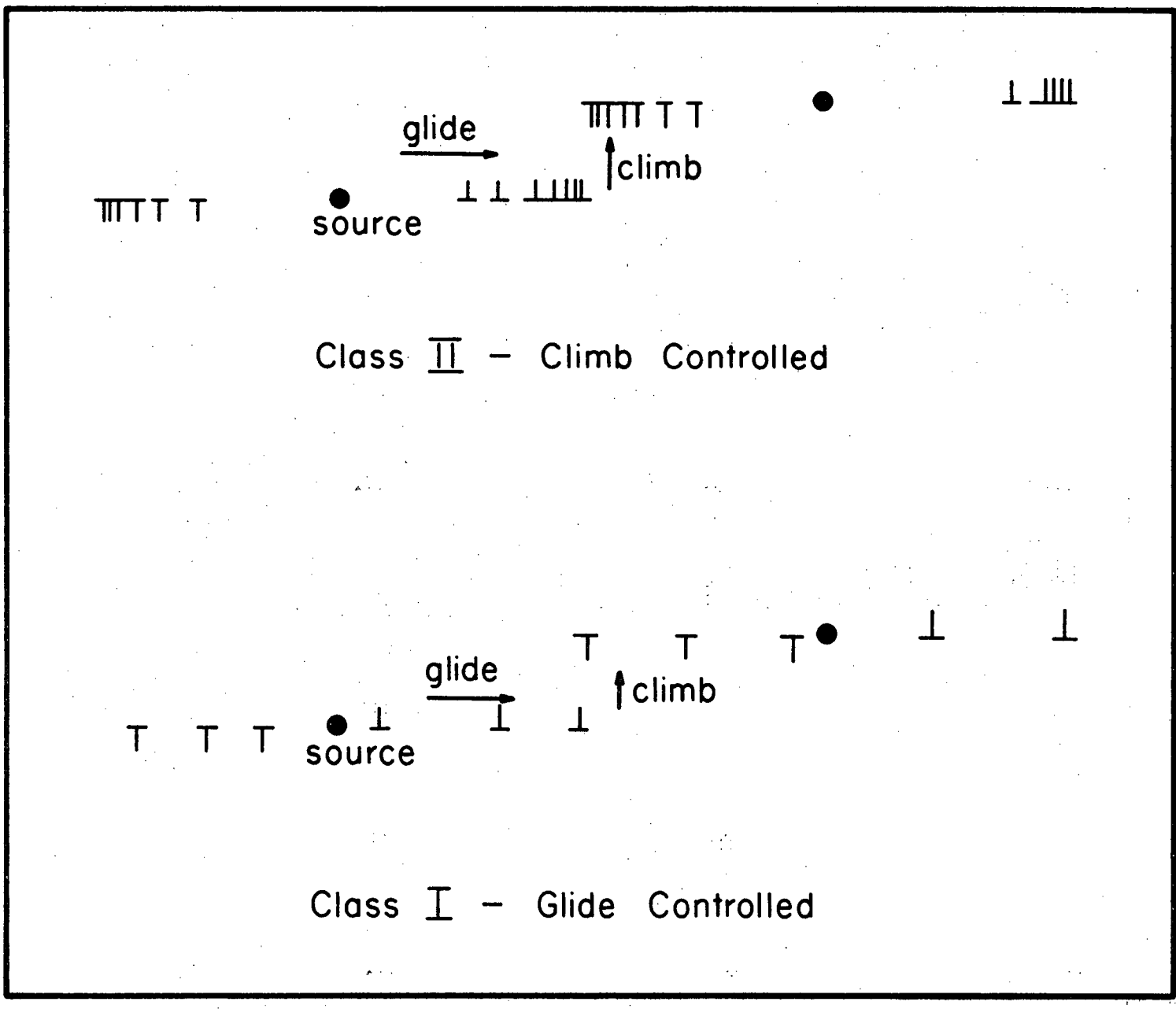

Figure 1.2. Dislocation models for climb and glide controlled creep (Weertman, 1955, 1957a, 1957b, 1968).

be a function of the applied stress, the number, N, of piled-up dislocations and the diffusivity of vacancies D_v:

$$\dot{\varepsilon}_s = f(\sigma, N, D_v) \ . \qquad (1.1)$$

In a binary alloy the vacancy diffusivity can be replaced by a weighted or average diffusivity representing a flux of both solute and solvent atoms:

$$\overline{D} = D_1 D_2 / (D_1 X_2 + D_2 X_1) \qquad (1.2)$$

with X_1, X_2 the fractional concentrations of the alloy species and D_1, D_2 their diffusivities (Herring, 1950, Weertman, 1960). The solute atom in the climb model affects the creep rate only by its influence on this diffusivity.

In the glide controlled model (Weertman, 1957), the solute atoms interact with the stress field around the dislocation forming atmospheres. Since movement of the dislocation then requires diffusion of the solute atmosphere, the glide rate is reduced sufficiently to become the rate controlling step. No pile-ups form in this model since the climb rate is faster than the glide rate. The requisite number of dislocations will be spaced across the slip plane between the source and the adjacent stress fields.

The strain rate is the product of the velocity of the dislocations and their density in the slip plane. Both applied stress and the diffusivity of the solute atoms D_s influence the velocity. The density will depend upon the applied stress overcoming the inherent repulsion force between the like sign dislocations. Therefore:

$$\dot{\varepsilon}_s = f(\text{velocity x density}) = f(\sigma, D_s). \qquad (1.3)$$

For both models mathematical development leads to an expression:

$$\dot{\varepsilon}_s = A\ \sigma^n \exp - \frac{Q}{RT} \qquad (1.4)$$

where A is a constant, n is the steady state stress exponent and Q is the activation energy. For the glide controlled case, n = 3 and Q is the activation energy for solute diffusion. For the climb controlled case, n = 4.5 and Q is the energy for self diffusion.

Thus there are two obvious ways of differentiating between the two mechanisms, the values of n and of Q. Because of the lack of data on diffusion coefficients in alloys, the value of the stress exponent has become the most important criterion for determining the rate controlling mechanism.

REFINED THEORIES

The simple theories previously described epitomize the general theoretical controversy between the reaction rate and recovery theories of high temperature deformation. In the reaction rate or glide theory (Kauzman, 1941; Cottrell and Stokes, 1955; Feltham, 1968), thermal activation aids the dislocation to overcome the obstacles impeding its motion; the obstacles are thermally penetrable. The strain rate is given directly by the Arrhenius equation:

$$\dot{\varepsilon}_s = \dot{\varepsilon}_0 \exp - \frac{Q}{RT} \qquad (1.5)$$

For example, in the Weertman glide model, thermal activation assists the dislocation movement through the diffusion of the solute atoms.

In the recovery theory (Bailey 1926; Orowan, 1946), the obstacles are thermally unstable and disappear with the assistance of thermal activation. The strain rate is given by the ratio of the recovery rate r to the strain hardening coefficient h:

$$\dot{\varepsilon}_s = \frac{r}{h} . \qquad (1.6)$$

Thermal activation influences the strain rate through its effect on the recovery rate. In the simple climb model the

removal of a dislocation from the piled-up group constitutes the recovery mechanism and permits further strain.

Although both theories offer reasonable explanations of the phenomenon of steady state creep, application to transient conditions is not so clear (Orowan, 1946; Alden, 1972). Modifications to the basic theories (Figure 1.3) do permit analysis of a wider spectrum of phenomena. The present thesis will invoke two such refined treatments, the "combined glide-recovery" model (Cottrell and Aytekin, 1950; Ahlquist *et al.*, 1970; Gasca Neri *et al.*, 1970) and the "rearrangement" theory (Alden, 1972).

As the name implies, the combined glide-recovery theory incorporates aspects of both fundamental concepts. A new idea of dividing the applied stress into effective and internal stress components is introduced. The internal stress component is necessary to overcome long range elastic stress fields of immobile dislocations. Dislocations cannot move unless the applied stress is greater than the internal stress, so that an effective stress component can assist the dislocation over short range obstacles.

Since the immobile dislocation density can be diminished through recovery and increased by entrappement of mobile dislocations, the internal stress is governed by a recovery-strain hardening competition. The microstructural model contains both short and long range obstacles. In alloys

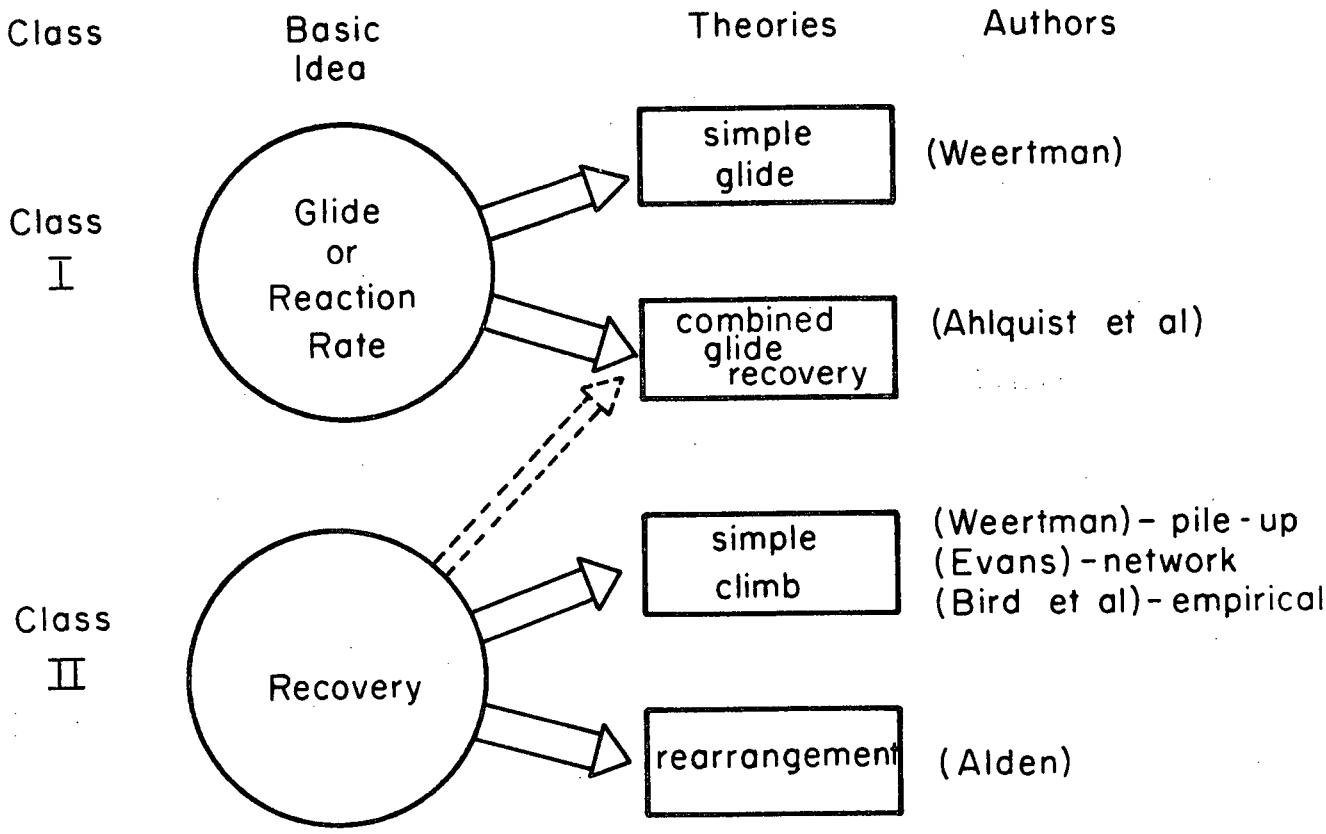

Figure 1.3. Interrelationships of several theories of creep for Class I and Class II alloys.

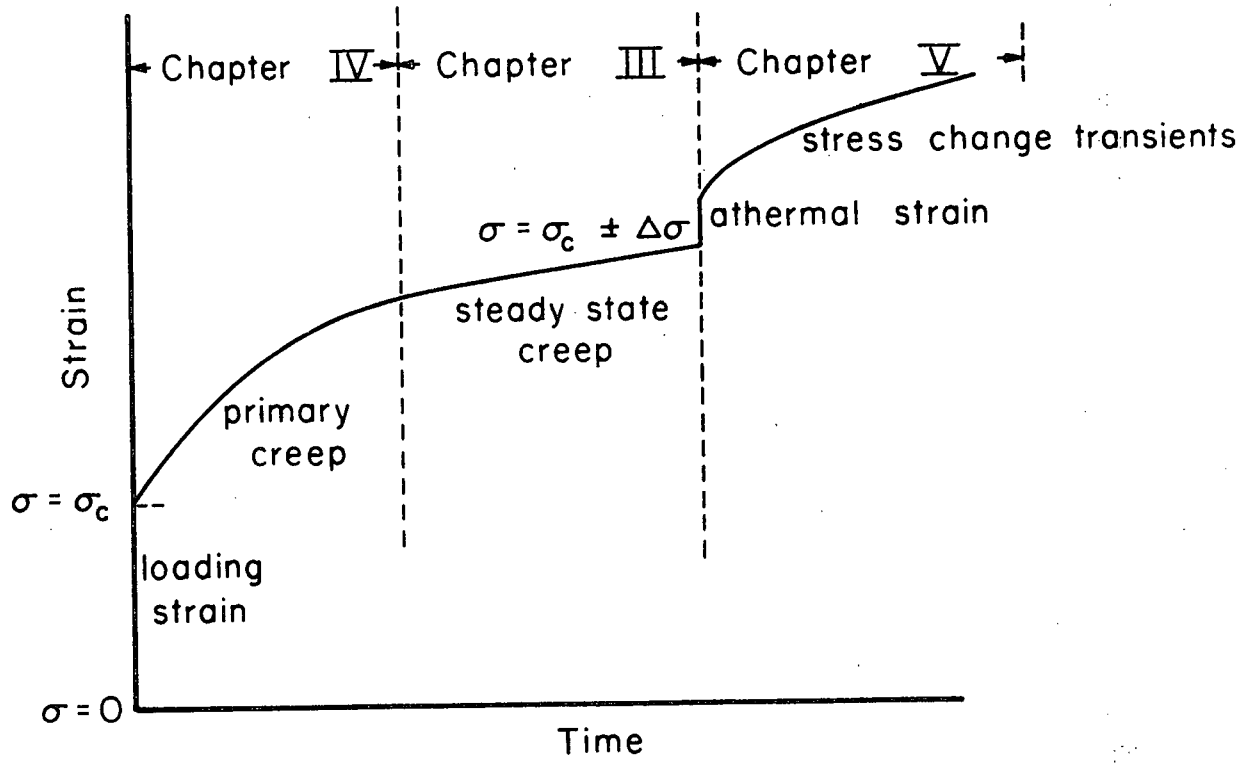

Figure 1.4. Organization of thesis as related to creep curve.

the short range obstacles could be the solute atmospheres, the long range the immobile dislocations.

The rearrangement theory is a new concept introduced within the framework of the recovery theory. There is only one set of obstacles, the forest dislocations, but their distribution is nonuniform. There are "soft" areas of low obstacle density where deformation is preferred. The obstacles can be lost by recovery but can also rearrange without loss to continually produce soft areas. The movement of the glide dislocation is athermal; thermal activation influences the recovery and rearrangement rates only.

The introduction of these new concepts, either a two obstacle structure or a spatial variation of single obstacles enable these two refined theories to deal with more complex deformation behaviour than the simple theories. Detailed discussion of the refined theories will be reserved until Chapter 4. Continual reference to Figure 1.3 will facilitate identification of the interrelationships between the theories.

SCOPE OF THE PRESENT WORK

In the creep literature, discussion of the two alloy classes has focussed on the simple theories of glide and climb. Differentiation of the alloy classes has been

done mostly on the basis of the steady state stress exponent. The intent of the present study was to examine the transient and steady state aspects of creep behaviour in alloys from each class and relate the results to the refined creep theories. Two principal transients were studied: 1) the initial transients from the condition of zero stress to attainment of the steady state creep rate and 2) the transients introduced by small changes in the creep stress in the steady state regime. Whenever possible, the effects of changes in the external variables, stress, temperature and solute content were assessed.

The alloy systems chosen for study were Pb-In and Pb-Bi which were previously categorized as Class I and Class II, respectively (Weertman, 1960). Both systems possess considerable solid solubility and low melting temperatures so creep temperatures are easy to attain. Bi is a larger atom than Pb with a positive volume size factor[3] of 7.04.% In is smaller with a negative size factor of 11.16 (King, 1966).

Polycrystalline sheet specimens were used with a grain size such that there were at least two to four grains across the specimen thickness. With this configuration grain boundary sliding should not contribute significantly to the creep strain (Bird, Mukherjee, and Dorn, 1969; Sherby and Burke, 1967). The measured deformation should be

representative of a polycrystal with all deformation occurring within the grains.

ORGANIZATION OF THE THESIS

The experimental results and discussion have been divided into three sections (Chapter 3, 4 and 5) corresponding to a portion of the creep curve (Figure 1.4).

In Chapter 3 the effects of stress, temperature and solute content upon the steady state strain rate are evaluated. Stress exponents are used to classify alloys in accord with the simple theories.

In Chapter 4 the initial transient region is examined under two subdivisions:

1) the loading strains upon initial application of the stress,

2) the primary creep transients.

The refined theories are elaborated and applied to the results.

Chapter 5 deals with the effects of small stress changes after the steady state is established. The emphasis is upon the "instantaneous" changes in strain during the stress change and on the transient effects until the re-establishment of steady state.

FOOTNOTES

[1]Barrett and Nix, 1965; Bonesteel and Sherby, 1966; Davies *et al.*, 1965; Evans and Wilshire, 1970; Feltham and Copley, 1960; Garofalo *et al.*, 1963; Hazlett and Parker, 1954; Hedworth and Pollard, 1971; Johnston *et al.*, 1972; Jones and Sellars, 1970; Karashima, Motomiya and Oikawa, 1968; Lawley *et al.*, 1960; Lytton, 1962; Monma *et al.*, 1964a, 1964b, 1964c; Pahutová, Čadek and Rys, 1969; Pahutová, Hostinsky, Čadek and Rys, 1969; Rossard and Blain, 1958; Russell *et al.*, 1968; Sidey and Wilshire, 1969; Weertman, 1960.

[2]Borch *et al.*, 1960; Brown and Lenton, 1969; Davies and Dennison, 1961; Fuchs and Ilschner, 1969; Hren, 1962; Jones and Sellars, 1970; Karashima, Oikawa and Watanbe, 1968; Laks *et al.*, 1957; Linga Murtz *et al.*, 1972; Oikawa and Karashima, 1974; Oikawa, Kariya and Karashima, 1974; Oikawa, Maeda and Karashima, 1972; Sellars and Quarrel, 1961; Sherby *et al.*, 1951, Vandervoort and Barmore, 1968; Weertman, 1960.

[3]Volume size factors represent the fractional differences between the effective atomic volume of the solute V_B^* and the atomic volume of the solvent V_A, i.e.

$$V_{sf} = (V_B^* - V_A)/V_A.$$

Chapter 2

EXPERIMENTAL

EQUIPMENT

All creep testing was done with machines fitted with Andrade-type constant stress lever arms (Figure 2.1). The samples were held in serrated split grips on the "short" arm side of the lever. To ensure axial alignment of the specimen, universal joints were connected to the grip assemblies.

Two machines were used; the larger gave a mechanical advantage on the lever of 4:1 and the smaller a 2:1 advantage.

The load was initially applied to the specimen by downward movement of the loading pan support. The movement of the support was controlled by either an hydraulic jack or an electrically driven screw gear. Rate of descent of the support was kept constant from test to test producing an initial elastic stress rate of approximately 1.5 Pa/min (Appendix 1).

The elongation of the specimen was measured with linear voltage differential transformers (Daytronic LVDT DF-160 or 300) by attachment of the iron core of the transducer

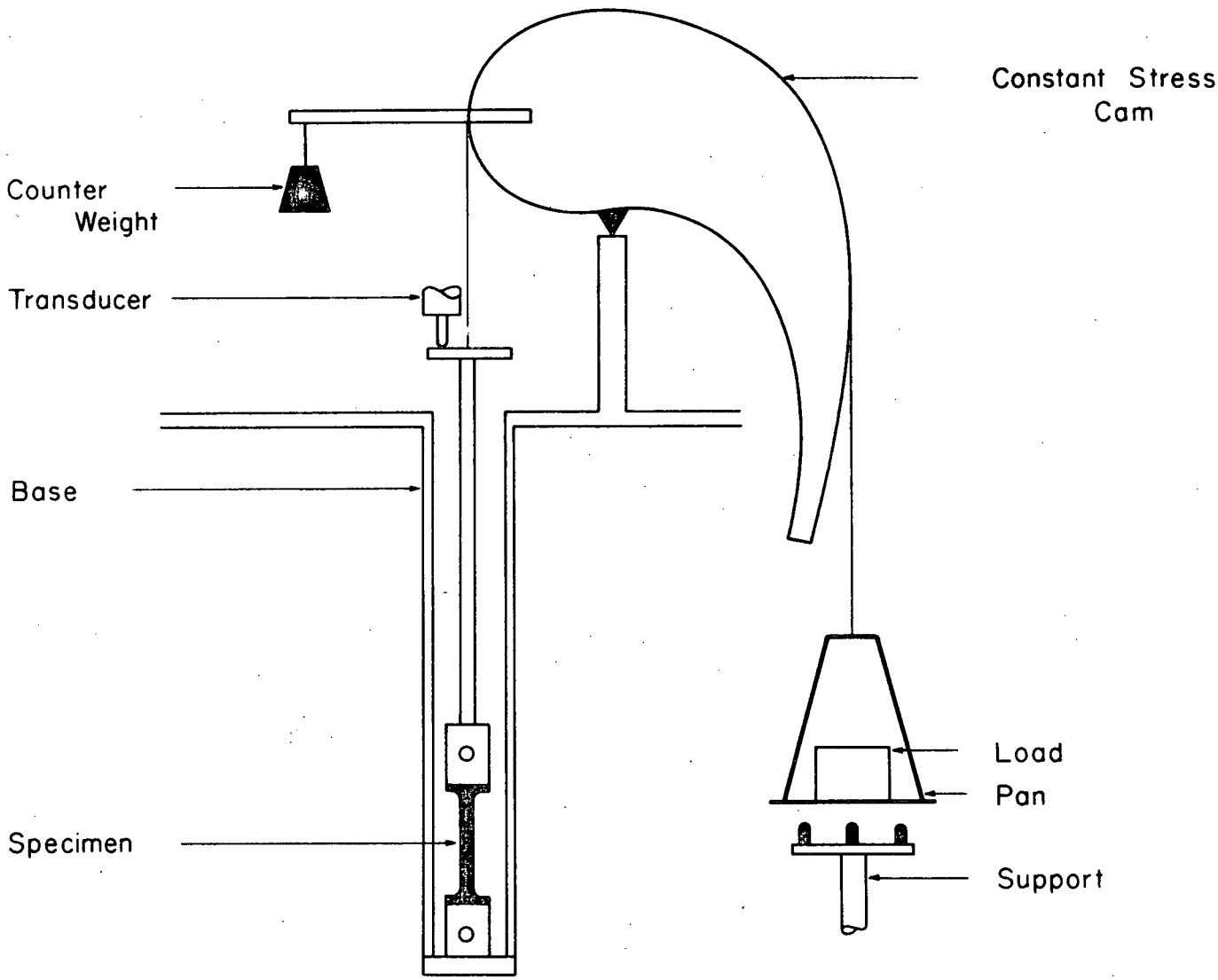

Figure 2.1. Creep testing apparatus.

to the upper grip assembly (Figure 2.1). Consequently some elastic extension of the grip assembly was detected as well as the plastic and elastic elongation of the sample. This machine deflection was included in all strain calculations. Output from the transformer was amplified by a Daytronic (Model 300D) amplifier and recorded on either a Heathkit chart recorder or a storage oscilloscope. The system was calibrated with dial gauges with divisions of 4×10^{-5} cm. Strains of 4×10^{-6} could be detected with this equipment. Stresses were accurate to ±.7%.

To achieve test temperatures greater than ambient, the sample and grips were immersed in an oil bath equipped with a magnetic stirrer and immersion heater. Temperature was maintained within ±2°C with a Honeywell on-off controller. For some temperatures close to or less than ambient, a water or ice-water bath was used. Actual specimen temperature was measured with a chromel-alumel thermocouple placed adjacent to the gauge section.

METHODS

Creep Curve Determination

Specimen Alignment. The upper and lower grip assemblies were clamped in 'vee' blocks mounted remote from the creep machine to permit the alignment and tightening

of the specimen in the grips. The whole grip and specimen assembly was transferred to the creep machine in a special clamp.

Loading Strain. After removal of the clamp and the preanneal treatment (see page 24), the constant stress cam was levelled and the transducer zeroed with a small load on the specimen (Point A, Figure 2.2). The pan support was raised to permit the specimen assembly to move downward in the central column (Point B, Figure 2.2) indicated by an apparent negative elongation reading. The small load was replaced by the required creep load P_c. The pan support was started downward at a fixed rate (Point C, Figure 2.2).

As the bottom grip assembly contacted the central column the loading of the specimen commenced causing a change in the measured elongation rate. The position of this change in rate indicated the zero strain condition in the specimen (Point D, Figure 2.2). Full application of load was achieved when the load pan no longer contacted the pan support (Point E, Figure 2.2). This occurrence was detected either visually or by the breaking of an electrical contact between the pan and support. The loading strain was defined as the difference between Points D and E.

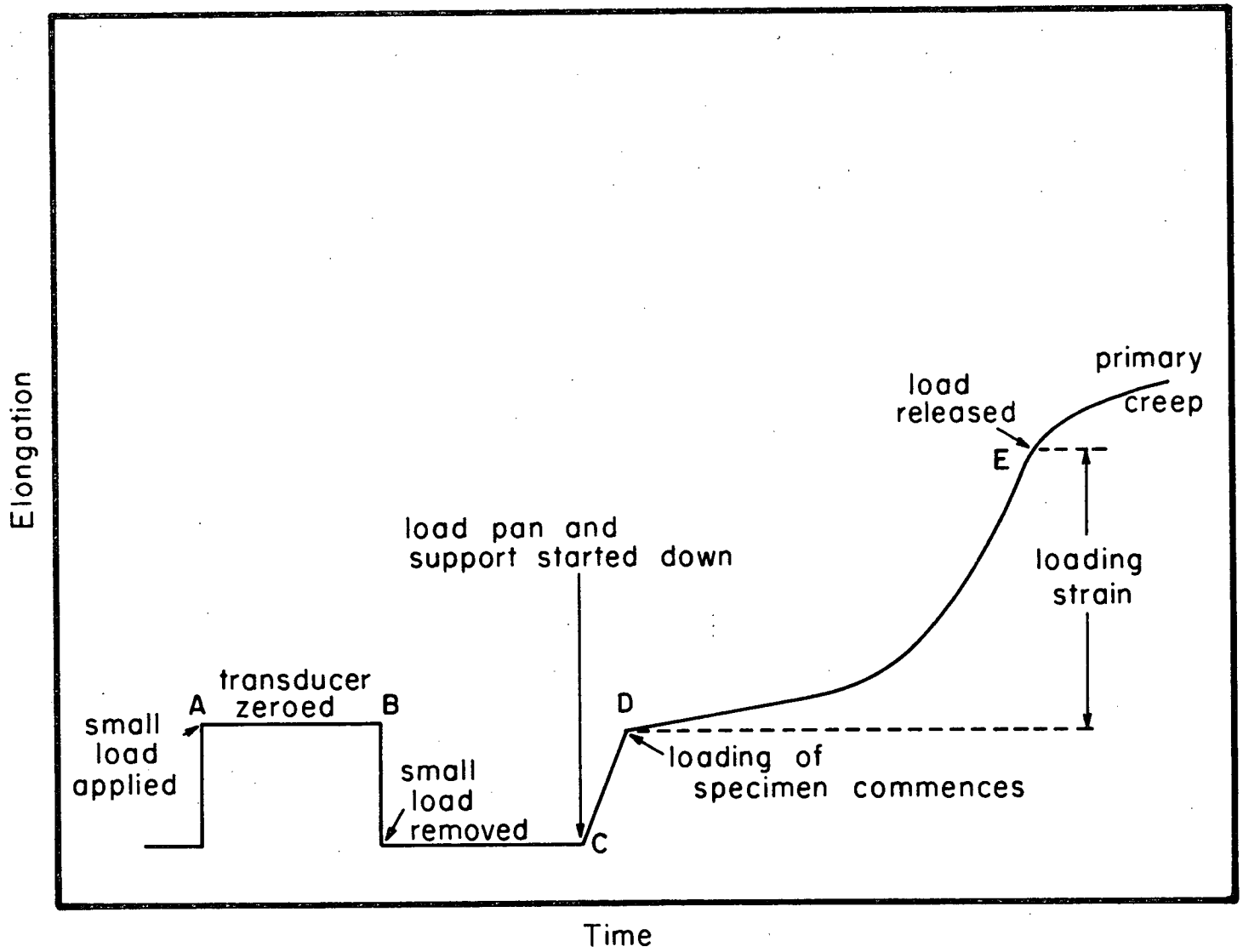

Figure 2.2. Elongation-time curve during the initial loading of creep specimen.

Creep Curve. The remainder of the creep curve was recorded continuously by the chart recorder. A computer program (Appendix 2) was used to convert the chart readings to true strain, to calculate the strain rate and to plot strain and strain rate as a function of time.

Stress Changes

The creep stress was changed when required during the course of a test by one of two methods, termed "rapid" and "slow." Rapid changes were achieved by adding or subtracting small counter weights to the negative side of the lever (Figure 2.1). For stress decreases the small weights were placed carefully on the lever by hand. For rapid stress increases the counterweight was suspended by a fine thread from the lever at the start of the test. At the desired time the thread was severed, releasing the weight and increasing the effective load rapidly.

The specimen elongations produced during stress increases were recorded by the oscilloscope with its rapid response time. The transients at later times were measured with the chart recorder. A stress rate of approximately .15 Pa/sec was achieved during these stress changes.

Slow stress increases were effected by adding small glass beads directly to the major weight from a reservoir

located over the load pan. A stress rate of approximately 1.1×10^{-3} Pa/sec was achieved by this method. Elongation in this case was measured with the recorder running at its highest chart speed (30.5 cm/min).

MATERIAL

All alloys were prepared from Pb, Bi and In of 99.999% purity. Melting, casting and cooling of the ingots were all done in a vacuum induction furnace (Vacuum Industries Inc.). The material was melted in a stainless steel crucible then poured into copper moulds to produce an ingot (16 x 6 x 1.3 cm). Ingots were annealed in oil baths for 24 hours at 200°C to reduce microsegregation. A thin layer ($\simeq$ 2 mm) was machined from all surfaces of the ingot to remove possible oxide skin or mould contamination. The top and bottom 10 mm of the ingot was discarded. The ingot was rolled at room temperature into sheets approximately 75 mm wide and either 2.0 mm or 1.7 mm thick. Spectrographic analysis revealed a total impurity content of approximately .01%, in the prepared sheet.

The Pb-Bi alloys were analyzed by standard chemical methods for the concentration of Bi. Difficulty was encountered in establishing a reliable chemical method for the Pb-In alloys. For these alloys differential thermal analysis

(Dupont 900 DTA unit) was used to establish the solidus and liquidus temperatures. Alloy content was estimated from the phase diagram. Table 2.1 shows the percentage of solute for the six alloys studied.

Tensile specimens were cut from the rolled sheet by clamping strips of the alloy between two mild steel templates of the required shape and cutting with a jeweller's saw. A good edge finish could be produced by smoothing with a sharp knife. Two specimen sizes were used; one with a reduced gauge section of (25.4 x 9.5 x 2.0 mm) for use in the large machine and the other (50.8 x 9.5 x 1.7 mm) for the small machine.

All specimens were annealed within 15°C of their respective solidus temperatures to produce recrystallization and the requisite grain size. This anneal was done in stirred oil baths with temperature control of ±2°C. Annealing times were adjusted to produce a grain size of 600 to 1000 μ.

For metallography the Pb-In alloys were electro-polished and etched in a solution of 60% perchloric acid — 40% distilled water at a temperature of -10°C. Current densities of 1 amp/cm^2 and .2 amps/cm^2 were used for polishing and etching respectively. Since a suitable etching solution for the Pb-Bi alloys was not available a different procedure was adopted. Small areas of the specimens were microtomed with a diamond knife ultramicrotome (Porter-Blum Co.) to

Table 2.1

Solute Content Analysis of Alloys

Bi		In	
Alloy	Solute Content	Alloy	Solute Content
	(At %)		(At %)
1.	1.3	1.	3.2
2.	8.8	2.	9.5
3.	16.2	3.	17.0

produce a suitably smooth surface (Clark, 1971). The specimen was deformed slightly in compression to induce some grain boundary sliding and delineate the grain boundaries. Grain size was determined by the intercept method using a 10 cm circumference circle (Hilliard, 1964).

Immediately before testing all specimens were annealed 'in-situ' to reduce the effects of any deformation introduced by handling. This anneal was also done within 15°C of the solidus for 1/10 the time of the previous treatment.

All test temperatures were less than the annealing temperature to minimize grain growth during creep. Examination of several specimens after creep did not reveal evidence of deformation induced recrystallization. Also the periods of accelerated creep usually associated with recrystallization were not found.

Physical processes such as diffusion and creep can often be correlated for different pure metals by use of relative or homologous temperature T/T_m where T_m is the melting temperature (Sherby and Simnad, 1961; Ashby, 1972; Gifkins, 1974). Since the melting temperature is an indication of the cohesive forces between atoms, the effectiveness of thermal assistance in overcoming the cohesive energy should, in principle, be equivalent at the same homologous temperature.

When comparing diffusion or creep rates in alloys T_m is not clearly defined. In this study T_m was taken as

the solidus temperature. Comparisons of the alloys were done mainly at homologous temperatures of .6, .8 and .95 with other temperatures used on occasion (Table 2.2).

Table 2.2

Relative and Homologous Temperatures

Atomic % Solute	Temperature (°K)			
	T_m	.95 T_m	.8 T_m	.6 T_m
16.2 Bi	493	468	394	296
8.8 Bi	543	516	435	326
1.3 Bi	588	559	471	353
17.0 In	553	525	443	332
9.5 In	572	544	457	343
3.2 In	588	559	471	353

Chapter 3

STEADY STATE CREEP

The relationship between the creep stress σ and the steady state strain rate $\dot{\varepsilon}_s$ is commonly used for determination of rate controlling mechanisms. In the intermediate stress ranges the functional form is usually a power law:

$$\dot{\varepsilon}_s = A\,\sigma^n \tag{3.1}$$

with n being termed the steady state stress exponent and A containing temperature and concentration factors.

Values of σ, $\dot{\varepsilon}_s$ were obtained in two ways:

1) One specimen for each creep stress and
2) A single specimen at several stresses and steady states.

Slight differences were discovered between the strain rates measured by the two methods. Therefore $\dot{\varepsilon}_s$ is not a unique function of stress and temperature, independent of the strain history. However since the variations between the two

techniques were small, a combination of both methods reflected the σ-$\dot{\varepsilon}_s$ relationship with sufficient accuracy.

Since activation energies have also been used to differentiate rate controlling mechanisms, the present study attempts to calculate activation energies from the σ-$\dot{\varepsilon}_s$ data.

In the RESULTS section the σ-$\dot{\varepsilon}_s$ function will be examined under three subdivision:

1) Stress exponent values
2) Activation energies
3) Strengthening effects

The influence of temperature and solute content will be examined for each subsection. Stress exponents will be calculated from the power law, activation energies by a modified Zener Hollomon method (Zener and Hollomon, 1944) and strengthening by the stress required to produce a constant strain rate.

The DISCUSSION section will deal with the predictions of the simple theories for the three subdivisions.

RESULTS

Stress Exponents

Stress-$\dot{\varepsilon}_s$ data were obtained for each alloy at the three principal temperatures of .95, .8 and .6 T_m (Figure 3.1 through 3.6). The curves through the points were

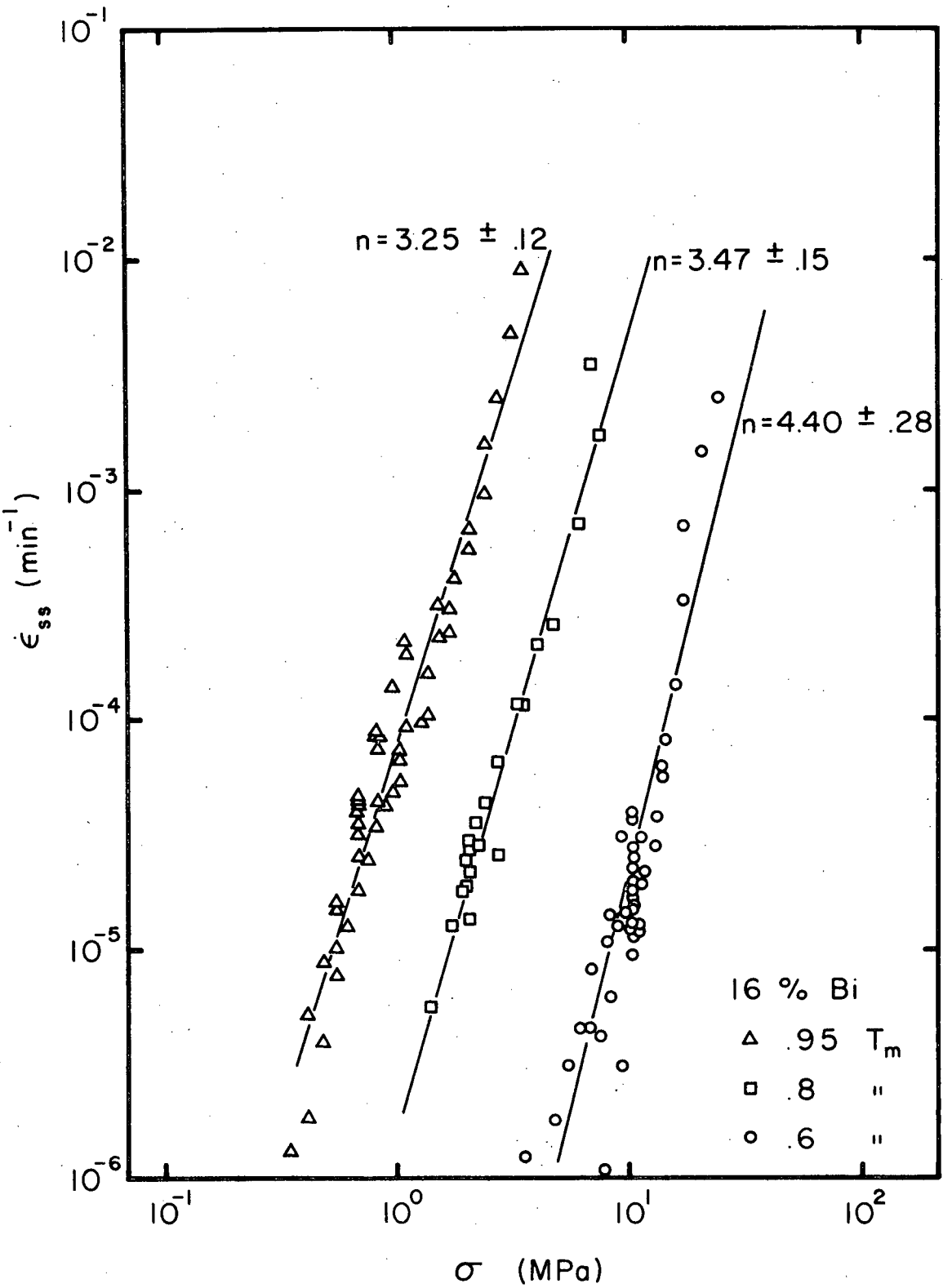

Figure 3.1. Steady state strain rate versus stress for 16% Bi alloy.

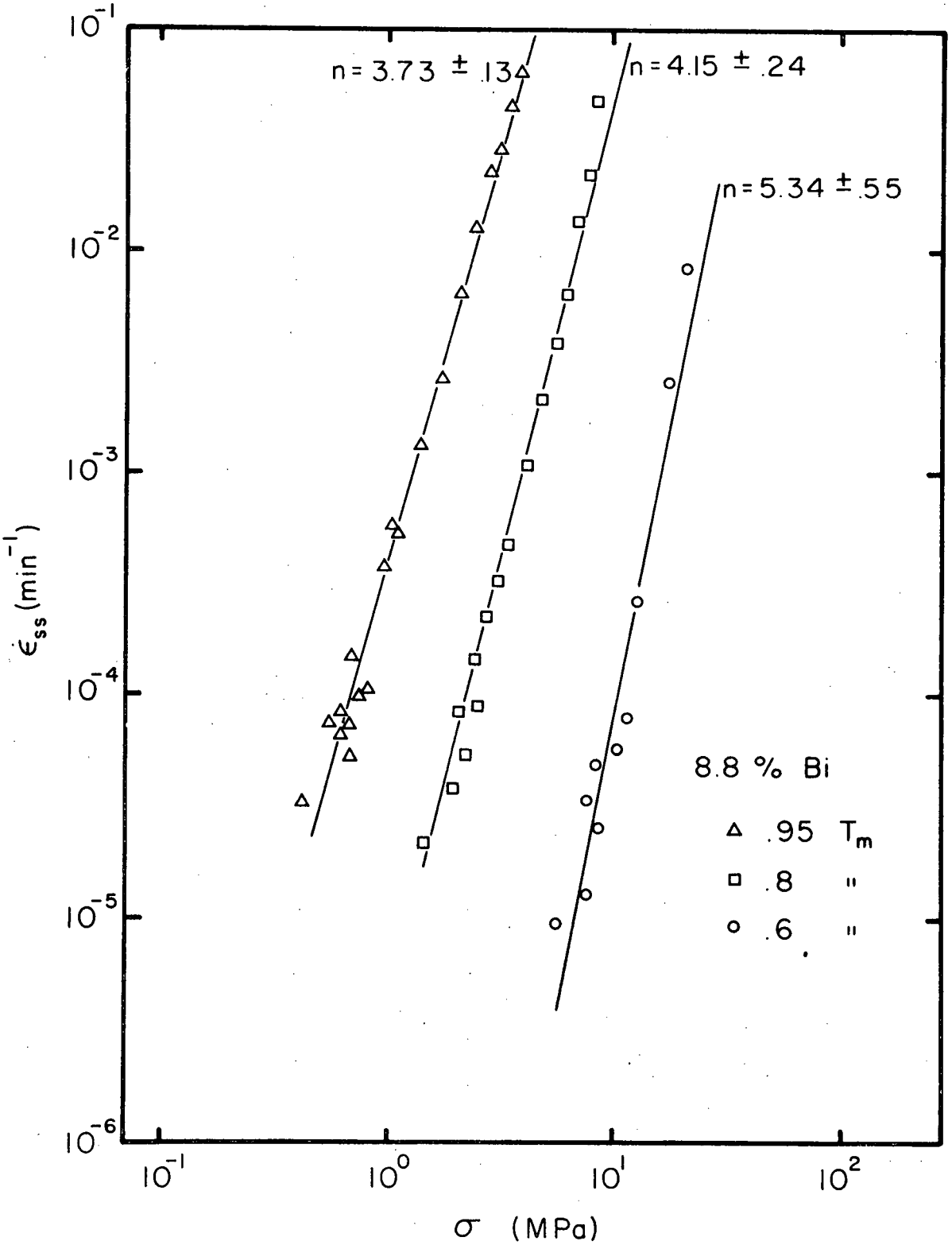

Figure 3.2. Steady state strain rate versus stress for 8.8% Bi alloy.

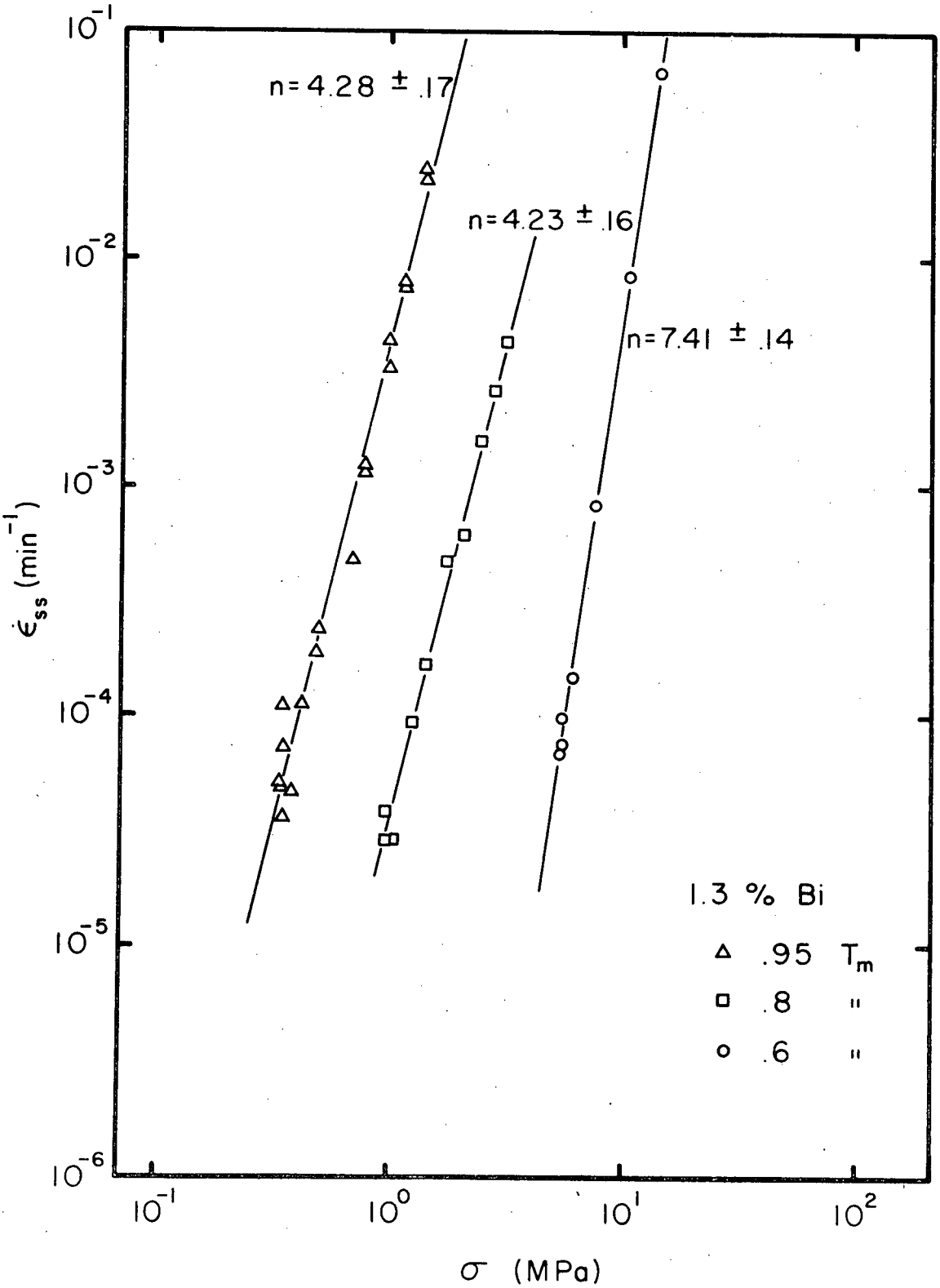

Figure 3.3. Steady state strain rate versus stress for 1.3% Bi alloy.

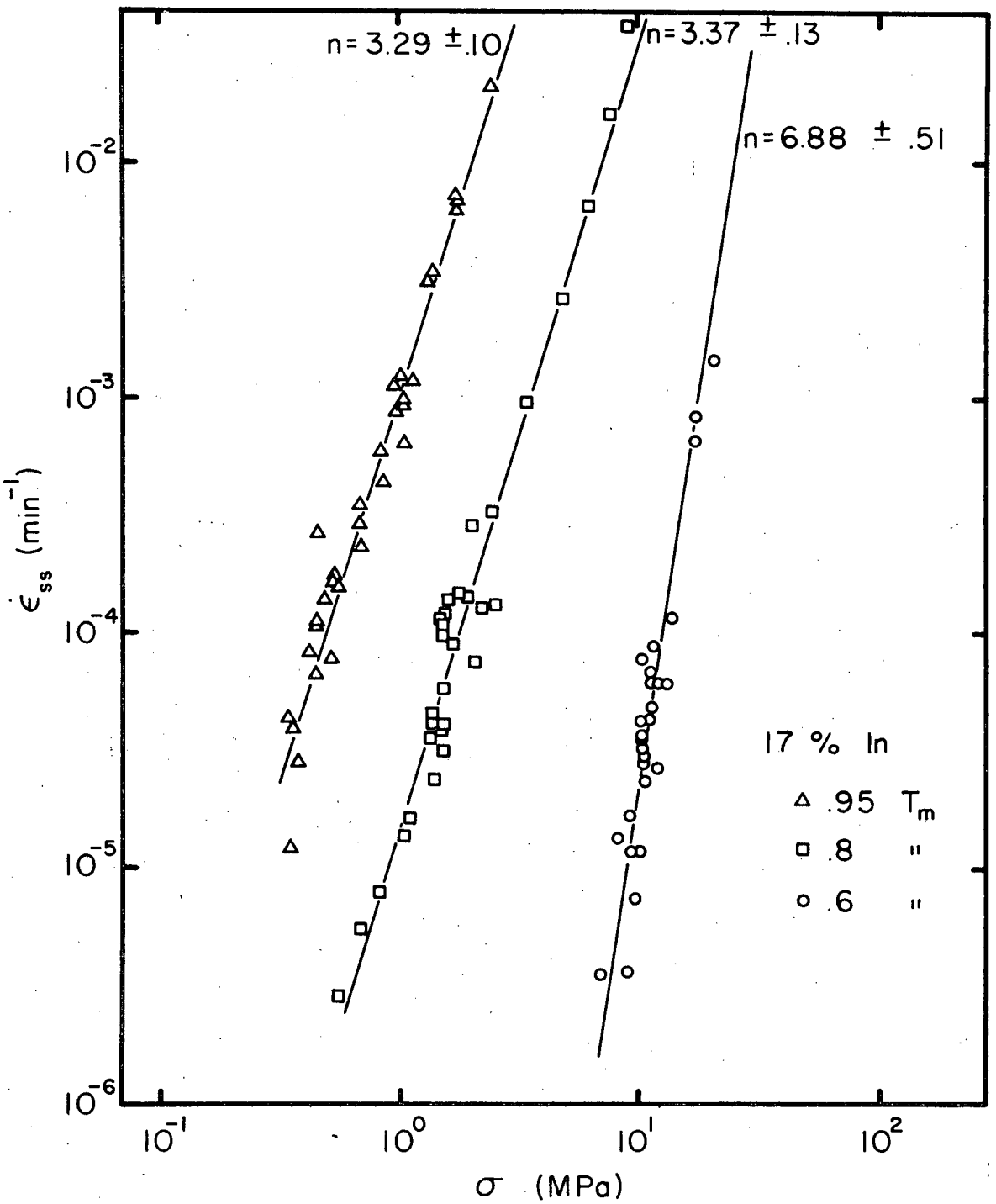

Figure 3.4. Steady state strain rate versus stress for 17% In alloy.

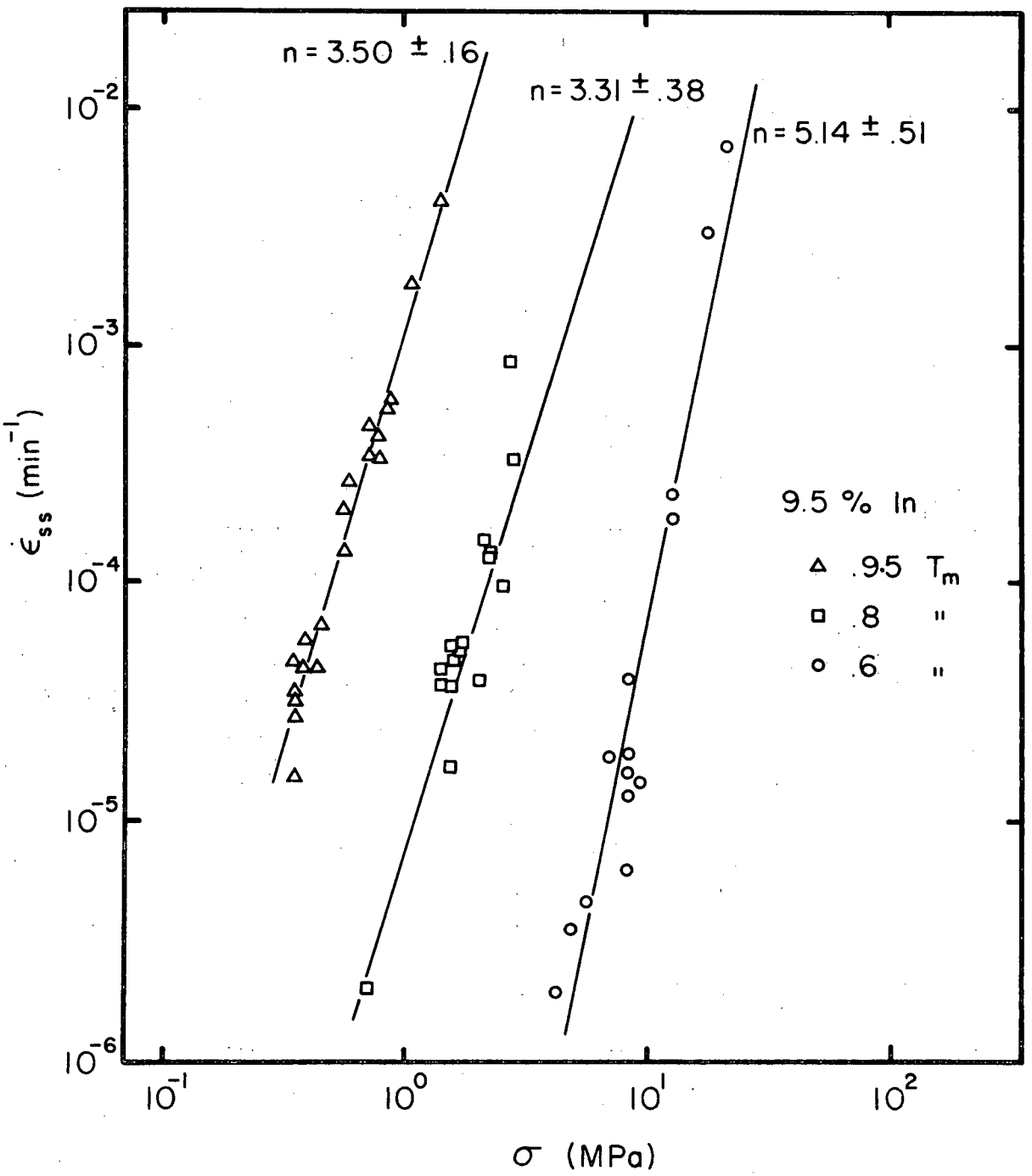

Figure 3.5. Steady state strain rate versus stress for 9.5% In alloy.

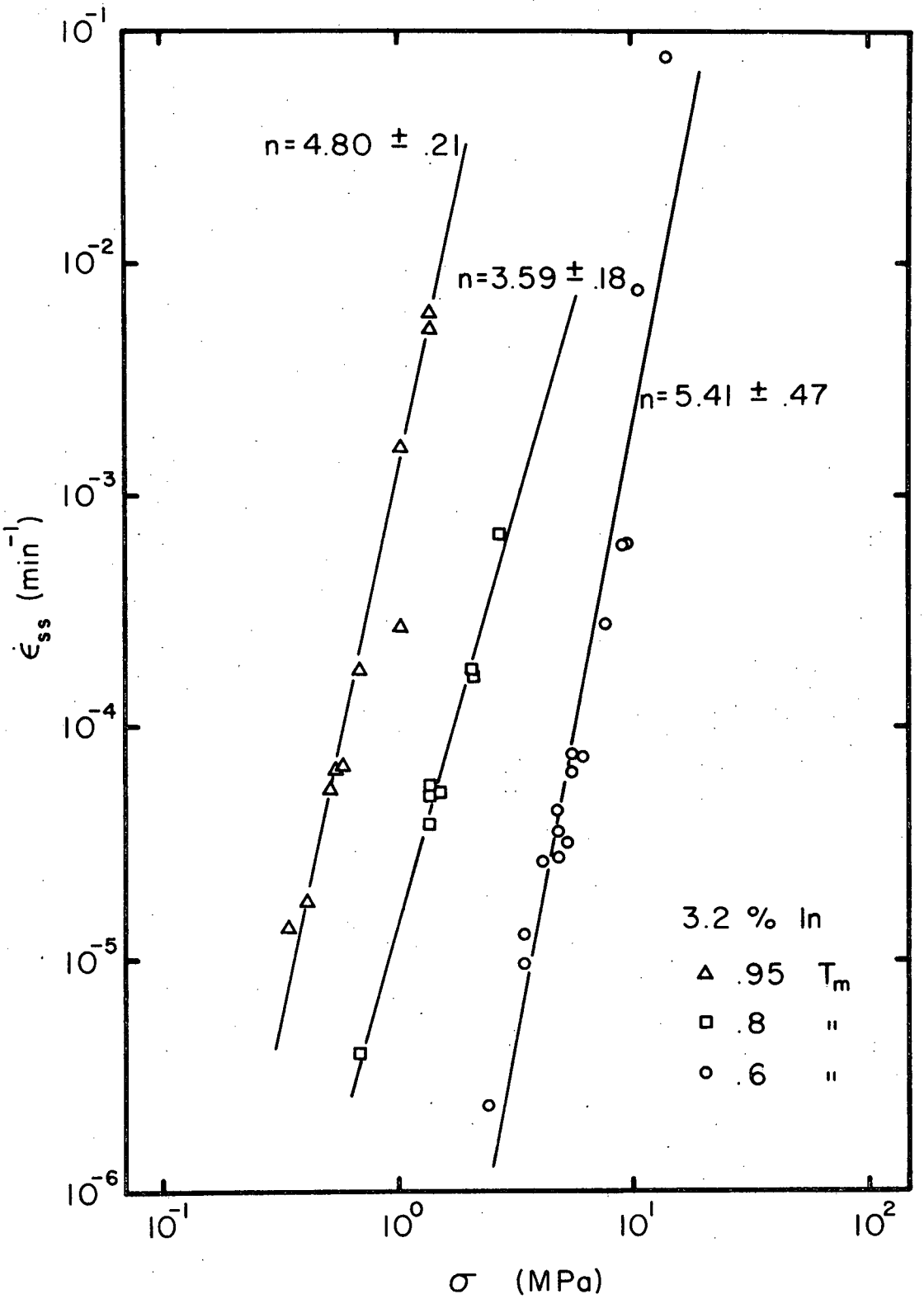

Figure 3.6. Steady state strain rate versus stress for 3.2% In alloy.

determined by least squares fitting to the power law equation (Eq..3.1), using computer programs (Bird, Moore and Streat, 1974). The ratio of the total error of estimate to the statistical error of estimate was always less than unity indicating 1) a good fit to the function and 2) the chief error source was random variation in $\dot{\varepsilon}_s$ (Rose, 1953). The quoted errors in n represent 56% confidence limits calculated from the total error of estimate parameter. The variation of the stress exponents with temperature and stress were evaluated.

Temperature. The general trend is a reduction of n with increasing temperature from .6 to .95 T_m (Figure 3.7) in both alloy systems. Only the 3.2% In alloy is an exception. The magnitudes of n at .6 T_m are somewhat above the usual range of 5 to 3. At higher temperatures the values of n from a previous study (Weertman, 1960) are comparable ($\simeq$ 20% difference) with the present determination for the Pb-In alloys (except for 3.2% In). For the 16% Bi alloy, the previous result is much higher (5.6 compared to 3.3). For this alloy the present results are based on a greater number of experimental points than the previous study.

It is possible that the high values of n at .6 T_m are due to incorrect application of the power law in this

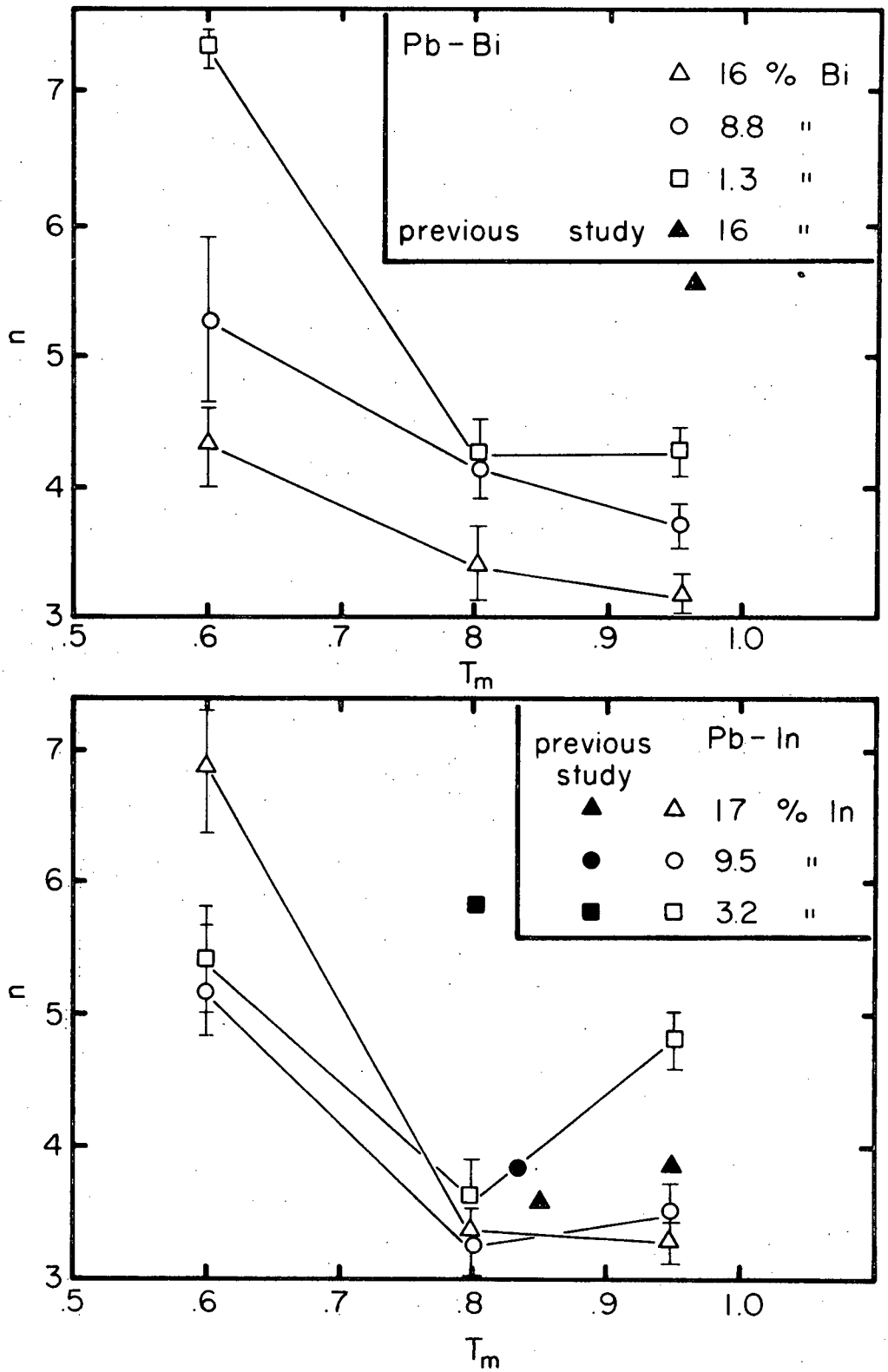

Figure 3.7. Steady state stress exponents versus relative temperature for all alloys.

stress range. Over wide stress ranges σ - $\dot{\varepsilon}_s$ can be more appropriately fitted by a hyperbolic sine function (Garofalo, 1965):

$$\dot{\varepsilon}_s = \beta\left[\sinh\alpha\sigma\right]^n \qquad (3.1A)$$

At low stresses this reduces to equation (3.1). At high stress it predicts a greater sensitivity of the strain rate to stress or higher apparent n values in a log $\dot{\varepsilon}$ - log σ plot. For this reason interpretation of the stress exponent results will emphasize the low stress (or high temperature) values.

Solute Content. The stress exponent decreases with increasing Bi content in the Pb-Bi system at all temperatures (Figure 3.8). In the Pb-In system a similar decrease with In is observed only at .95 T_m. At other temperatures n remains constant (.8 T_m) or increases (.6 T_m) with solute additions.

Activation Energy

Activation energies are commonly calculated from σ - $\dot{\varepsilon}_s$ plots such as Figures 3.1 to 3.6 (Garofalo, 1965; Zener and Hollomon, 1944). A thermally activated process controlling the creep rate implies that:

$$\dot{\varepsilon}_s = A' \sigma^n \exp\left(-\frac{Q}{RT}\right) \qquad (3.2)$$

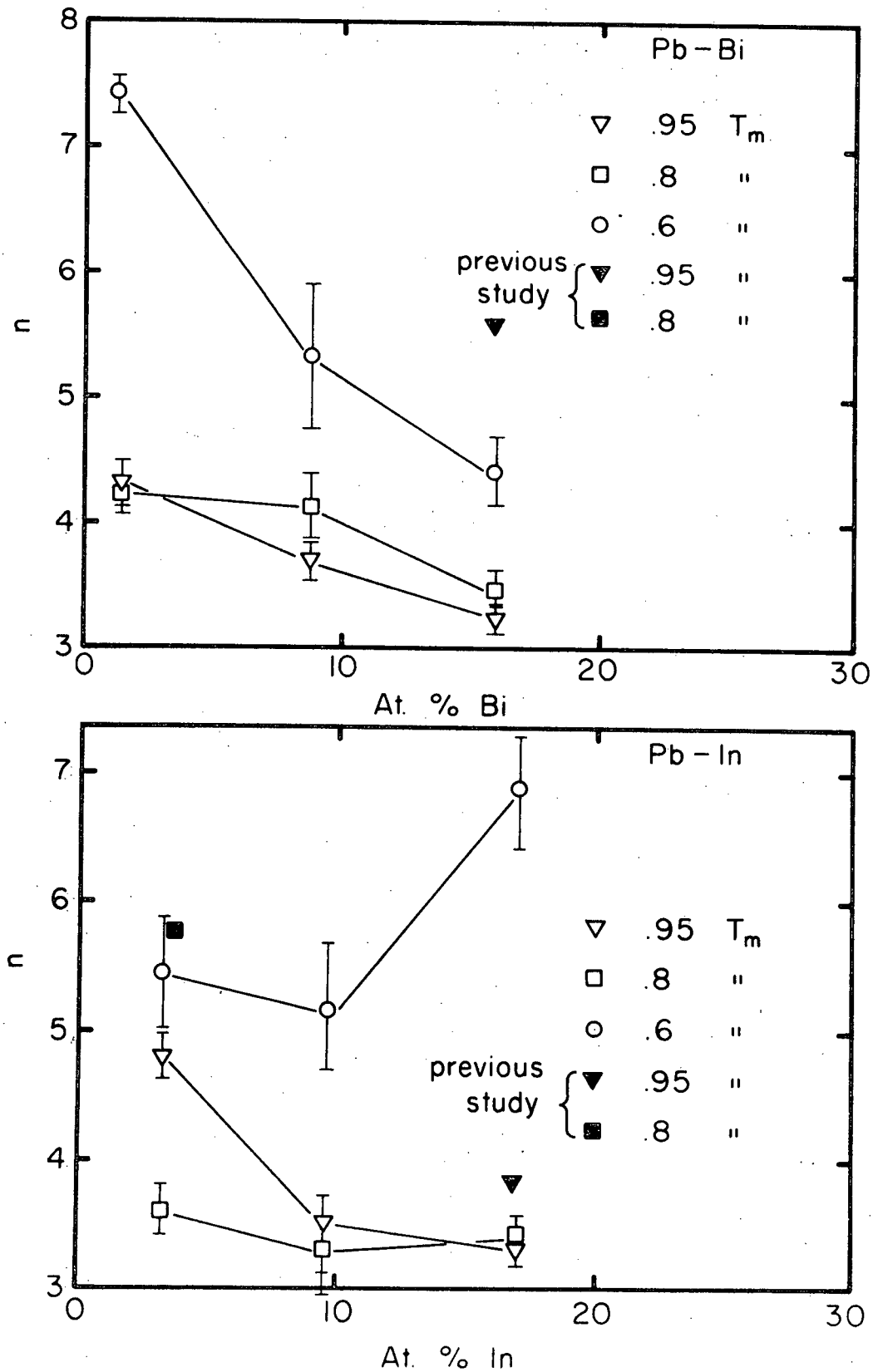

Figure 3.8. Steady state stress exponents versus solute content.

where Q is an apparent activation energy. In general all three parameters, A', n and Q could be functions of stress, temperature and/or structure (prior strain). To calculate a 'true' activation energy from $\sigma - \dot{\varepsilon}_s$ data by using equation (3.2) requires that:

1) The stress, structure and temperature dependent terms in A' are accounted for.

2) Q and n are constant over the stress and temperature ranges used.

Three equations that purport to represent these terms for A' have been considered. The first, a semi-empirical equation, supposedly correlates creep results from a number of different metals (Mukherjee, Bird and Dorn, 1969):

$$\dot{\varepsilon}_s \frac{T}{G} \exp \frac{Q}{RT} = A'' \left(\frac{\sigma}{G}\right)^n \qquad (3.3)$$

where Q and n are now 'true' estimates of activation energy and stress exponent, G is the shear modulus and A" is now stress and temperature independent.

Two other equations are based on Weertman's theoretical formulations for climb and glide controlled creep respectively:

$$\dot{\varepsilon}_s \; T \exp\left(\frac{Q}{RT}\right) G^{3.5} = A''' \; \sigma^n \qquad (3.4)$$

and

$$\dot{\varepsilon}_s \; \frac{1}{T} \exp\left(\frac{Q}{RT}\right) G^{4} = A'''' \; \sigma^n \qquad (3.5)$$

In the following analysis all three equations plus (3.2) are analyzed to determine which is the best representation of the data.

The second assumption of the stress and temperature independence of n and Q is not consistent with the present data. The stress exponents did vary widely with temperature (see Figure 3.7). Determination of apparent activation energies at three stress levels (Figure 3.10) using equation (3.2) also revealed some dependence of Q on stress. It was therefore necessary to use *average* values for both Q and n($\overline{Q}$, $\bar{n}$). A special double averaging technique (Matlock and Nix, 1974) using the original σ, $\dot{\varepsilon}_s$ data points and n values was employed to compute simultaneously both $\overline{Q}$ and $\bar{n}$.

The process is illustrated schematically in Figure 3.9 (for equation 3.2). First values of $\dot{\varepsilon}_s$ were taken from Figures 3.1 to 3.6 at three stresses (1.38, 2.78 and 5.52 MPa) extrapolating if necessary using the fitted curves at .95, .8 and .6 T_m. Since only limited data were determined for

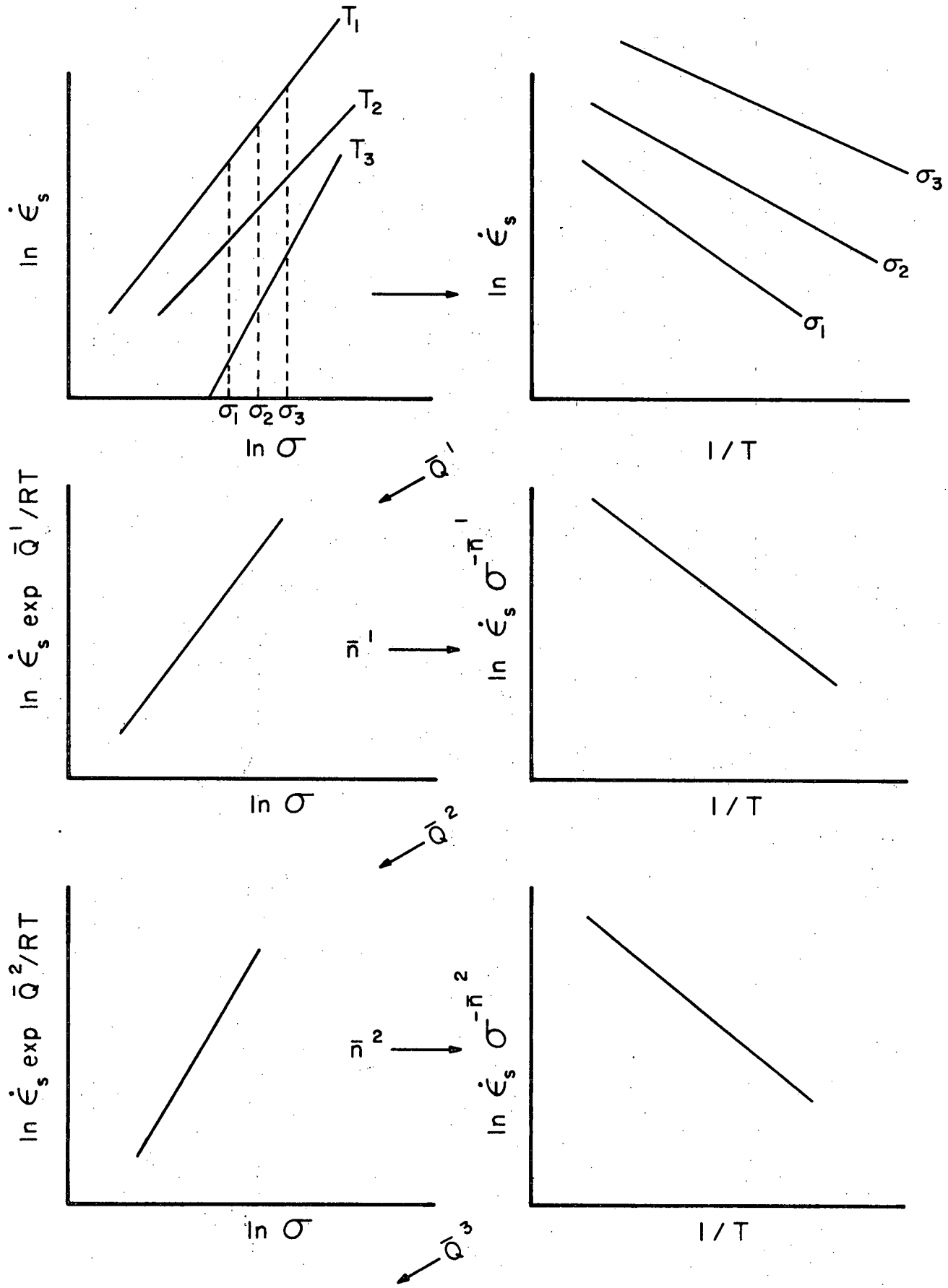

Figure 3.9. Schematic illustration of averaging procedure for activation energy and stress exponents.

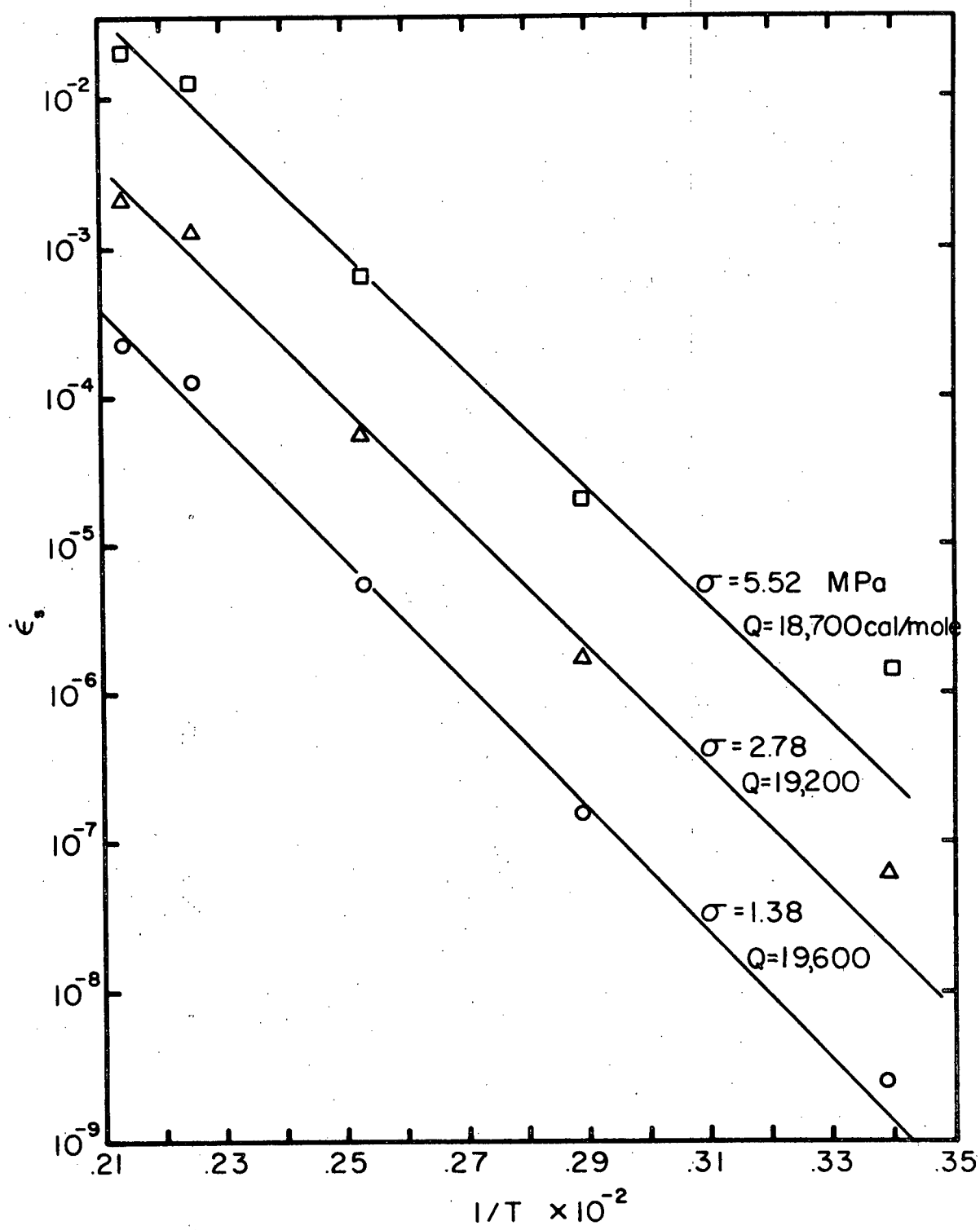

Figure 3.10. Arrhenius plot for 16% Bi alloy at various stresses.

.9 and .7 T_m, σ - $\dot{\varepsilon}_s$ curves were drawn through the available points using n values for the closest available temperature, i.e. for .9 T_m the stress exponent for .95 T_m was used. Standard Arrhenius plots ($\ln \dot{\varepsilon}_s$ vs. 1/T) were then produced for values of Q at each stress (Figure 3.10). A simple average from these three stresses gave an initial estimate of $\bar{Q}^1$. If each σ - $\dot{\varepsilon}_s$ data point is multiplied by $\exp \bar{Q}/RT$, points from all temperatures can be represented by one curve in a $\ln \dot{\varepsilon}_s$ vs. $\ln \sigma$ plot. The slope of this curve gave an initial average stress exponent $\bar{n}'$. This $\bar{n}'$ was applied in a $\ln \dot{\varepsilon}_s \sigma^{-\bar{n}}$ versus 1/T plot which produced a better estimate of the activation energy, $\bar{Q}^2$. Now $\bar{Q}^2$ could be used for a better value of $\bar{n}$. This procedure was continued for three or four iterations until the values of $\bar{n}$ and $\bar{Q}$ were invariant.

All calculations were done by computer with curves fitted by least squares analysis. Since the sum of squares parameter decreased during the iterative procedure indicating a progressively better fit, the final values of $\bar{n}$ and $\bar{Q}$ were the best possible averages for the data.

All four equations (3.2, 3.3, 3.4 and 3.5) were employed with the averaging technique. The temperature dependence of the shear modulus for pure Pb (Cardinal and Hart, 1968) was used in those equations containing G. The criterion for determining the best equation was the fit in the final $\ln \dot{\varepsilon}_s$ - $\ln \sigma$ plot (Figure 3.11). The normalized

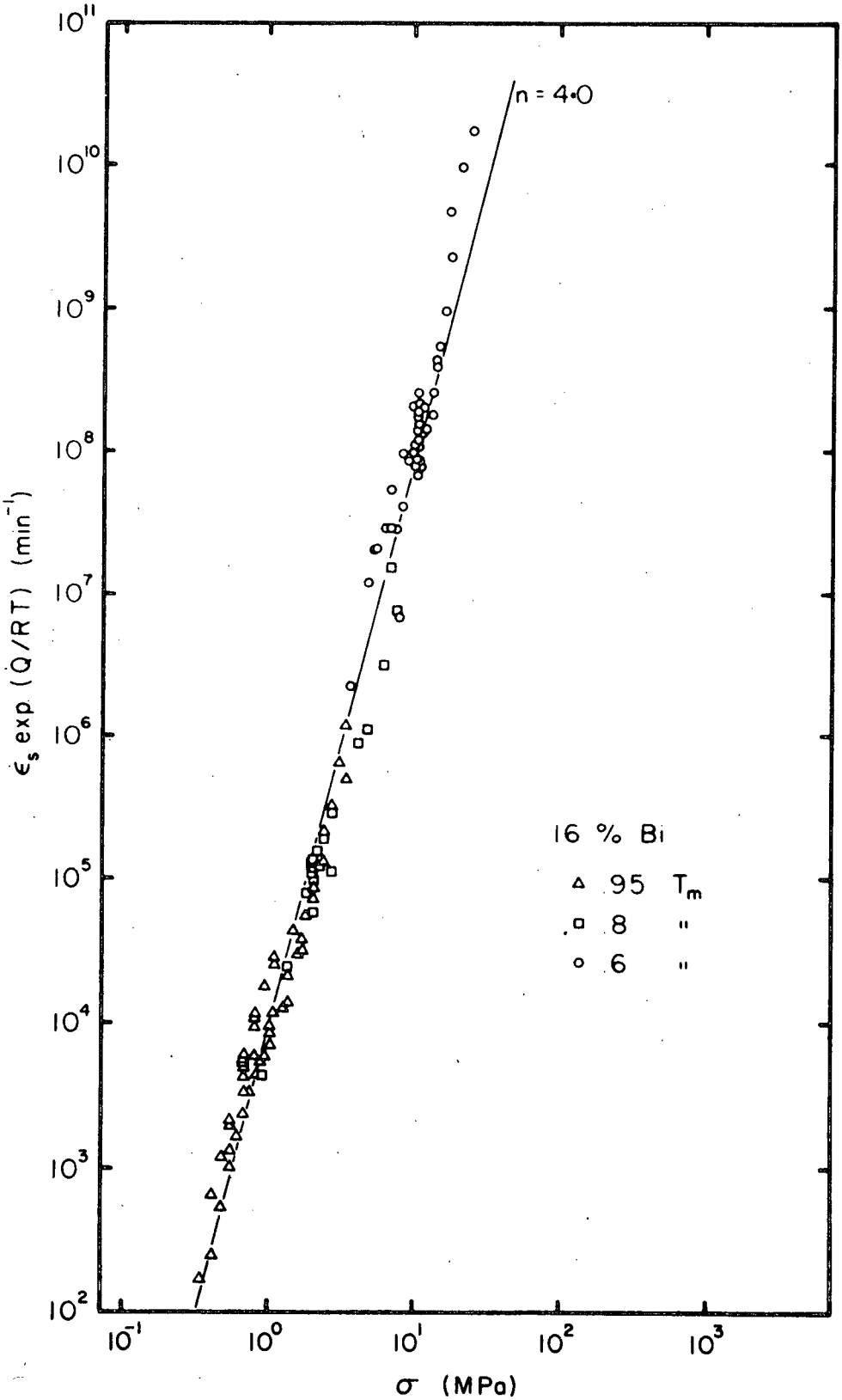

Figure 3.11. Final compensated strain rate versus stress using 'true' activation energy for 16% Bi alloy.

sum of squares parameter which is equivalent to the ratio; total error of estimate/statistical error of estimate (Rose, 1953) determined the best fit. Because of the high values of n at .6 T_m (Figure 3.7) two temperature ranges were studied: 1) $.6 \leq T \geq .95\ T_m$ and 2) $.7 \leq T \geq .95\ T_m$.

The semi-empirical equation (3.3) and the Weertman climb equation (3.4) produced very similar sum of squares values for all alloys. Equation (3.4) was a slightly better fit particularly for the wider temperature range. This equation thus gave the best estimates of the 'true' activation energy (Table 3.1). Standard deviations (56% confidence limits) were calculated from the total errors of estimate to the final $\ln \dot{\varepsilon}_s - \ln \sigma$ plot.

Some differences in $\bar{Q}$, $\bar{n}$ and the sum of squares are apparent between the two temperature ranges. The high temperature range (.7 to .95 T_m) gave the best fit, however. In this range the effect of increasing the solute content was to decrease the activation energy in both systems. The activation energies were always higher in the Pb-In system than the Pb-Bi system at equivalent solute contents. The value of the creep activation energy extrapolated to 0% Bi is close to the activation energy for pure Pb self diffusion.

Table 3.1

"True" Average Activation Energy, $\bar{Q}$, and Stress Exponent, $\bar{n}$ values using Weertman's Climb Controlled Equation Temperature Range .6 to .95 T_m

Alloy	$\bar{Q}$ cal/gm-mole	$\bar{n}$	Normalized Sum of Squares $\bar{Q}$
16.2 Bi	16,100 ± 500	3.82 ± .05	.20
8.8 Bi	19,100 ± 600	4.11 ± .11	.24
1.3 Bi	22,500 ± 1300	4.89 ± .88	.88
17.0 In	27,000 ± 1400	4.72 ± .08	1.43
9.5 In	21,500 ± 1000	3.90 ± .12	.43
3.2 In	18,000 ± 1600	4.61 ± .15	1.17
Temperature Range .7 to .95 T_m			
16.2 Bi	17,400 ± 500	3.33 ± .07	.08
8.8 Bi	19,700 ± 1600	3.66 ± .11	.12
1.3 Bi	23,500 ± 2400	3.96 ± .11	.25
17.0 In	23,500 ± 600	3.38 ± .06	.24
9.5 In	26,100 ± 4200	3.31 ± .10	.008
3.2 In	30,000 ± 2800	4.74 ± .17	.32

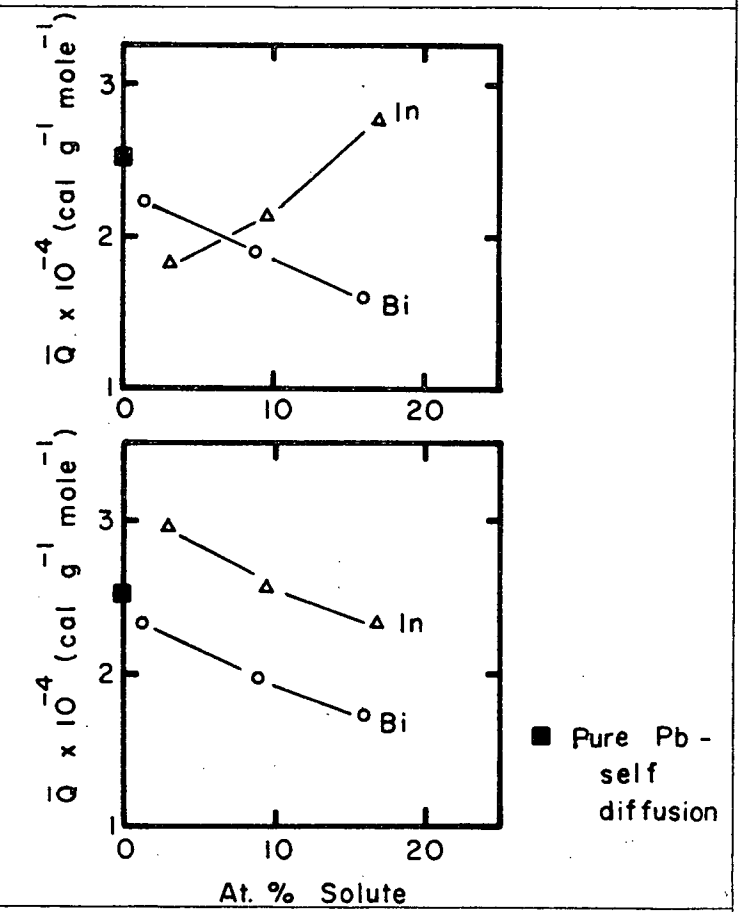

Strengthening Effects

Temperature. Information about the strengthening effects of alloying additions can be obtained from Figures 3.1 to 3.6 by determining the creep stress required to produce a constant steady state strain rate (4×10^{-5} min^{-1}) in each of the alloys. Data were obtained at the intermediate temperatures using n values of the nearest principle temperature.

The creep stress to produce this strain rate decreased markedly as the creep temperature increased (Figure 3.12) in both alloy systems. The hardening effects of both alloying elements were appreciable only at the lower temperatures ($\leq .6\ T_m$).

Solute Content. At high temperatures the effect of solute additions was evaluated by determining the σ at constant strain rate and temperature (Figure 3.13). The chosen temperature (200°C) was in the range .8 to .95 T_m for all the alloys. In the Pb-In system only the 3.2% In alloy was harder than the pure Pb. Increased In additions then produced a weaker material. All concentrations of Bi softened the Pb matrix but the 8.8% alloy was slightly more resistant to creep than either the 1.3 or 16% alloy.

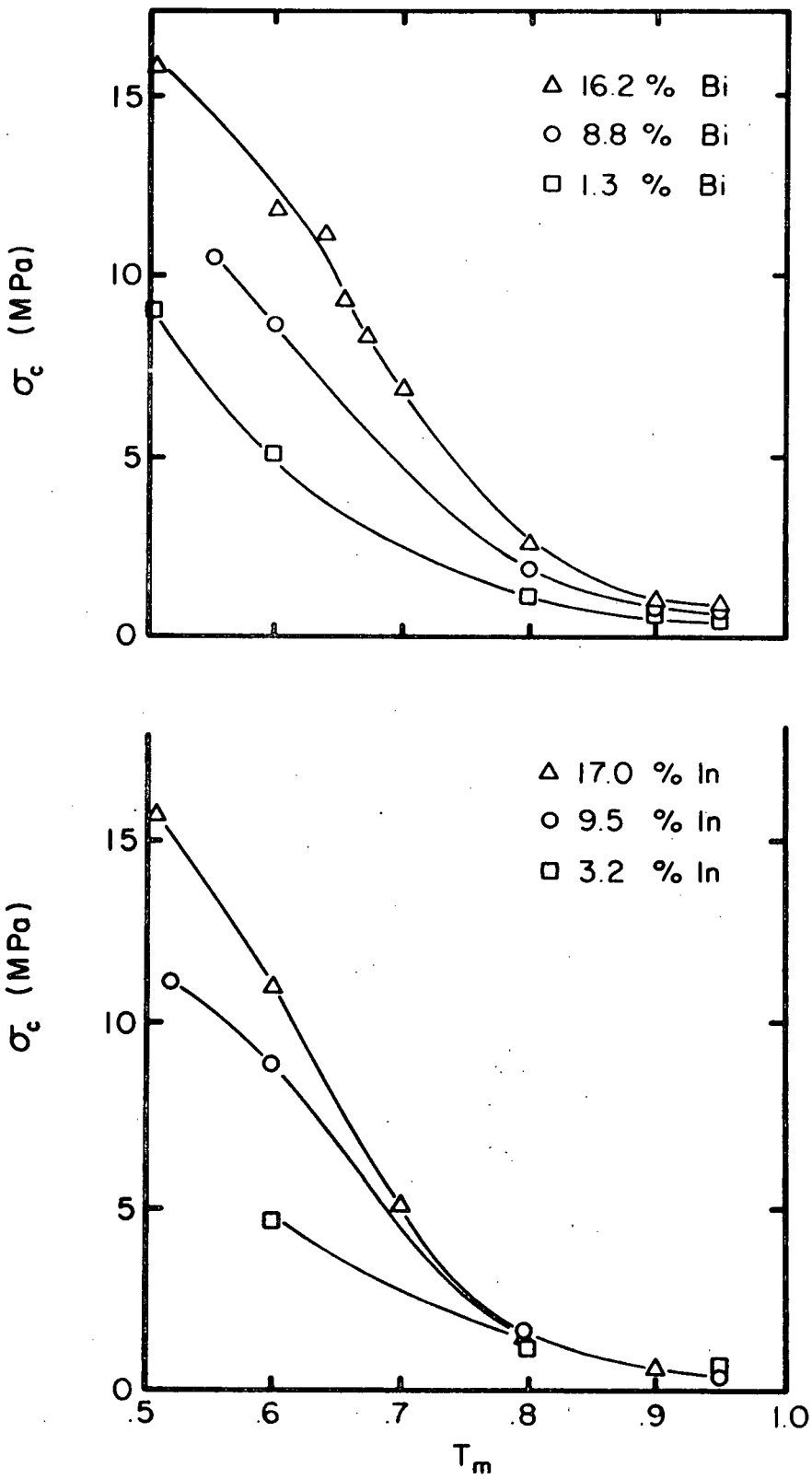

Figure 3.12. Creep stress at $\dot{\varepsilon}_s = 4 \times 10^{-5}$ min^{-1} versus relative temperature for all alloys.

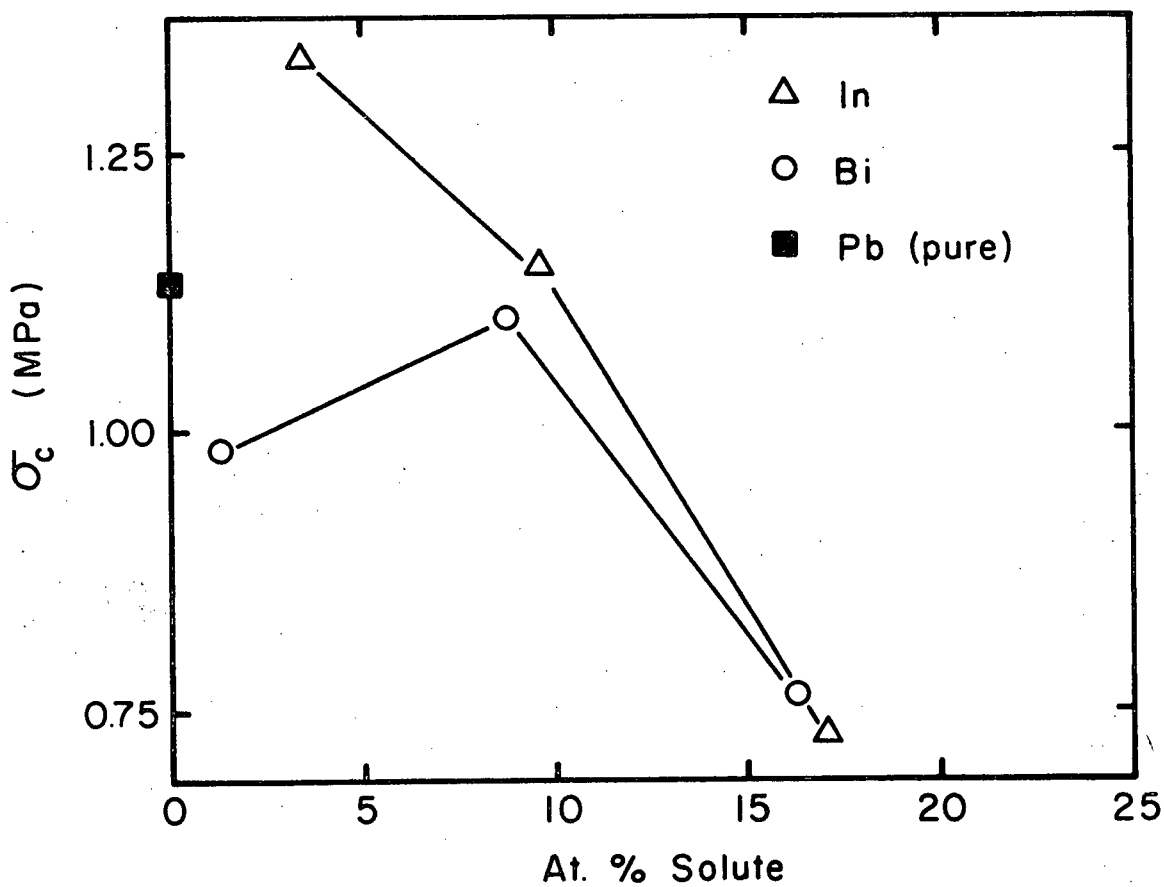

Figure 3.13. Creep stress at $\dot{\varepsilon}_s = 4 \times 10^{-5}$ min^{-1} and 200°C versus solute content for both systems.

DISCUSSION

The preceding results will be discussed under the subdivisions of stress exponent, activation energy and strengthening effects but with the application of only the simple creep theories. The utility of the simple theories is their ability to deal adequately with the steady state.

Stress Exponents

Two attempts have been made to delineate which material parameters and external variables are important in determining whether glide or recovery are rate controlling (Cannon and Sherby, 1970; Mohamed and Langdon, 1974). The following discussion will concentrate on the more detailed treatment of Mohamed and Langdon.

When glide is rate controlling the steady state creep rate was represented by:

$$\dot{\varepsilon}_g = \frac{\pi(1-\nu)\ kT\ D_s}{6\ e^2\ cb^5\ G} \left(\frac{\sigma}{G}\right)^3 \qquad (3.6)$$

where D_s is the diffusivity of the solute atom, e is the linear size factor (a measure of the solute-solvent size difference), and c is the solute concentration. This equation represents the Weertman glide model with the interaction between solute atmospheres and the moving dislocations

governing the viscous glide movement (Cottrell and Jaswon, 1949).

For the creep rate when recovery is rate controlling, Mohamed and Langdon used the semi-empirical equation (Bird, Mukherjee and Dorn, 1969):

$$\dot{\varepsilon}_c = A_0 \left(\frac{\gamma}{Gb}\right)^3 \frac{\overline{D}\, Gb}{kT} \left(\frac{\sigma}{G}\right)^5 \qquad (3.7)$$

where γ is the stacking fault energy, A_0 is a constant and $\overline{D}$ is the Herring-Weertman weighted diffusion coefficient. This equation is similar to Weertman's climb equation except for the stacking fault energy factor. Climb is considered to be the recovery mechanism.

Since the glide-climb processes are sequential, the slower of the two will always be rate controlling; for example, when $\dot{\varepsilon}_c < \dot{\varepsilon}_g$, climb controls the deformation rate.

A transition in controlling mechanism can occur when the two rates are equal:

$$\dot{\varepsilon}_g = \dot{\varepsilon}_c$$

or upon substitution,

$$\frac{\pi(1-\nu)\, kT\, D_s}{6\, e^2\, cb^5\, G} \left(\frac{\sigma}{G}\right)^3 = A_0 \left(\frac{\gamma}{Gb}\right)^3 \frac{\overline{D}\, Gb}{kT} \left(\frac{\sigma}{G}\right)^5$$

or

$$\frac{T^2}{e^2\ cb^6} = \frac{1.9A_0}{k^2(1-\nu)} \cdot \frac{\bar{D}}{D_s} \cdot \sigma^2\left(\frac{\gamma}{Gb}\right)^3 \qquad (3.8)$$

Thus a plot of $T^2/e^2\ cb^6$ versus $\sigma^2(\gamma/Gb)^3$ will define a map (Figure 3.14) which can be used to predict the type of mechanism that will be rate controlling. (For lack of data $\bar{D}/D_s$ is usually taken as 1. Determination of A_0 will be described below.)

In the area to the right of the transition line $\frac{T^2}{e^2\ cb^6} < \sigma^2\left(\frac{\gamma}{Gb}\right)^3$, which means that $\dot{\varepsilon}_g < \dot{\varepsilon}_c$ and glide should be rate controlling. Similarily, to the left of the transition line the recovery process climb, will control. With a given alloy and temperature, as the creep stress is increased from point A to point B (Figure 3.14) the transition boundary will be crossed, and the rate controlling mechanism will shift from recovery to glide. This transition with stress will be manifested experimentally by a stress exponent decrease from 5 to 3 (Figure 3.15). Thus any alloy that shows such a decrease in stress exponent with increasing stress provides support for this simple sequential model.

Mohamed and Langdon attempt to show that several alloys do display such a transition, namely Al-Mg, Pb-Sn, Pb-Cd and Pb-In. Data from a previous study (Weertman, 1960) were used for one demonstration (Figure 3.16). Further support for the theory would be provided by a correspondence

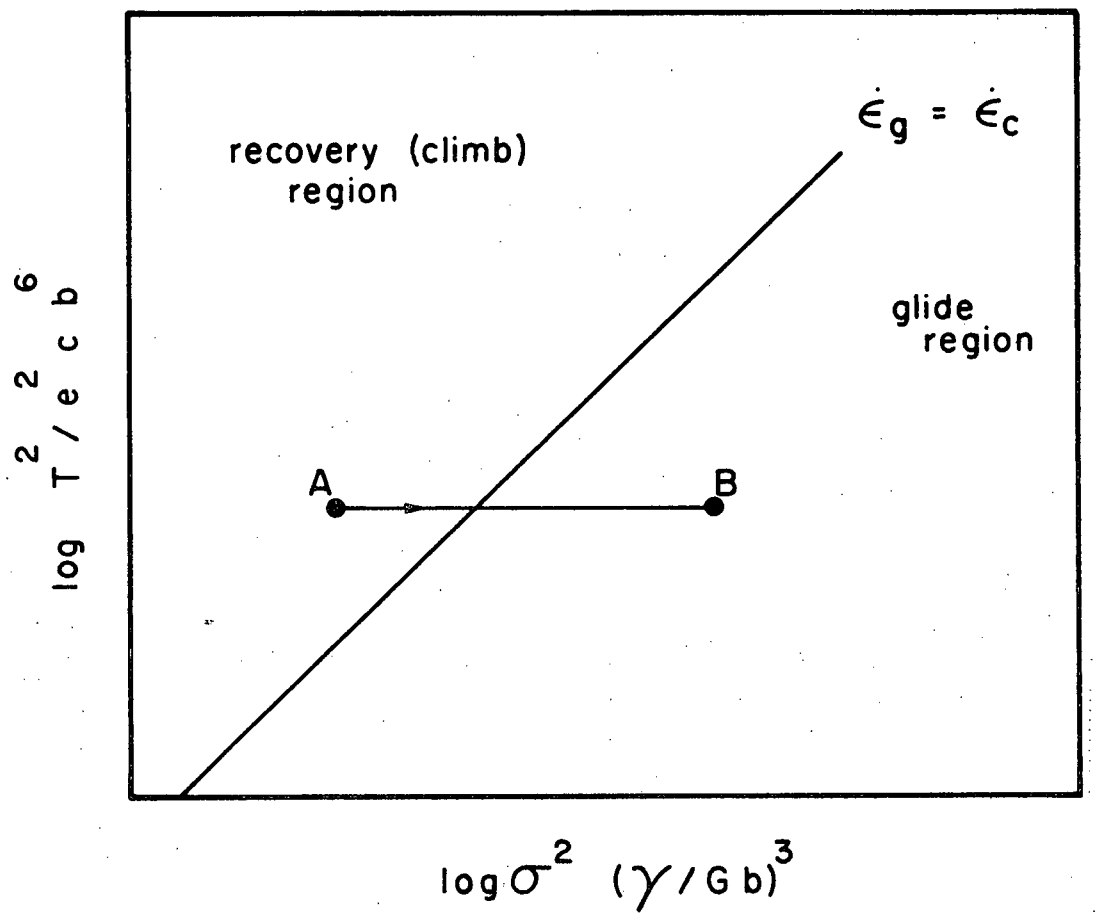

Figure 3.14. Criterion for the climb to glide transition (after Mohamed and Langdon, 1970).

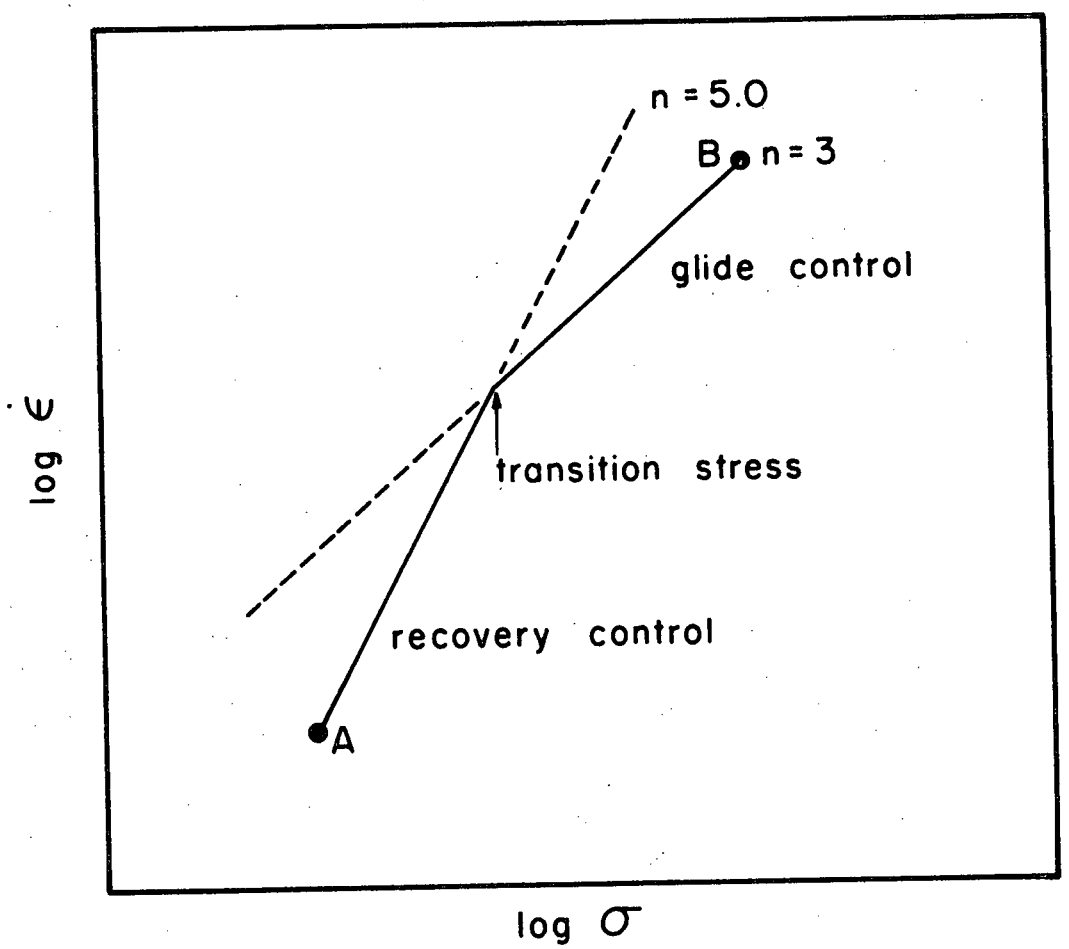

Figure 3.15. Change in stress exponent for the climb to glide transition.

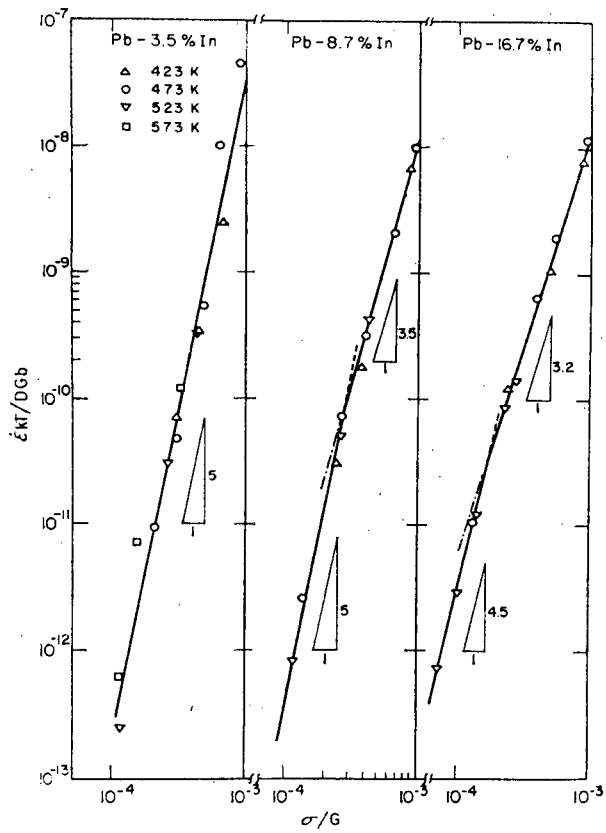

Figure 3.16. Normalized strain rate versus normalized stress for Pb-In alloys (Weertman, 1960) (after Mohamed and Langdon, 1970).

between the experimental stress where the exponent changes and the transition boundary of Figure 3.14. Unfortunately the position of the transition line depends upon one parameter that cannot be obtained independently, A_0. Therefore A_0 was chosen such that the experimental transition stress for Al-3% Mg (Linga Murty, Mohamed and Dorn, 1972) coincided with the boundary. The transition stress for other alloys could be predicted from Figure 3.17. For Pb-Bi alloys the theoretical prediction was that all alloys should be in the recovery region with no transition to glide control. This prediction was in agreement with the results of a previous study (Weertman, 1960) in which the stress exponent was 4.5 with no transition.

Transitions were predicted for the Pb-In. The predicted transition stress was higher than the experimental value if the γ value for pure Pb (37 ergs/cm^2) was used to compute the position of the stress ranges (for example 16.7% In in Figure 3.17). If the stacking fault energy was arbitrarily increased (to 65 ergs/cm^2 for 16.7% In) coincidence was obtained. Thus some flexibility of stacking fault energy values is required for the model to correctly predict the observed behaviour of the previously studied Pb-In alloys.

When the present results are plotted in a similar fashion to Figure 3.16, good is agreement is obtained in terms of absolute values of the creep rates. However, when the

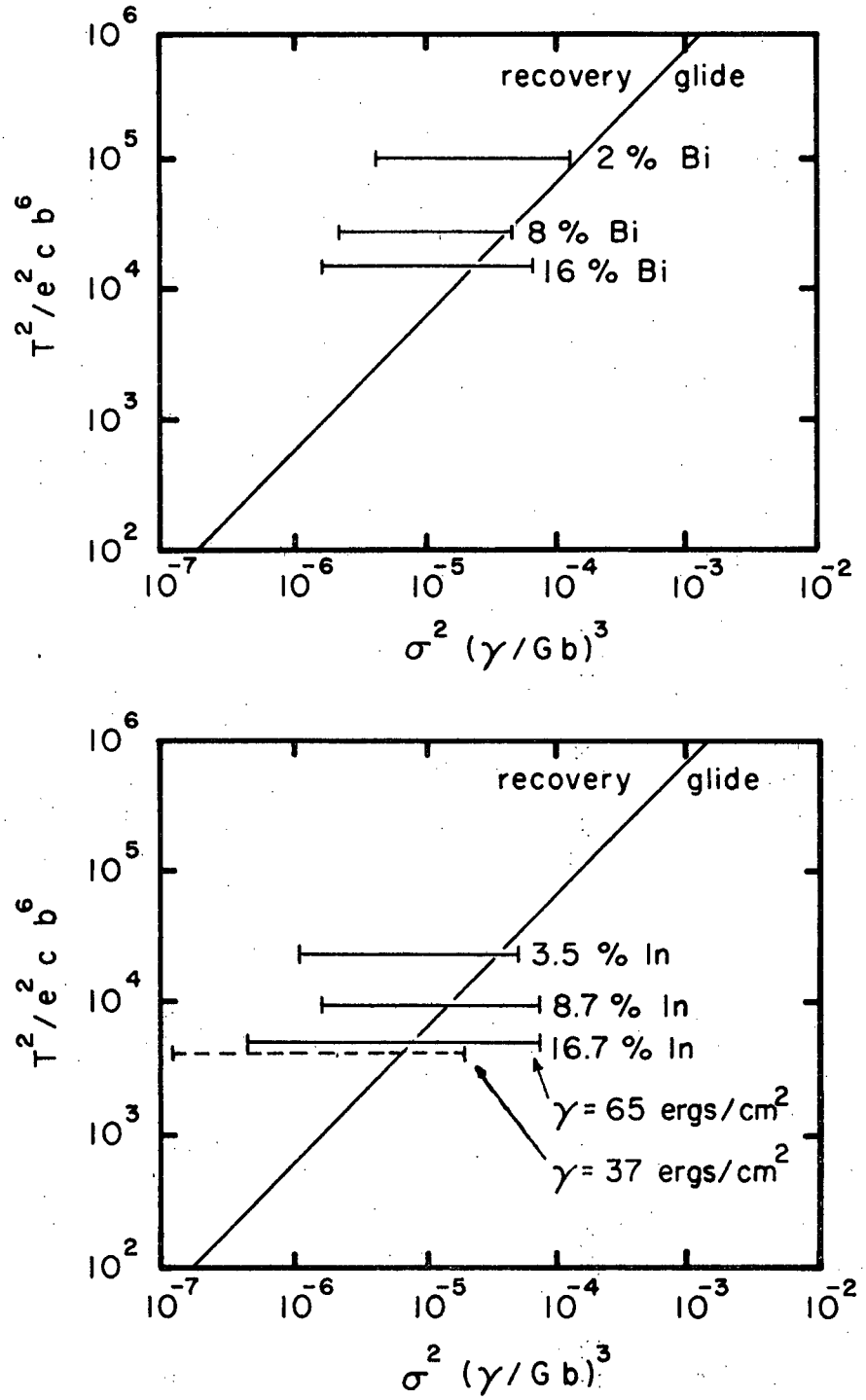

Figure 3.17. Theoretical predictions for the climb to glide transition for previous study (Weertman, 1960) on Pb-Bi and Pb-In alloys.

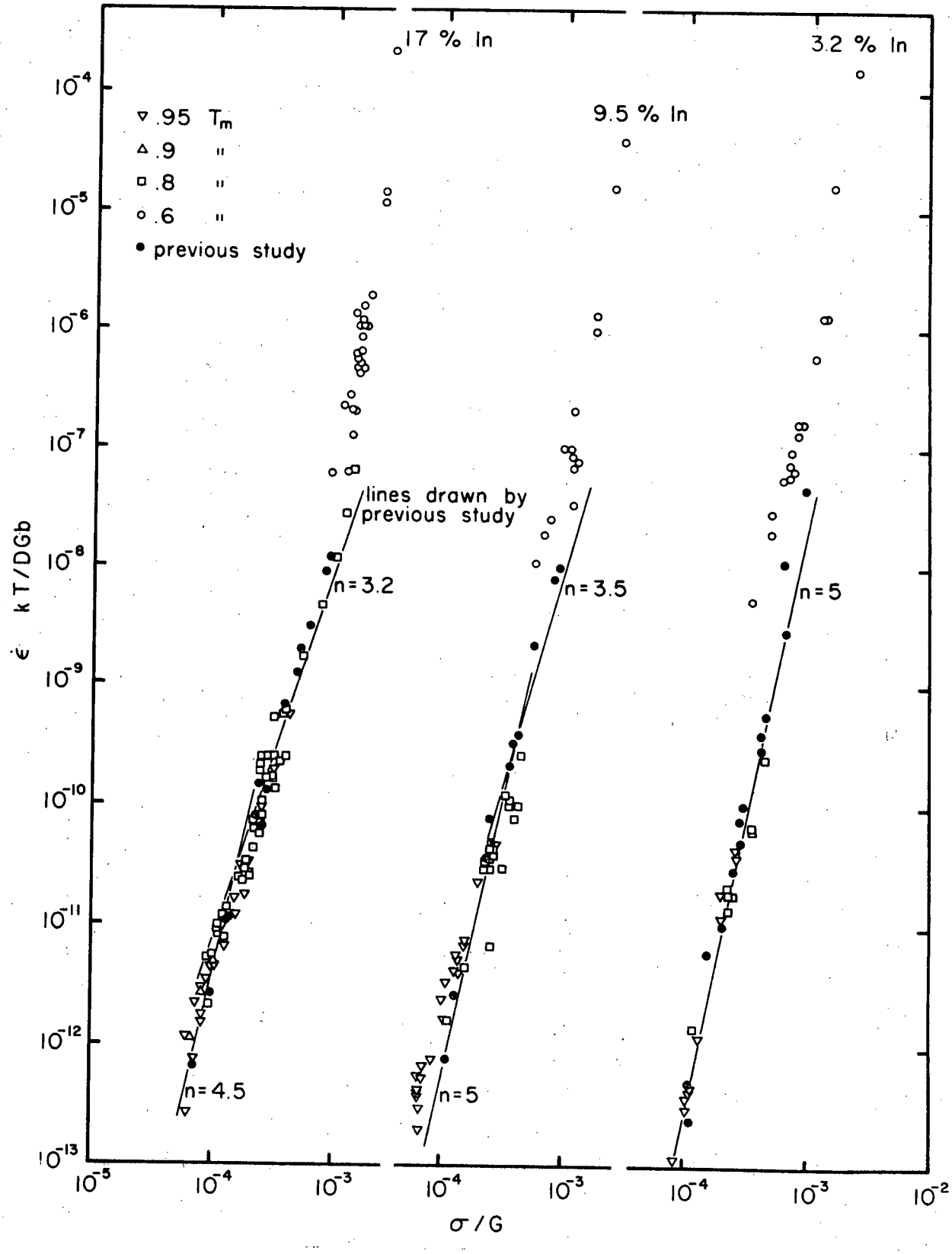

Figure 3.18. Normalized strain rate versus normalized stress for present study of Pb-In alloys.

curves drawn by Mohamed and Langdon are placed on these plots, they fall within the scatter band. A transition from recovery to glide control is therefore not established (Figure 3.18).

For the 17% In alloy an exponent of 3 at low $\frac{\sigma}{G}$ and higher values at increased stress are more appropriate. However, the slope (stress exponent value) in these kinds of plots depends upon the values of D since they influence the shift of different temperature points. By contrast, the individual n values at each temperature (Figure 3.7) are independent of diffusivity.

For comparison with the Mohamed-Langdon model, stress exponents at 200°C were taken from Figure 3.7 interpolating if necessary (Table 3.2). For the 17% In alloy the low value of 3.3 for n and the lack of a transition point indicate that glide is rate controlling in the stress range studied. Thus the alloy must lie totally in the glide region rather than across the transition boundary. Similarly the 9.5% In and 16% Bi alloy must be glide controlled. The 8.8 and 1.3% Bi can possibly be considered recovery controlled since their n values are closer to 4.5. The 3.2% In is indicated as also glide controlled at 200°C. However, a slight increase in temperature to 286°C produces an apparent transition to climb control since n equals 4.8 (see Figure 3.7). The alloy probably does undergo a transition from climb to glide in this stress and temperature range.

Table 3.2

Stress Exponents for Present Study at 200°C. Data Obtained From Figure 3.7 Interpolating if Necessary

Alloy	n at 200°C	Suggested Mechanism
16 Bi	3.25	Glide
8.8 Bi	3.9	Climb
1.3 Bi	4.2	Climb
17 In	3.3	Glide
9.5 In	3.3	Glide
3.2 In	3.6	Glide[1]

[1]Possible transition to Climb (see text)

Thus the present stress exponent values require, for the In alloys and the 16% Bi alloy, further adjustments in stacking fault energy to reposition their stress ranges with respect to the transition boundary (Figure 3.19). For the 16% Bi and 17% In alloys, stacking fault energies of the order of $\simeq$ 100 ergs/cm^2 are required as compared to 37 ergs/cm^2 for pure Pb. Lack of stacking fault energy data in these systems makes it difficult to assess the validity of these increases with alloy content.

One study (Bolling, Massalski and McHague, 1961) reported large decreases in stacking fault probabilities in Pb - 20% In as opposed to pure Pb indicating that γ increases with In content. This increase in γ was connected with a decreased electron to atom ratio. Bi additions, on the other hand, increase the electron concentration, therefore γ should decrease with Bi content. Thus the required increase in γ for 37 to $\simeq$ 100 ergs/cm^2 for the 16% Bi alloy seems unrealistic. If the stress exponent is to be the only criterion for determination of the rate controlling mechanism, then the present results with 16% Bi are not compatiable with the Mohamed-Langdon correlation or the simple models of creep.

Activation Energy

In the equations for the two rate controlling mechanisms:

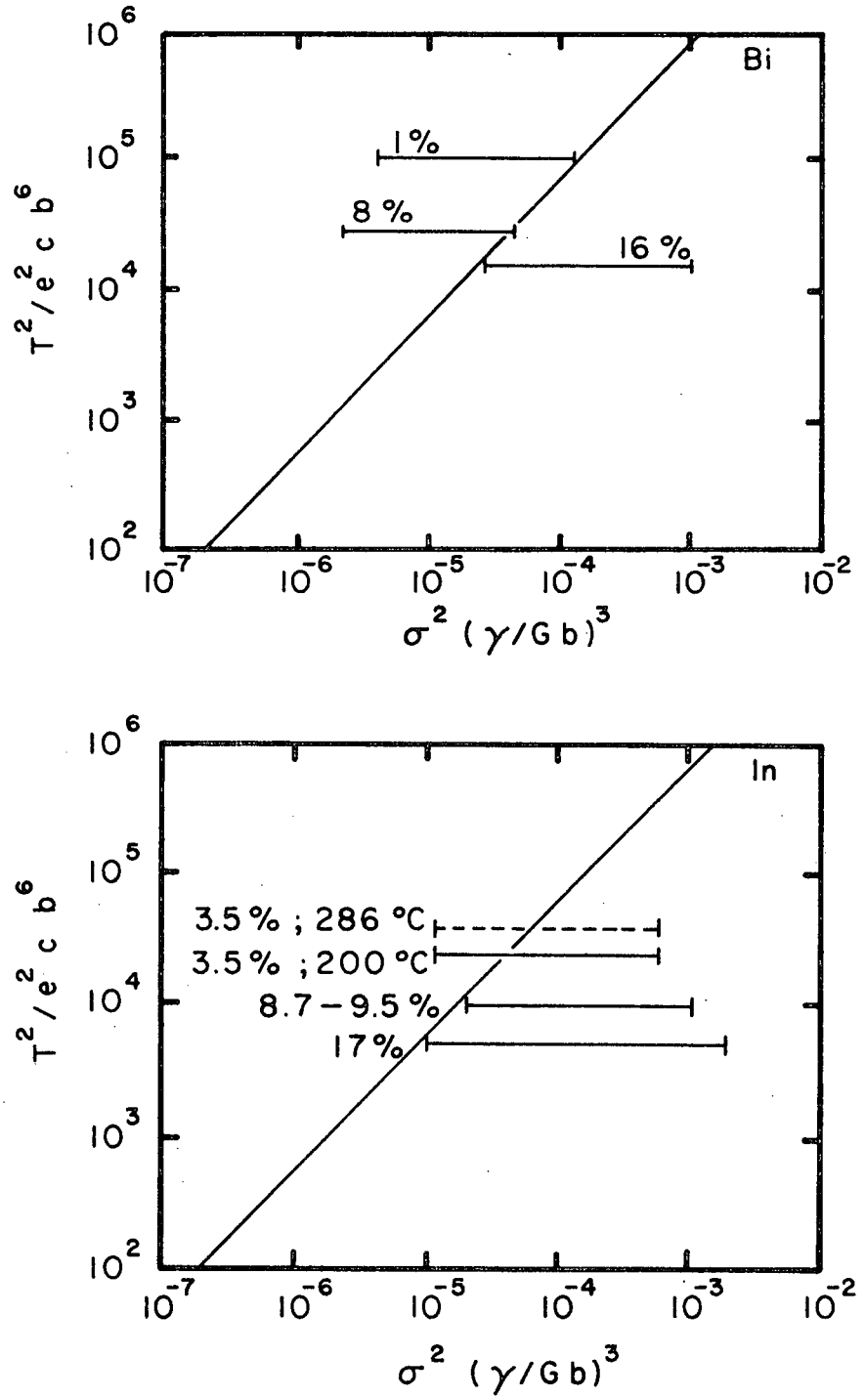

Figure 3.19. Theoretical predictions for the climb to glide transition for the present study on Pb-Bi and Pb-In alloys.

$$\dot{\varepsilon}_g = \frac{\pi(1-\nu)\ kT\ D_s}{6\ e^2\ cb^5\ G}\left(\frac{\sigma}{G}\right)^3$$

and

$$\dot{\varepsilon}_c = A'\left(\frac{\gamma}{Gb}\right)\ \frac{\bar{D}\ Gb}{kT}\left(\frac{\sigma}{G}\right)^5$$

the effects of thermal activation enter through the diffusivity of the solute D_s and the Herring-Weertman self diffusivity $\bar{D}$. Since diffusion coefficients are thermally activated, they can be represented by:

$$D = D_0 \exp - \frac{Q_D}{kT}$$

If the strain rate equations truly represent the creep process, the measured creep activation energies should be equal to the appropriate diffusion activation energies.

The general lack of diffusion data for alloys and the difficulties of determining a 'true' activation energy (see page 39) has made definitive comparison difficult. In one "recovery-controlled" system (Johnson, Barrett and Nix, 1972), Q for creep correlated with the Herring-Weertman activation energy. In only one glide controlled system (Sellars and Quarrel, 1962), could Q for creep be identified with Q for solute diffusion of one component. All other solid solution creep studies would not relate creep energies to diffusion energies.

Since there are few diffusion data for Pb-Bi or Pb-In systems, meaningful comparisons between the measured trends of $\overline{Q}$ and diffusion energies are not possible (Table 3.3). One measurement (Kureca and Stransky, 1969) of In diffusion in Pb single crystals (less than 5% In) found the impurity activation energy was slightly higher than that for pure Pb self diffusion. Both the past and present studies indicate that the creep energies decrease with additions of both In and Bi. However, the standard deviations in the present results preclude any definite comparisons or conclusions. It is thus not possible to even postulate about rate controlling mechanisms on the basis of activation energy measurements.

Strengthening Effects

Temperature. A strong effect of temperature on the stress to produce a given strain rate was found (Figure 3.12). Equations (3.6) and (3.7) can be rewritten:

$$\sigma^3 = \dot{\varepsilon}_g \left(\frac{G^4}{TD_s}\right) \cdot \frac{6\, e^2\, cb^5}{k\, \pi(1-\nu)} \tag{3.6A}$$

$$\sigma^5 = \dot{\varepsilon}_c \left(\frac{G^7 T}{\overline{D}}\right) \cdot \frac{k\, b^2}{A_0 \gamma^3} \tag{3.7A}$$

Table 3.3

Comparison of Activation Energies for Creep and Diffusion

Material	Activation Energies cal/mole		
	Diffusion	Creep Past Studies	Creep Present Study
Pure Pb	25,500[1]	26,400[2]	—
		26,000[3]	
Pb-In	26,800[4]	25,000[5]	30,000 ± 2800-3.2%
			26,100 ± 4200-9.5%
			23,500 ± 600-17%
Pb-Bi	—	22,000[5]	23,500 ± 2400-1.3%
			19,700 ± 1600-8.8%
			17,400 ± 500-16%

1 - Millar, 1969

2 - Feltham, 1956

3 - Wiseman, Sherby, and Dorn, 1957

4 - Kucera and Stransky, 1969 (Up to 5% In)

5 - Weertman, 1960 (Independent of composition)

with the strongly temperature dependent factors bracketed. Thus a decrease of stress with temperature must be due to decreases in shear modulus and/or increases in diffusivity. Both theories are capable of predicting the general trends in σ but discrimination between the two theories is not possible.

Solute Content

The most common consequence of solute additions is an increase in the creep strength (Monma Sato and Oikawa, 1964; Davies, Davies and Wilshie, 1965; Linga-Murty, Mohamed and Dorn, 1972). However, some metals can be softened by alloy additions at high temperatures (Monma, Sato and Oikawa, 1964B; Sellars and Quarrel, 1961).

A possible explanation for this anomalous behaviour is apparent from equations (3.6A) and (3.7A). For the glide controlled case increasing solute concentration will increase the creep stress. In the climb case, the usual hardening mechanism is the decrease in stacking fault energy with solute additions. However, simultaneous increases in D_s or $\overline{D}$ or decreases in shear modulus by the alloy additions could offset this increase producing a net softening.

Again the lack of data in the Pb-Bi, and Pb-In systems preclude any assessment of the theories.

SUMMARY

In this chapter the steady state region of the creep curve for all alloys was examined and the results evaluated in terms of the simple glide and climb theories. Comparison with past work on the alloys was done whenever possible. The following conclusions may be drawn:

1. On the basis of the steady state stress exponent, the present study has confirmed the previous categorization of Pb-In alloys as Class I — glide controlled and the Pb-Bi alloys up to 9% Bi as Class II — recovery controlled. The Pb-16% Bi alloy, however should be reclassified as "Class I" contrary to past results.

2. A transition from glide to recovery control at low stress for the Pb-9.5% In and Pb-17% In alloys, as suggested by Mohamed and Langdon, was not confirmed by this study.

3. These contradictions with previous studies emphasize the danger of using only the stress exponent values to determine the rate controlling mechanisms, particularly when few data are available.

4. Activation energy measurements or 'strengthening' effects of solute addition could not be used to distinguish the rate controlling process.

Despite the doubts raised about the validity of determining rate controlling mechanisms solely on the stress exponents, the classification suggested for the alloys will be adopted for evaluation purposes in subsequent sections.

A summary chart will be used to assist in such evaluation. The 16% Bi alloy has been included in both classes in the chart because the ensuing results will contradict its categorization as glide controlled. The 3.2% In alloy will be treated as a predominately glide alloy despite some evidence of a transition to recovery control.

Table 3.4

Summary Chart

	Theory	Alloys	Stress Exponent	ε_0	Primary Creep	Athermal σ-ε	Δ_σ Transients
CLASS I -GLIDE	Simple Glide	3.2 In	✓				
		9.5 In	✓				
		17 In	✓				
		16 Bi	✓				
	Combined Glide-Recovery	3.2 In					
		9.5 In					
		17 In					
		16 Bi					
CLASS II -RECOVERY	Simple Climb	1.3 Bi	✓				
		8.8 Bi	✓				
		16 Bi	X				
	Rearrange-ment	13. Bi					
		8.8 Bi					
		16 Bi					

Chapter 4

INITIAL TRANSIENT

The initial portion of the creep curve can be divided into two sections: 1) the loading strain produced as the stress is increased from zero to its final value and 2) the primary creep deformation from time = 0 until establishment of a steady state strain rate. The two classes of alloys apparently behave differently in both these regions (Mohamed and Langdon, 1974; Sherby and Burke, 1967; Cannon and Sherby, 1970). Some investigators suggest that the "glide control" Class I alloys exhibit little or no loading strains but the "recovery control" alloys have comparatively large amounts.

Distinctions are also made about:

1) The shape of the strain-time curve in the primary creep region, and

2) The amount of strain or time that occurs before steady state.

Generally Class II "recovery" alloys undergo appreciable amounts of creep with a continually decreasing strain rate

(normal transient) (Figure 4.1A). The "glide control" alloys can have complex shaped curves, either inverted, linear or sigmoidal (Figure 4.1B) but with a rapid establishment of the steady state.

In this chapter, these features of the initial transients will be examined for the present alloys to ascertain if the preceding generalizations are consistent with the glide-recovery classification of Chapter 3. The results will be presented in three subsections: 1) Loading strain, 2) Shape of primary transient and 3) Extent of primary region. The discussion section will apply the simple theories to the results. The inadequacies of the simple theories will necessitate the introduction of the refined theories.

RESULTS

Loading Strain

Loading strain measurements usually exhibit considerable experimental scatter due to a number of factors: 1) the difficulty of determining $t = 0$, the time at full application of the load, 2) differences in loading rates and 3) structure differences in the specimens. Efforts have been made to minimize the first source of error with the loading method described in Chapter 2 (p. 18). The rate of loading was kept constant from test to test. Each specimen was

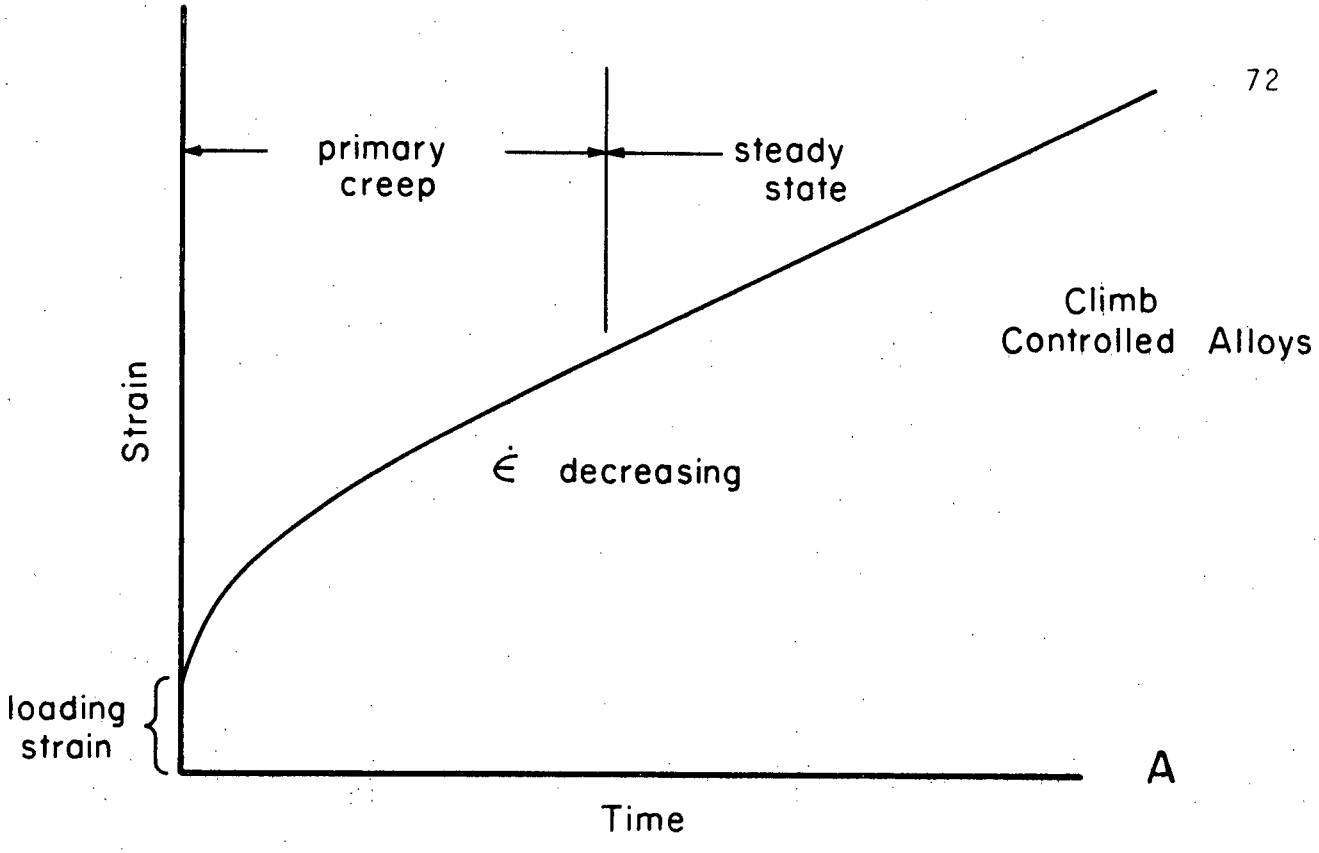

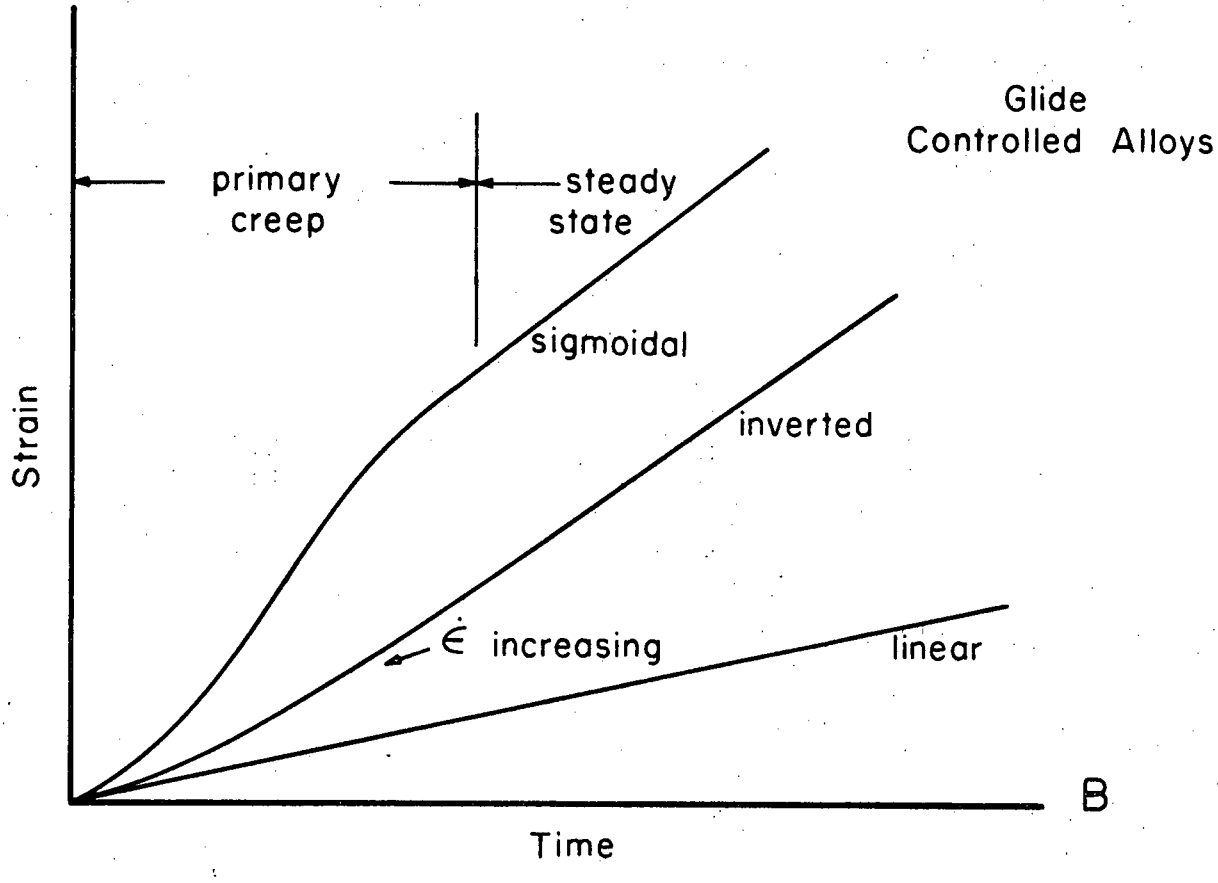

Figure 4.1. Generalized primary creep curves for climb and glide controlled alloys.

annealed immediately prior to testing to reduce the effects of handling damage on specimen structure.

Several measurements (4 to 12) were made at each test condition to enable calculation of an average value and 95% confidence limits. Any points plotted without error bars represent only one or two results. Most comparisons of results were done for tests at a constant steady state strain rate of 4×10^{-5}/min.

Temperature. The two high solute content alloys (16% Bi and 17% In) were both classified as "glide controlled" in the preceding section. The loading strains of both these alloys were identical when compared at the same absolute temperature and steady state strain rate (Figure 4.2). The trend to lower loading strains at the high temperatures may be indicative not of a temperature effect per se but a reflection of a stress effect since the stress for constant strain rate decreases with temperature.

Stress. When these points from several temperatures are plotted versus the creep stress (Figure 4.3) the trend can be represented by one curve. The important variable in determining the loading strain magnitude is therefore the stress rather than the temperature.

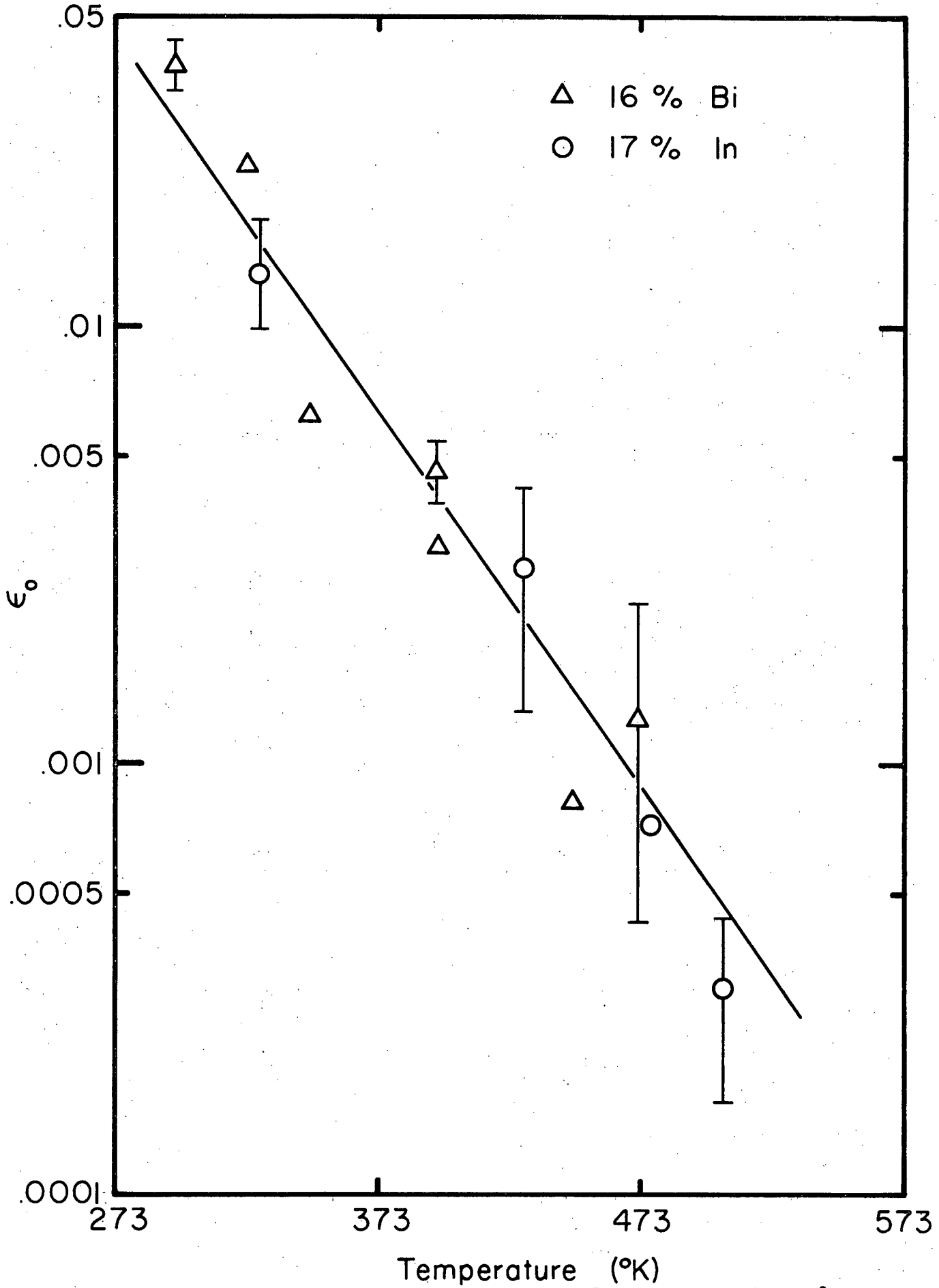

Figure 4.2. Loading strain versus absolute temperature for 16% Bi and 17% In alloys.

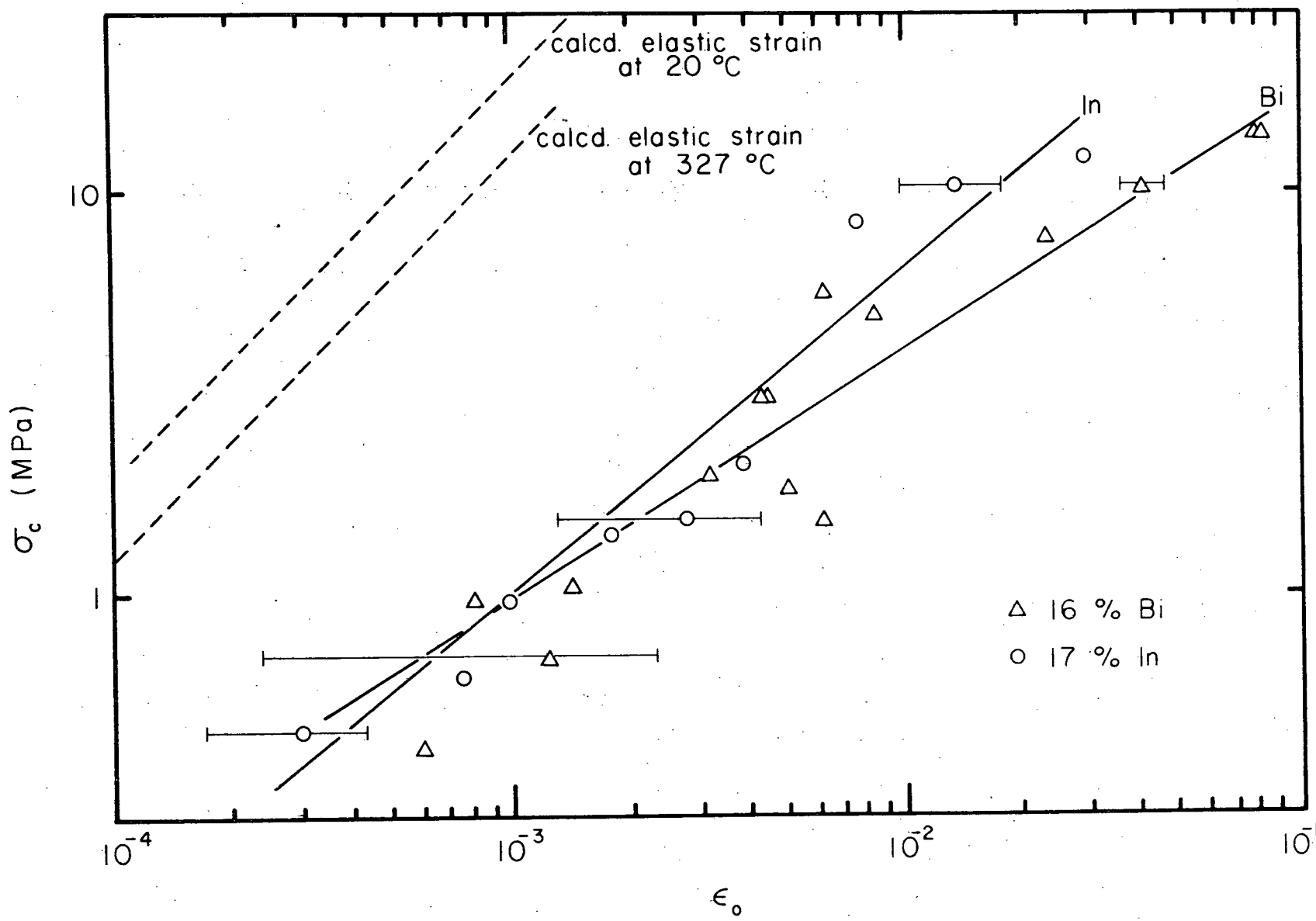

Figure 4.3. Creep stress versus loading strain for 16% Bi and 17% In alloys.

There seems to be little difference between the loading strains for the two alloys at equivalent stresses. The curves in Figure 4.3 were drawn using linear regression analysis to a power law equation:

$$\sigma_c = x\epsilon_0^c \qquad (4.1)$$

There was a slight difference in the slope of the lines; c was .62 for Bi and .80 for In. At all stresses the loading strain included considerable plastic deformation.

Solute Content. Since a smaller number of loading strain measurements were done on the low solute content alloys, evaluation of the effects of solute were difficult. In the high temperature range (.8 to .95 T_m) the loading strain did increase somewhat with Bi content (Figure 4.4). The In content had little effect on the loading strain.

Insufficient results were obtained to permit a quantitative assessment of the power law equation for the low solute content alloys. The results did follow the same general trend with stress (Figure 4.5). The magnitude of the loading strains at equivalent creep stress did not vary appreciably with solute content. Significantly, the two "recovery controlled" Class II alloys (1.3% Bi and 8.8% Bi) did not exhibit larger strains than the "glide" alloys.

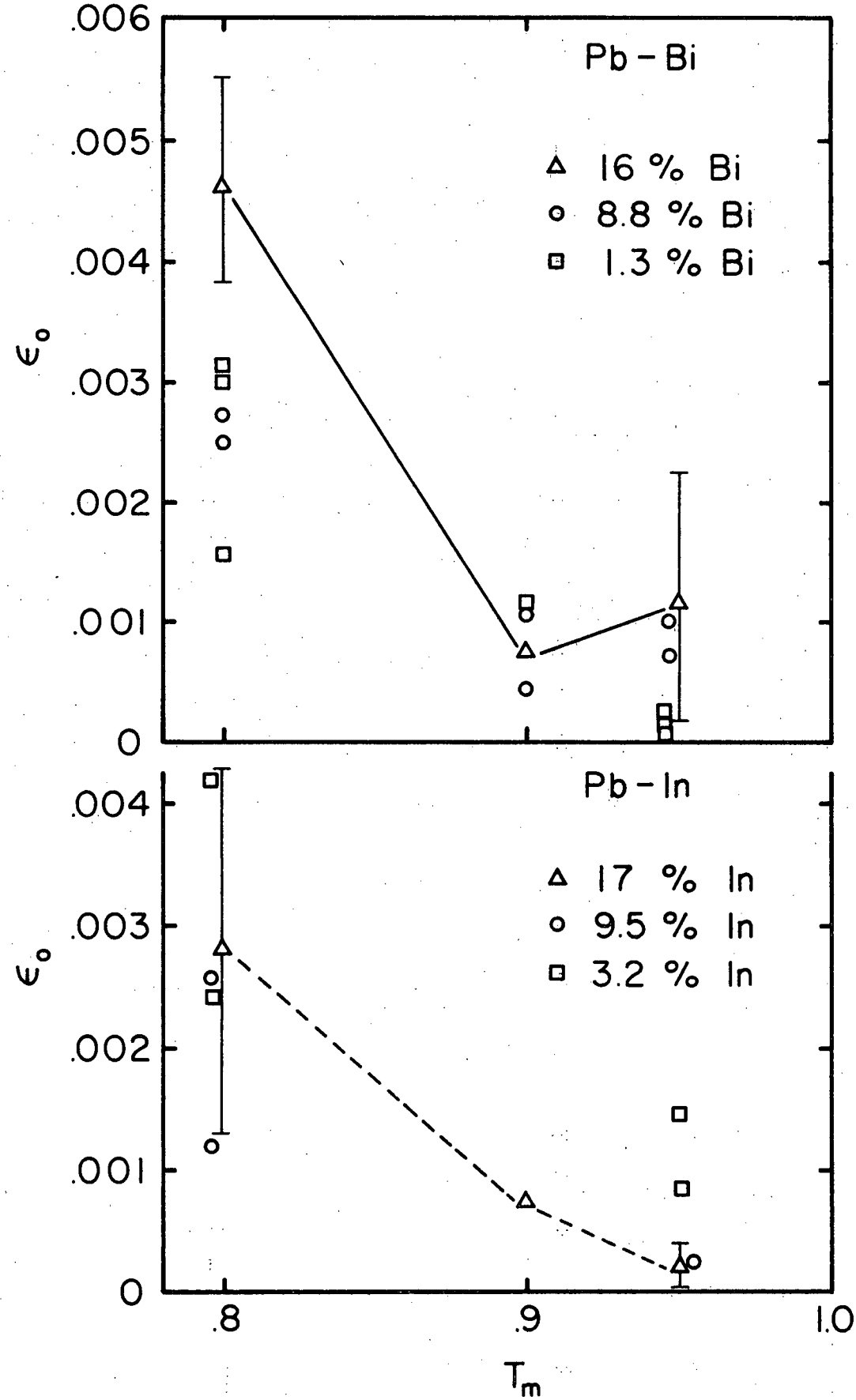

Figure 4.4. Loading strain versus relative temperature for all alloys.

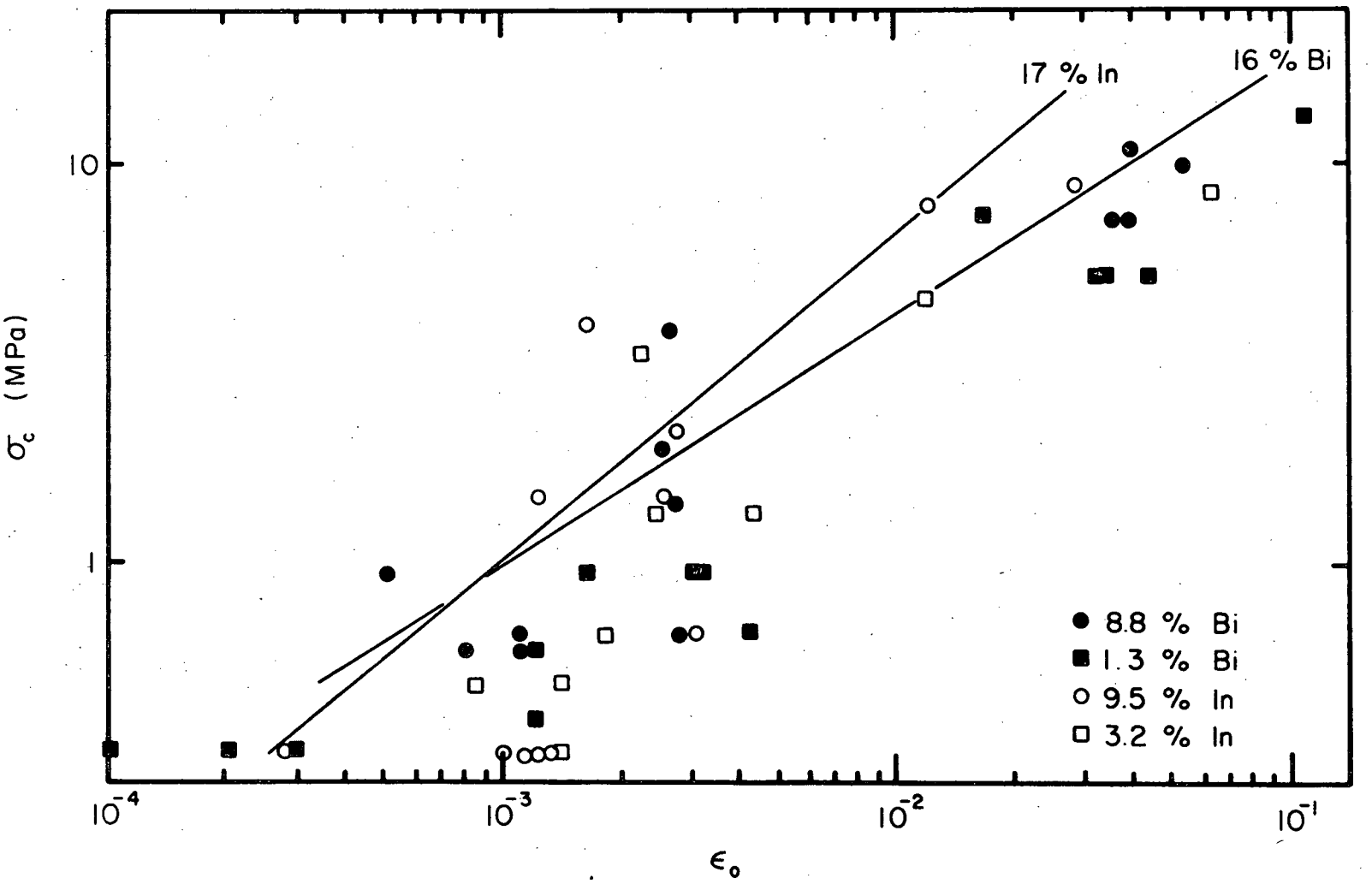

Figure 4.5. Creep stress versus loading strain comparison for all alloys.

Shape of Primary Transients

The results of this section were, in most cases, produced from the computer plots of creep strain versus time. In some cases visual examination of the elongation-time curve was sufficient to determine the shape of the transient.

Stress. For the "glide controlled" 16% Bi alloy, normal decreasing $\dot{\varepsilon}$ transients were found at all stress levels (Figure 4.6). On the other hand, the 17% In, also a "glide" alloy, exhibited non-normal transients at some stresses (Figure 4.7). At low stress at a particular temperature (.95 or .8 T_m) normal transients occurred, but at higher stresses either inverted or sigmoidal shapes appeared.

Temperature. No change in transient shape with temperature was found in any of the Bi alloys; normal transients predominated. In the Pb-In system the non-normal transients occurred at high temperatures (greater than .7 T_m). At .6 T_m only normal transients prevailed.

Solute Content. The amount of solute affected the transient shapes only in the Pb-In system (Figure 4.8). The low content (3.2% In) alloy possessed only normal transients at all temperatures and stresses. With increased

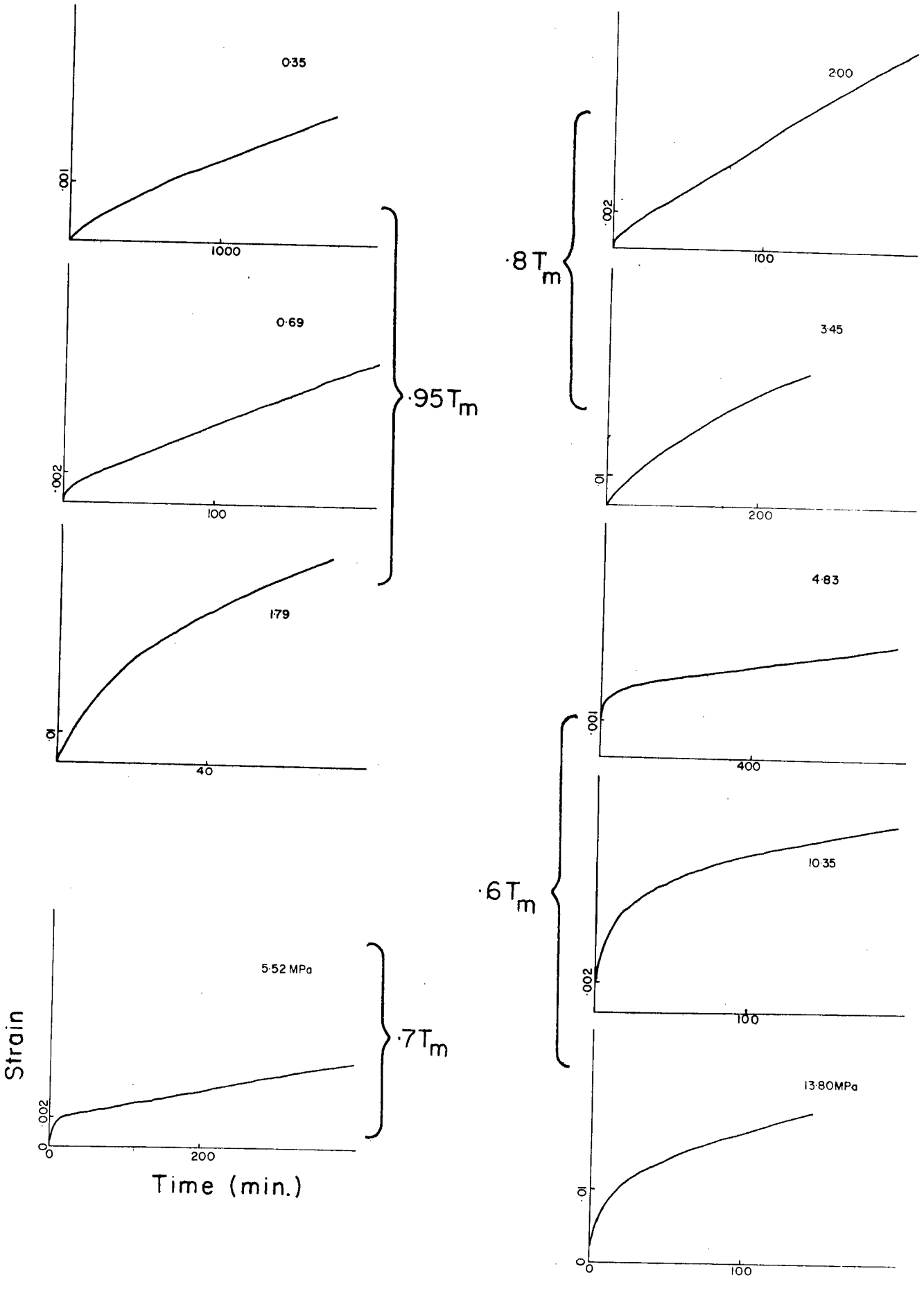

Figure 4.6. Primary creep transients for 16% Bi alloys at several stresses and temperatures.

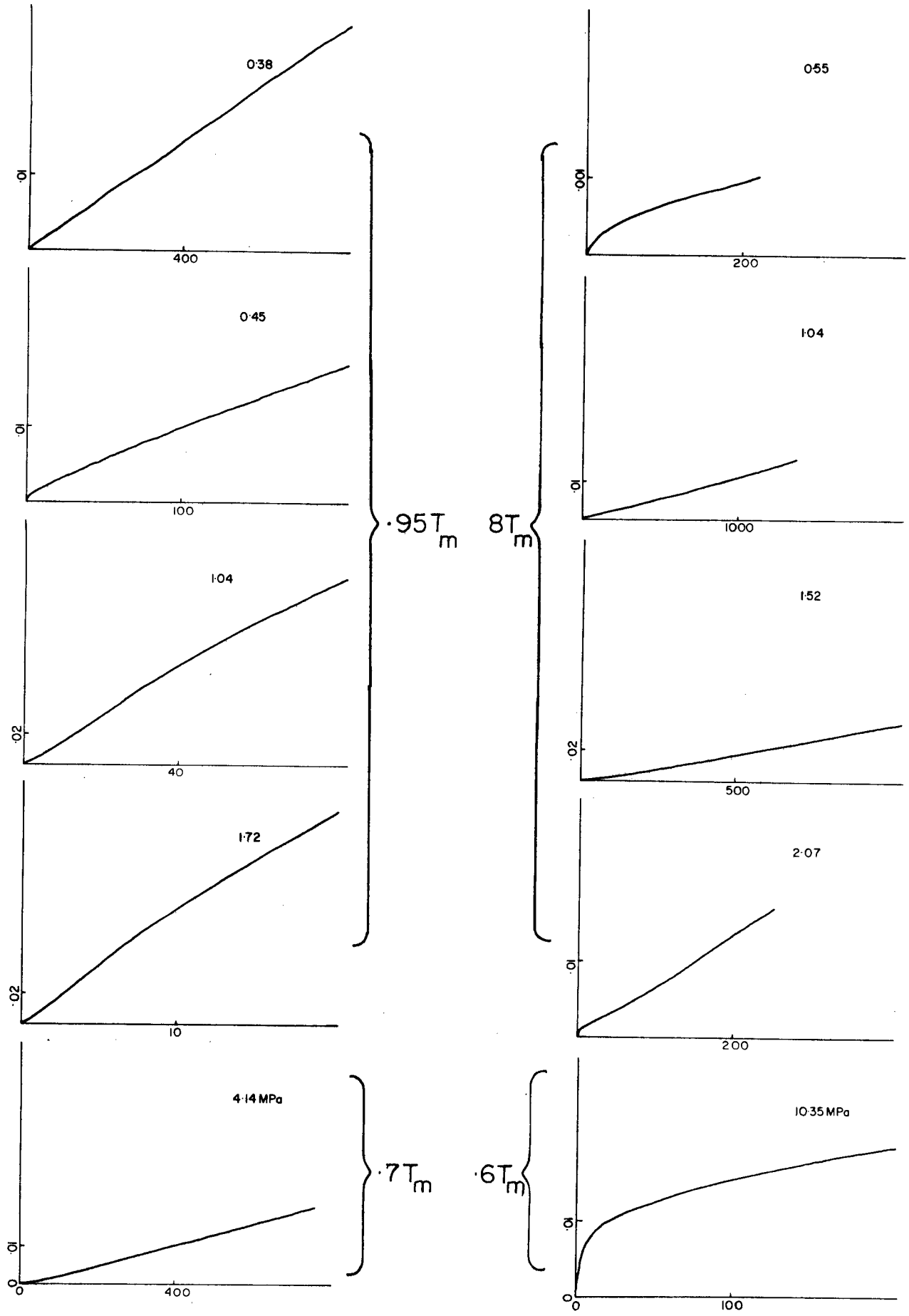

Figure 4.7. Primary creep transients for 17% In alloy at several stresses and temperatures.

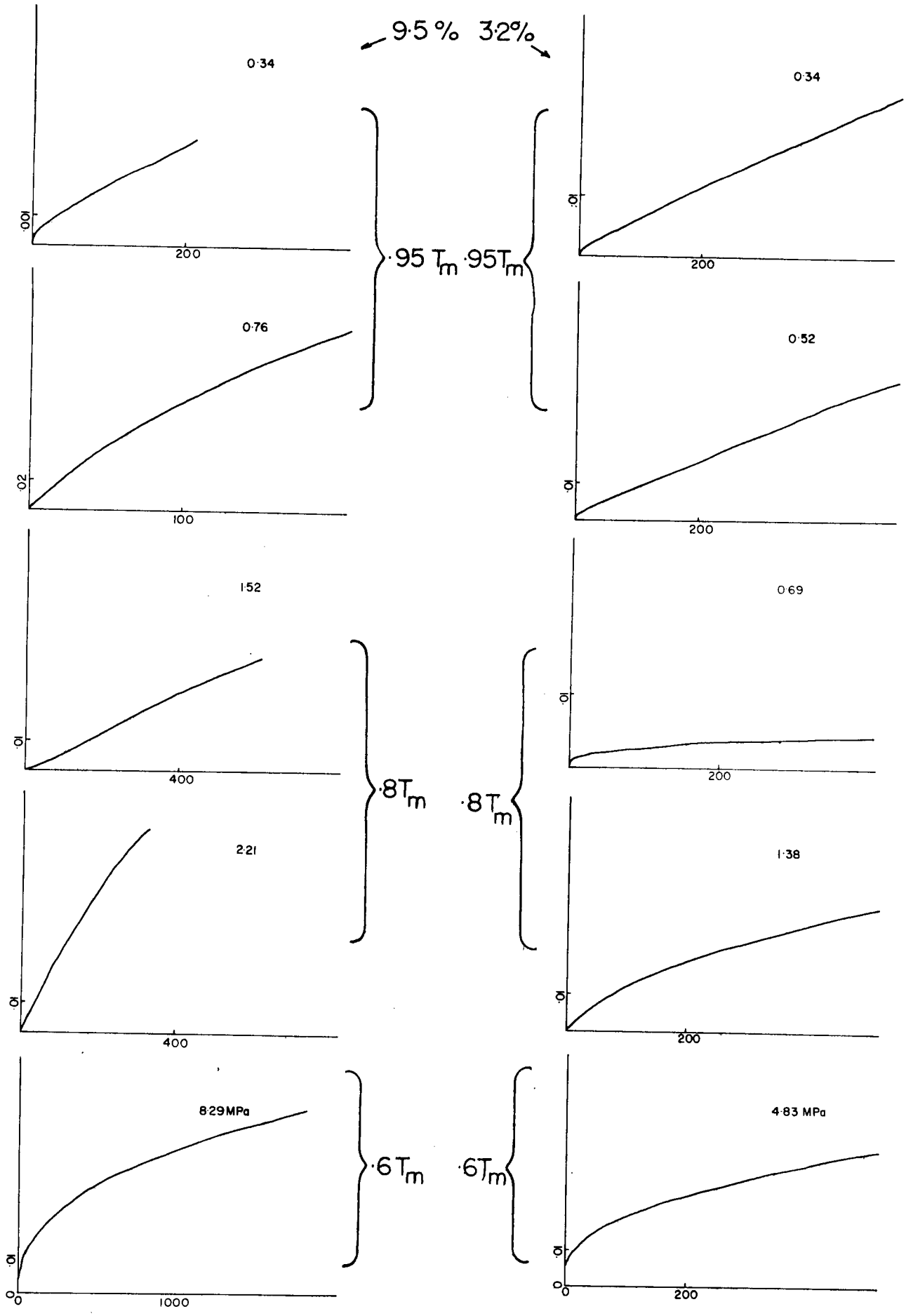

Figure 4.8. Primary creep transients for 9.5 and 3.2% In alloys at several stresses and temperatures

solute (9.5% In), sigmoidal transients occurred in a narrow stress range at .8 T_m. In the high In content alloy non-normal transients were more common (Figure 4.8).

Extent of Primary Region

Two methods were employed to measure the extent of the primary creep region: the first involved a measure of the *transient strain*, the second the *time* for attainment of steady state creep. To estimate the transient strain, the Garofalo equation (Garofalo, 1965) was used:

$$\varepsilon_c = \varepsilon_T\left(1 - e^{-mt}\right) + \dot{\varepsilon}_s\, t \qquad (4.2)$$

where ε_T is the limiting transient creep strain and m is a parameter related to the time to establish steady state. This equation can approximate the creep curves in pure metals and several "recovery controlled" alloys (Evans and Wilshire, 1970; Garofalo *et al.*, 1963; Sidey and Wilshire, 1969).

A graphical method (Conway and Mulliken, 1966) was used to evaluate the parameters of equation (4.2) for all the normal transients (Figure 4.9). The transient strain ε_T is determined by extrapolating the strain-time curve to t = 0 from the steady state region. Values of δ (see Figure 4.9) are measured from the ε-t curve and linear regression

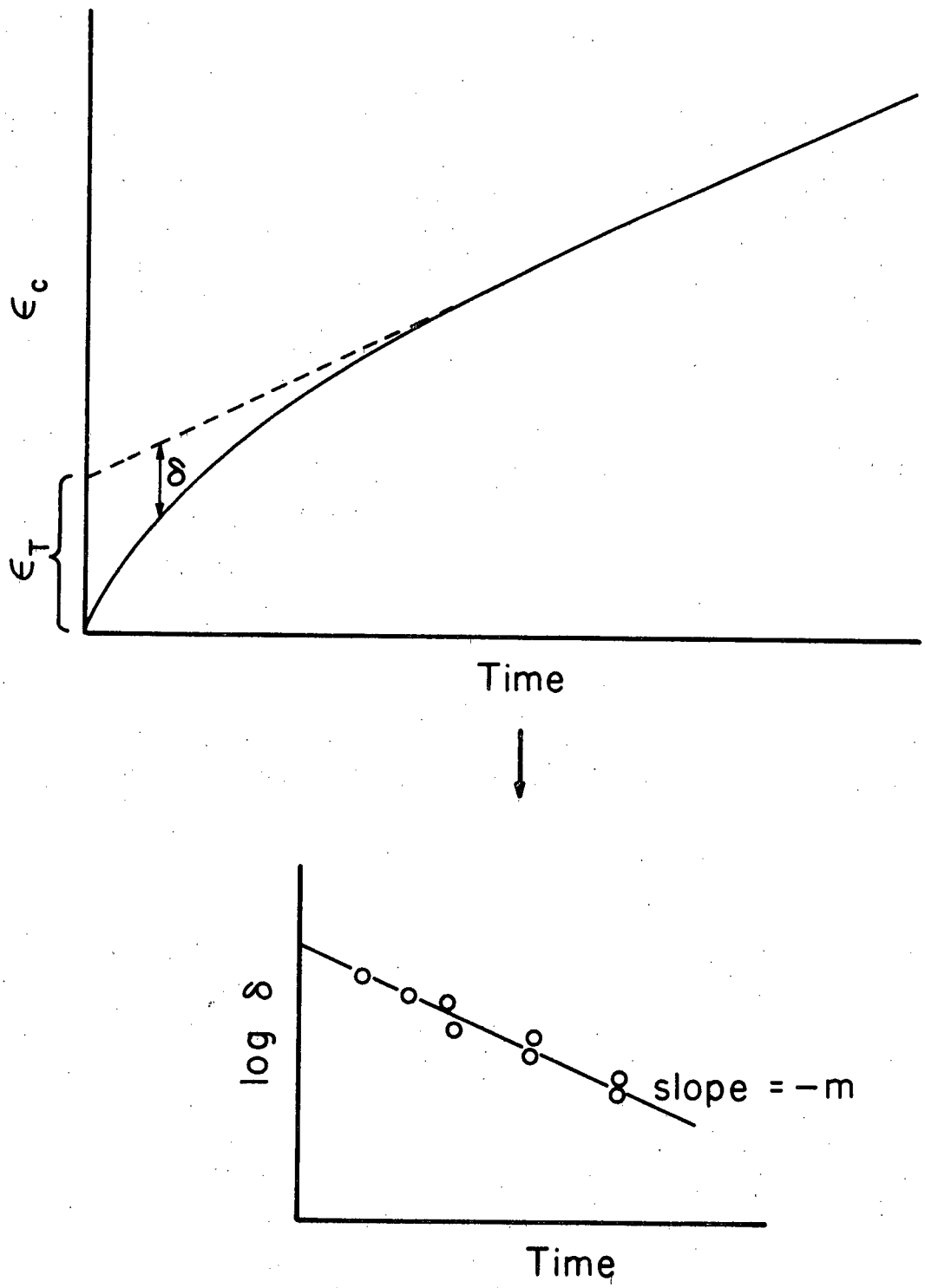

Figure 4.9. Graphical method for determining the parameters of Equation (4.2).

analysis used to fit a straight line to log δ versus time. The slope of this line can be shown to be equivalent to m. The fit of the equation to the experimental curves was good but with an underestimation of the creep strain in the early stages (Figure 4.10). This poor approximation to initial portion has been found in other systems (Sidey and Wilshire, 1969; Evans and Wilshire, 1968).

The curve fitting procedure could be applied to only the normal shaped transients. For the inverted or sigmoidal shaped transients, the time required for the establishment of the steady state strain rate was used. This measure of the extent of transient creep could be defined for both normal and non-normal transients.

The results will be presented in two subsections: transient strain ε_T and time to steady state. All evaluations were done for the same steady state rate of 4×10^{-5}/min.

Transient strain, ε_T. i) Stress — The transient strain was found to increase with stress at all temperatures (Figure 4.11) for the 16.2% Bi alloy. The occurrence of the non-normal transients in the 17% In alloy did not permit similar plots. The stress range was also too small for 8.8 and 1.3% Bi alloys to be analyzed for stress variations.

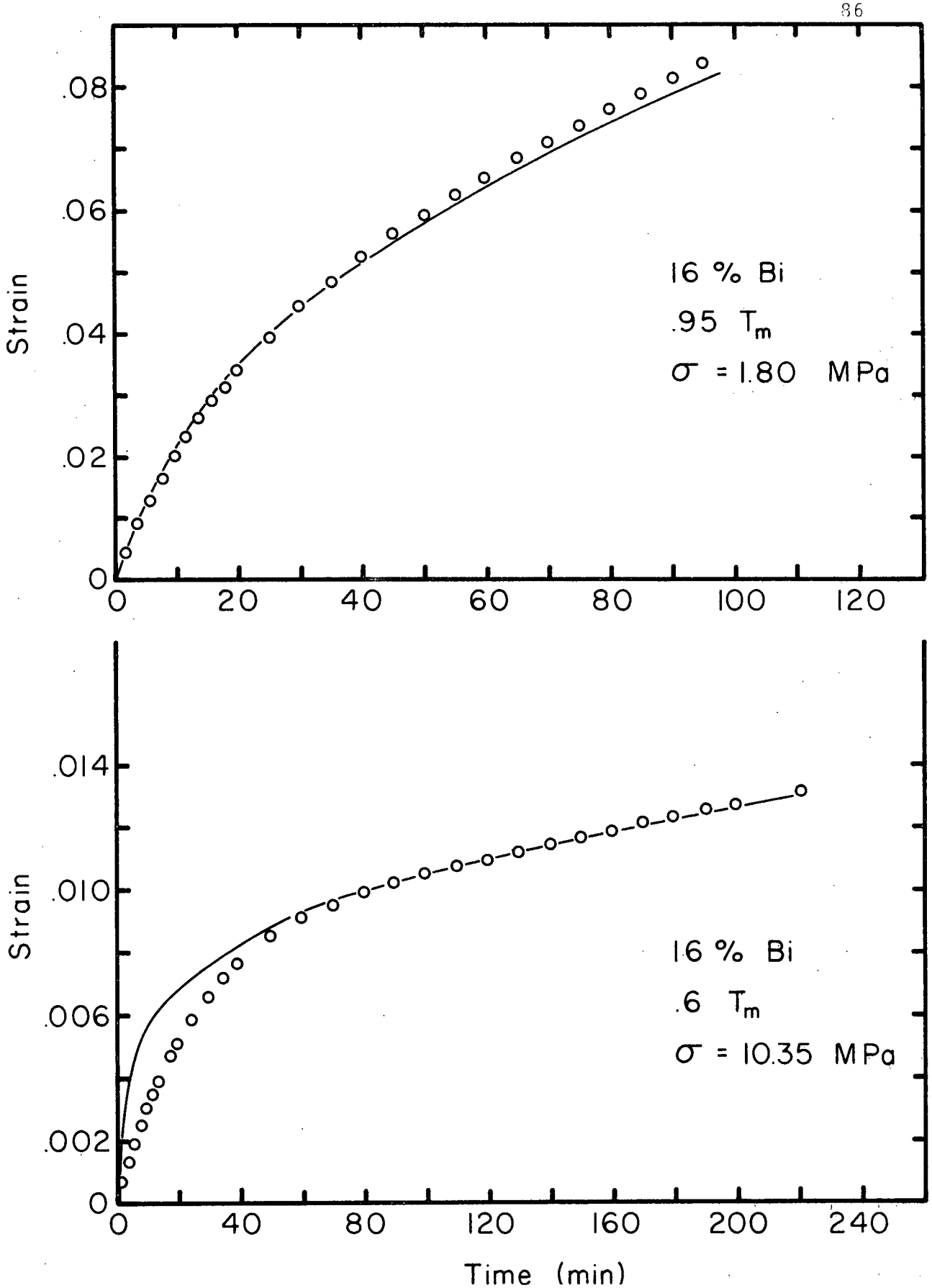

Figure 4.10. Comparison of strain versus time curves calculated from Equation (4.2) with experimental points.

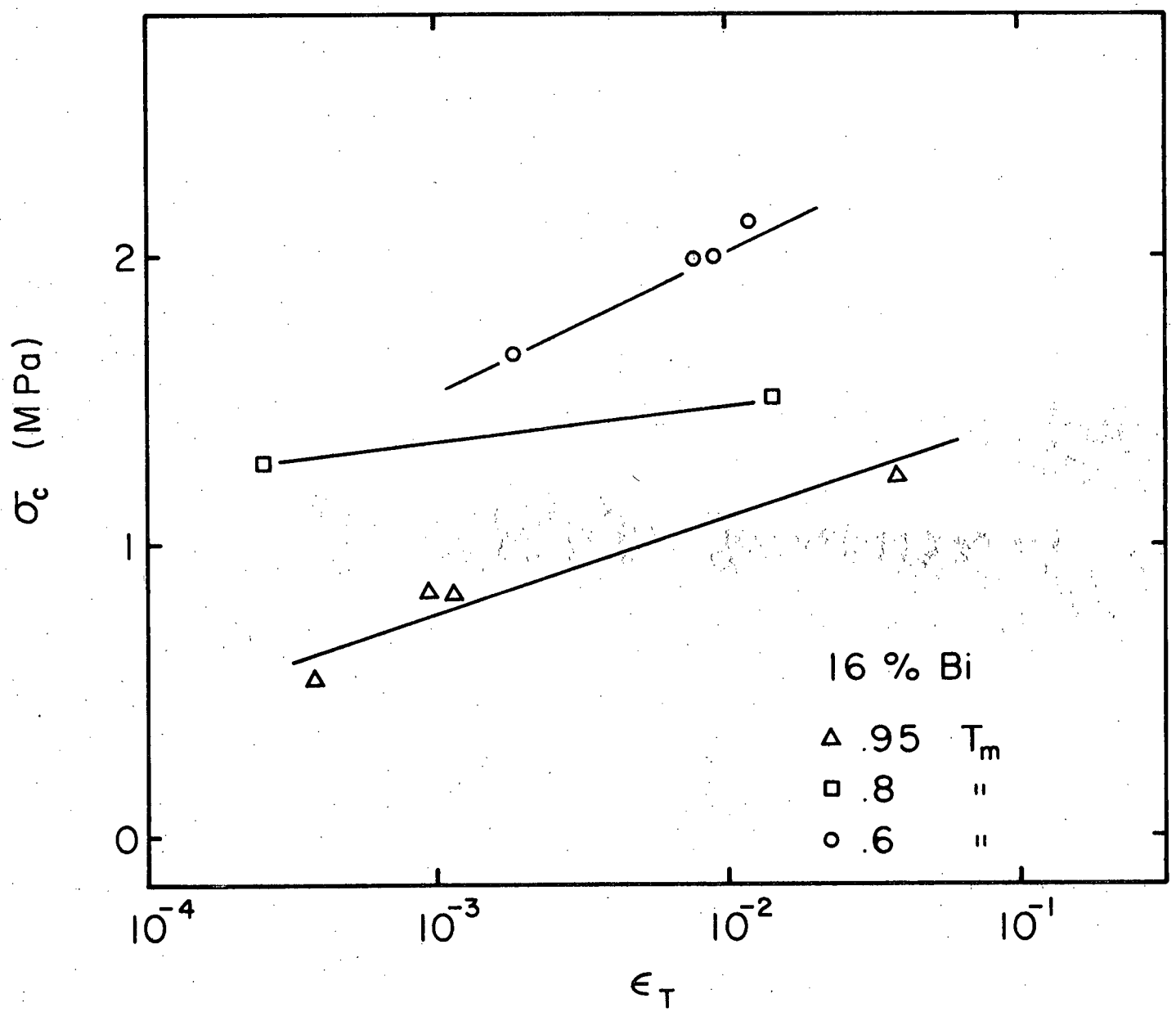

Figure 4.11. Creep stress versus transient strain for 16% Bi alloy.

ii) Temperature — The transient strain did not vary appreciably with temperature for all alloys. The 16.2% Bi alloy did show slightly less transient strain at the higher temperatures of .8 and .95 T_m than at .6 T_m (Figure 4.12). The In alloys with normal transients followed a similar trend of less transient strain at the higher temperatures.

iii) Solute Content — A pronounced effect of solute content was found in the Pb-Bi system; the 16.2% Bi alloy transient strain was lower than in the 8.8 and 1.3% alloys (Figure 4.13). The transient strain in the Pb-In system was independent of solute content (see Figure 4.12).

Time to Steady State. When the extent of primary region was measured by this method, very little difference was found between the two alloy systems (Figure 4.14) at equivalent solute concentrations and temperatures. Both the 16% Bi and 17% In alloys took slightly less time to achieve steady state than the low concentration alloys. The extent of primary creep in the non-normal curves was comparable to that of the normal type.

Summary

Based on previous investigations the "recovery controlled" alloys should have had normal transients and

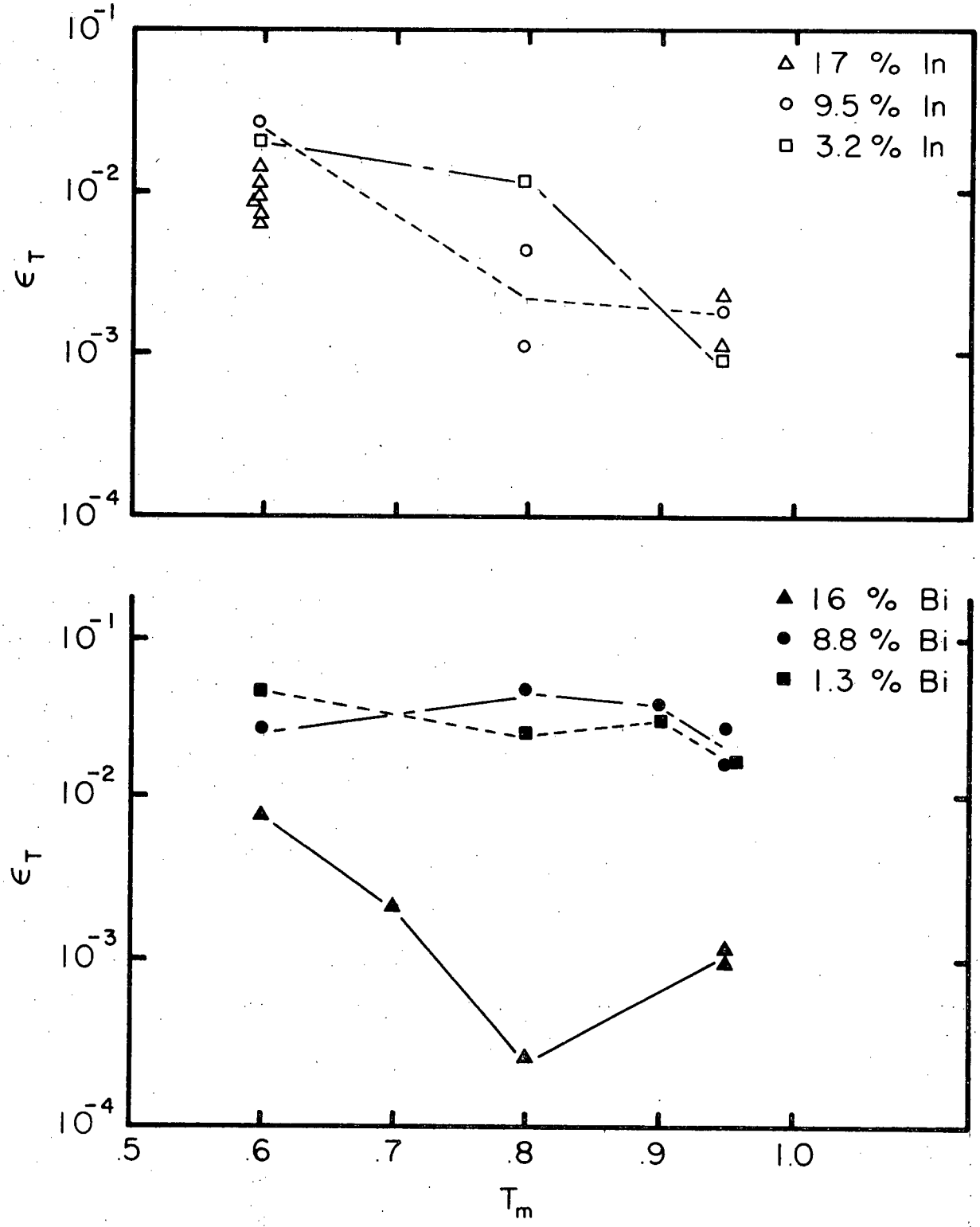

Figure 4.12. Transient strain versus relative temperature for all alloys.

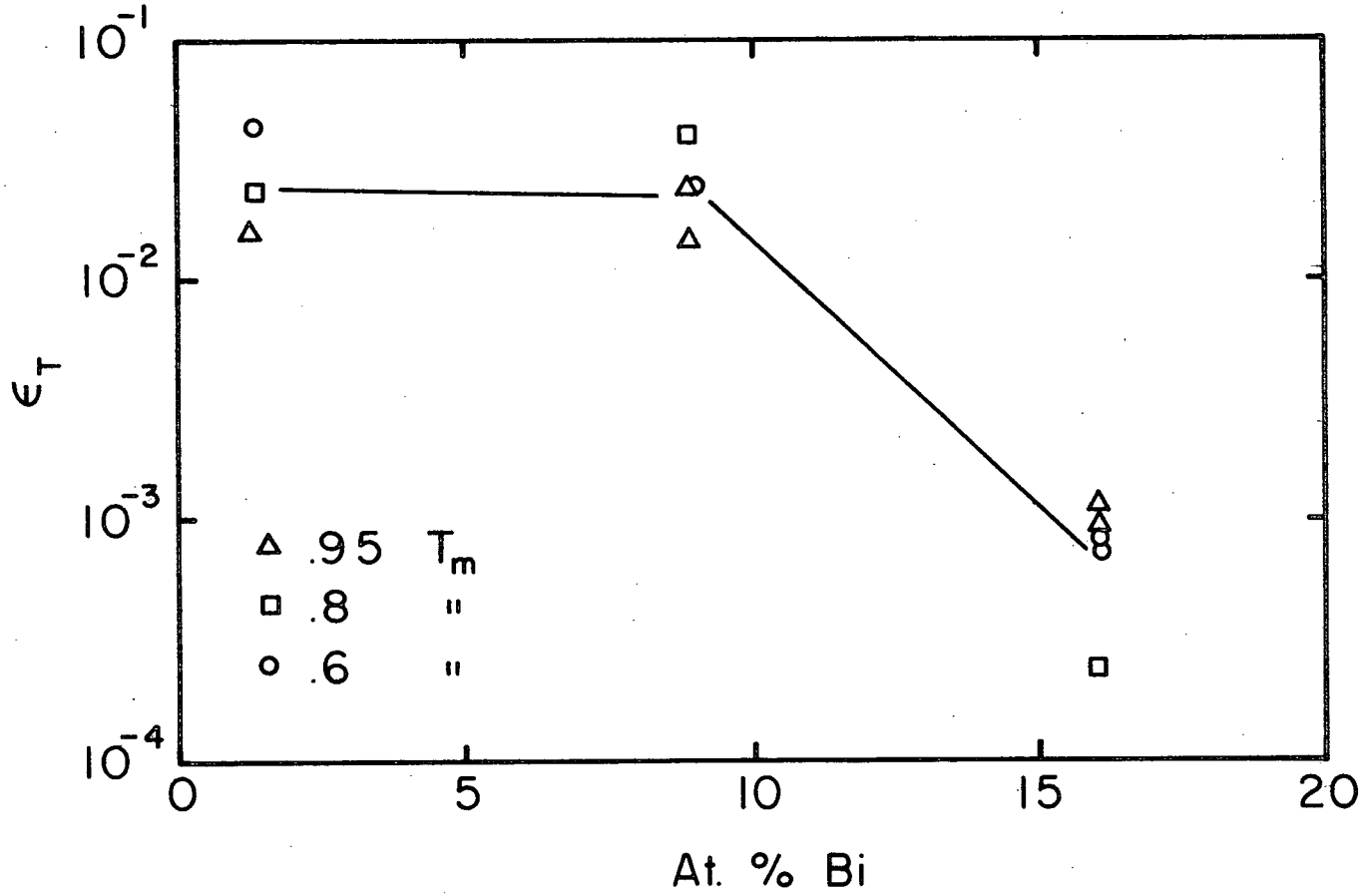

Figure 4.13. Transient strain versus solute content for Pb-Bi alloys.

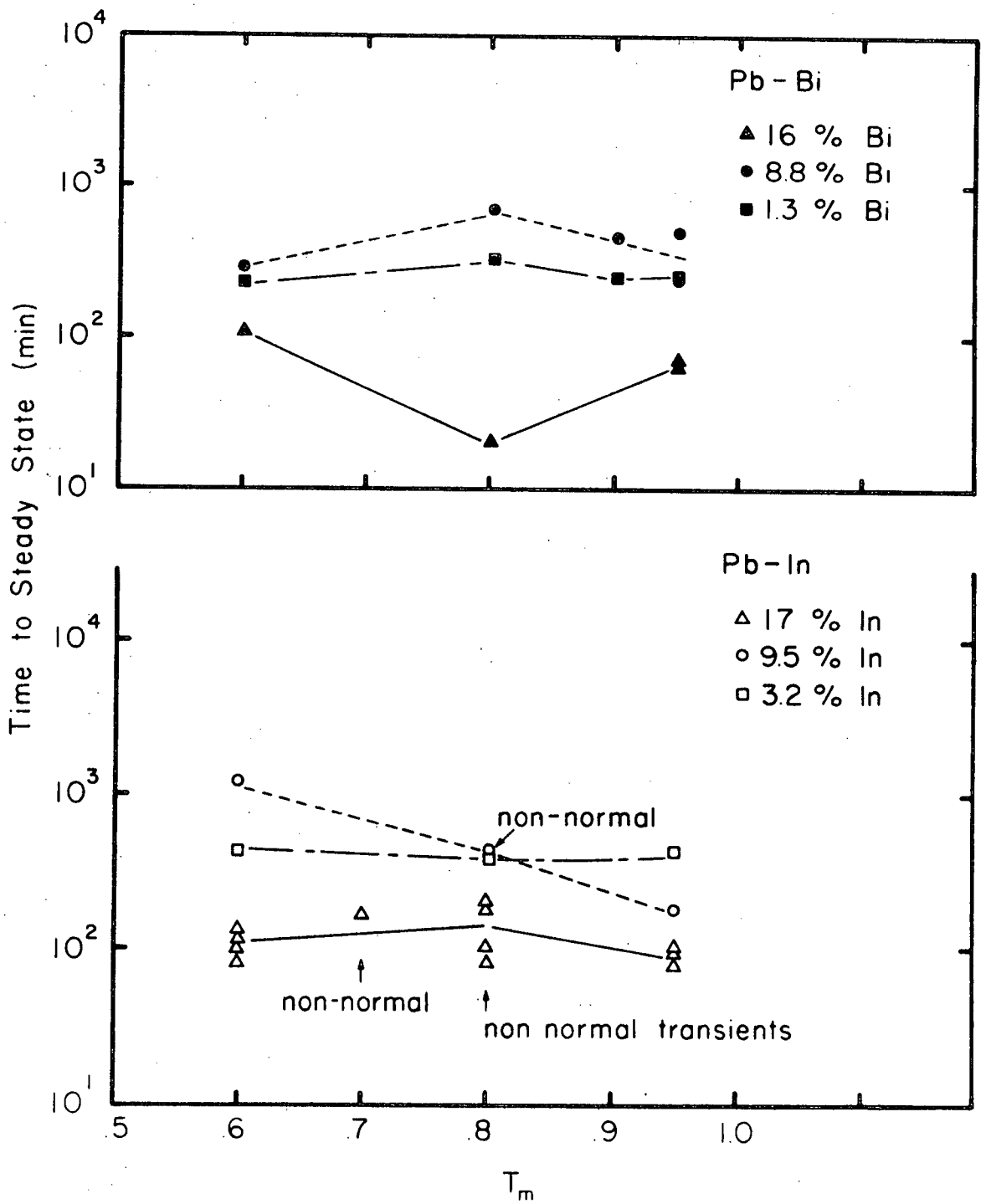

Figure 4.14. Time to steady state versus relative temperature for all alloys.

loading strains, the "glide controlled" non-normal transients of short duration and negligible loading strains. Some of the alloys did behave as expected from their stress exponent classification. The 1.3 and 8.8% Bi alloys (recovery controlled) had normal transients and appreciable plastic loading strains at all stresses and temperatures. The In alloys (17 and 9.5%), classified as "glide controlled" displayed inverted and sigmoidal transients at some stresses. However, the loading strains were not negligible as expected but were of the same order as the "recovery" alloys. The extent of the primary region was also of equivalent magnitude to the normal transients.

The other alloys also had results anomalous to their classification. The 3.2% In alloy which underwent a transition from $n \simeq 4.5$ to $n \simeq 3$ did not have any non-normal transients. The 16.2% Bi alloy, "glide controlled" had only normal transients and large loading strains.

DISCUSSION

This section will consider the results of the loading strain and primary creep measurements initially in terms of the simple creep theories. As these will be found

inadequate, the rearrangement theory will be applied to the Bi alloys and the combined glide-recovery theory to the In alloys.

Loading Strain

Weertman's two theories of "glide" and "climb" control make different predictions about the loading strain. In the climb model at steady state, the back stress from dislocation pile-ups control the dislocation generating source. Since the glide process is very fast, production and movement of dislocations can occur during the fast initial loading to create these pile-ups. Considerable loading strain is thus possible.

On the other hand, in the glide controlled case, the movement of the dislocations is time dependent in that it requires thermal activation for diffusion of solute atmospheres. Any dislocations existing prior to loading will be pinned by their atmospheres in the time span of the loading period and will be incapable of producing strain.

In the results section, the loading strain varied with the creep stress according to equation (4.1):

$$\sigma_c = x\ \varepsilon_0{}^c \qquad (4.1)$$

for both "glide" and "recovery" controlled alloys. Other investigations of "recovery" controlled solid solutions have successfully applied this equation to the loading strain (Davies, Davies and Wilshire, 1965; Feltham and Copley, 1960; Garofalo *et al.*, 1963).

The similarity between equation (4.1) and the parabolic work hardening "law" for polycrystalline metals at low temperature implies the initial strain is an essentially athermal plastic deformation. The coefficient x is also of the same magnitude as the low temperature value E/400 (Honeycombe, 1968). In creep tests, x does vary with temperature (Feltham and Copley, 1960) implying that some time dependent strain can occur concurrently with the athermal strain.

The loading strain results on the "recovery controlled" alloys, 1.3 and 8.8% Bi, are in qualitative agreement with the Weertman climb model since the loading strains followed the trend indicated by equation (4.1) (Figure 4.5). The loading strain can be considered an athermal plastic strain associated with the pile-up creation.

The present study is the first discovery of appreciable loading strains and the parabolic relationship in "glide controlled" alloys (16% Bi and all the In alloys). The values of the exponent c in equation (4.1) for 16% Bi

and 17% In were somewhat higher than the usual 0.5 found in "recovery controlled" alloys. The coefficient values x are also larger, E/250 and E/70 respectively for Bi and In. If a value of 0.5 is assumed for c as previous studies have done and x recalculated, the respective values become E/330 and E/200 which are similar to the low temperature coefficient (E/400). Thus the loading strains in the "glide" alloys also represent largely athermal plastic strain. These results are in obvious conflict with the Weertman glide theory.

If the 16% Bi alloy is regarded as "recovery" controlled, the loading strain results agree with the Weertman climb model.

The conclusions of this section are summarized in the chart on page 118.

Normal Transients

Kinetics. The strain-time relationships during normal transients in both alloys systems were approximated by the Garofalo equation. If it is assumed that the change in strain rate during the normal transient follows the principle of first order chemical kinetics, the Garofalo equation can be derived and its parameters be given a theoretical meaning (Webster Cox and Dorn, 1969). First order kinetics means that the

rate of change of $\dot{\varepsilon}$ is proportional to the difference between its current and steady-state values:

$$\frac{d\dot{\varepsilon}}{dt} = -m(\dot{\varepsilon} - \dot{\varepsilon}_s)$$

Integrating

$$\frac{\dot{\varepsilon} - \dot{\varepsilon}_s}{\dot{\varepsilon}_i - \dot{\varepsilon}_s} = \exp(-mt)$$

with $\dot{\varepsilon}_i$ being the initial creep rate. Integrating again gives the Garofalo equation:

$$\varepsilon = \left(\frac{\dot{\varepsilon}_i - \dot{\varepsilon}_s}{m}\right)(1 - \exp -mt) + \dot{\varepsilon}_s\, t \qquad (4.2)$$

with $$\frac{\dot{\varepsilon}_i - \dot{\varepsilon}_s}{m} = \varepsilon_T$$

Such a derivation implies that the process controlling the steady state strain rate also governs the transient rate. Some structure parameter responsible for the creep rate must change continuously from an initial value at t = 0 to a value characteristic of the steady state. For additional support of this notion, some attributes of ε_T, m and $\dot{\varepsilon}_i$ can be compared with deductions based on the kinetic theory (Mukherjee, Bird and Dorn, 1969). This comparison has been done for the present measurements of transient

creep (Appendix 3). The analysis generally lends support to the first order kinetics idea and hence to the conclusion that the same process governs the primary transient and the steady state creep rate.

Recovery Theories. If a material has been deformed to some point on its stress-strain curve (at 0°K or after the loading strain) its internal structure is characterized by a yield strength τ_y which exactly balances the applied stress σ (Orowan, 1946). An incremental increase in the applied stress produces strain and an increase in the yield strength:

$$d\sigma = hd\varepsilon = d\tau_y \tag{4.3}$$

where h is the coefficient of strain hardening. Deformation can also occur if the yield strength is decreased by a recovery process (above 0°K)

$$d\tau_y = rdt \tag{4.4}$$

where r is the rate of recovery.

During steady state creep any fall in τ_y will result in strain which maintains the yield strength equal to the constant applied stress:

$$d\tau_y = hd\varepsilon = rdt$$

or

$$\frac{d\varepsilon}{dt} = \frac{r}{h} = \dot{\varepsilon}_s \qquad (4.5)$$

This is the basic equation of the recovery model of creep. Steady state creep is the result of a balance between a process of softening (recovery) and a simultaneous hardening.

In attempting to analyze primary creep some workers (Evans and Wilshire, 1968; Sidey and Wilshire, 1969) have used equation (4.5) and considered the effects of an imbalance in r and h. For instance, if the hardening rate remains constant but the recovery rate continually decreases from an initial high value to the steady state value it would appear that the strain rate would also continuously decrease. The recovery process then controls both the transient and steady state rates consistent with the Garofalo equation analysis. However, since equation (4.5) can only be derived by invoking the steady state condition, the basic theory cannot admit such an imbalance in r and h; transient states are not possible (Alden, 1972; Orowan, 1946).

Consideration of the microstructural recovery models also confirms the non-existence of transients. Weertman's climb

model can be considered as a simple recovery model with the recovery step being the climb process of the dislocations from the pile-ups. Strain hardening is associated with the generation and release of a dislocation at the source and its addition to the pile-up or entanglement. In the steady state, these two processes are in balance since the generation step follows reduction of the back stress by the climb of one of the piled-up dislocations. The recovery rate is governed by the stress field of the pile-up which is a function of its dislocation population. If the loading strain creates pile-ups with more than the requisite dislocations for steady state, there would be a fast initial recovery rate. This rate could then decline as some of the dislocations climbed out of the slip plane. However, until the number of dislcations and consequently the back stress on the source are reduced to their steady state values, no generation of dislocations and no strain can take place. Steady state must be established immediately; the loading strain produces exactly the steady state dislocation configuration. Hence Weertman's pile-up model is not capable of predicting a decreasing rate transient.

An alternate recovery theory using a network microstructural model has been applied to primary creep. A three-dimensional network of dislocations interconnected at nodes supposedly occupies the volumes of the material between more

dense entanglements or subboundaries. Elements or mesh links of this network, which thread the glide plane act as forest obstacles to mobile dislocations. The yield strength is associated with the average size of this network. As the network coarsens to reduce its line energy, the yield strength is reduced (recovery). The network can be refined as glide dislocations are stopped at the forest obstacles and become incorporated into the network (strain hardening). The recovery rate will vary inversely as the mesh size x or directly as the dislocation density ρ:

$$r \alpha \frac{1}{x} \alpha \rho^{\frac{1}{2}}$$

To explain normal primary creep, it must be assumed that after the loading strain the network is very fine. Consequently the recovery rate will be high and will decrease with time as the network coarsens. If the hardening coefficient is constant with mesh size (Evans, 1973), the creep rate should fall continuously (Eq. 4.5). Two objections can be raised against this idea.

If the mesh size is initially very fine, high stresses will be required to move dislocations between the dense forest obstacles. If the applied stress is too low, dislocations will not be able to move appreciable distances. Since the distribution of mesh lengths is thought to be narrow (Mclean, 1968; Evans, 1973) and the applied stress

is constant, the network must grow to critical mesh size before strain occurs. This critical length will be characteristic of steady state. The situation is analogous to the pile-up model; the loading strain must produce the steady state dislocation configuration. Therefore primary creep is not predicted.

Also the contention that the mesh is small initially and then coarsens implies that τ_y decreases during primary creep . Measurements during the initial transient region in pure Pb (Fox, 1969) show that τ_y increases with strain.

Rearrangement Theory. Thus on both theoretical and experimental grounds the simple recovery models are not adequate to explain a decreasing strain rate transient. A new concept that the obstacle structure is non-uniform and that its thermal "rearrangement" can produce strain has amplified the recovery theory concepts to include the possibility of transients (Alden, 1972).

Instead of characterizing the solid by a single or average yield strength as in the simple recovery theories, the rearrangement theory postulates the existence of a non-uniform obstacle structure. Again a network of dislocations threading the glide plane acts as the "forest" to the slip dislocations. In the network-recovery model, the slip area

available to a released dislocation was governed by the *average* mesh spacing of the network. Only changes in the average spacing could influence this area. A statistical analysis of a random distribution of such forest obstacles (Kocks, 1966) showed that at low stresses a dislocation can move over only a small area of the slip plane where the forest dislocation density is low. As the stress increases, progressively larger areas become accessible to the dislocation until it can move over virtually all the slip plane. Some volumes of the crystal are softer than others and the distribution of the obstacles is also important as well as their average spacing. A new material parameter must be introduced to describe this non-uniformity.

At high temperature a material deforms by using only its "soft-spots," areas of low dislocation density (Alden, to be published). If only the soft spots deform, only they will be strain hardened.

To allow for continuing deformation, new areas of low density must be produced either by loss of obstacles (recovery) or by changes in their distribution (rearrangement). Thus strain can be produced in three ways:

1) an increase in the applied stress
2) a decrease of average obstacle density (recovery), and
3) production of a soft area (rearrangement).

These concepts have been expressed mathematically. At 0°K the stress-strain relationship is represented by:

$$d\varepsilon = \frac{d\sigma}{\theta_y} \exp - \left(\frac{\tau_y - \sigma}{\tau_v}\right) \tag{4.6}$$

where θ is a "strain hardening coefficient"

τ_y is an average yield strength

τ_v is a new parameter which expresses the degree of non-uniformity of the structure. In a regular or uniform structure τ_v will be small. In a non-regular (or cellular) structure τ_v will be large (Alden, to be published).

The exponential term is called the relative free area function and is a measure of the amount of the slip plane accessible to the dislocation. The strain rate equation at high temperature is:

$$\dot{\varepsilon} = \frac{1}{\theta_y}\left(\dot{\sigma} + r_y + r_v\right) \exp - \left(\frac{\tau_y - \sigma}{\tau_v}\right) \tag{4.7}$$

where r_y and r_v are recovery and rearrangement rates.

Transient creep can be explained with this new concept. Immediately after the loading strain the yield strength will equal the applied stress ($\tau_y = \sigma$) and the relative free area will be unity. No further strain will

be produced until the processes of recovery and rearrangement occur. If only loss of dislocations takes place, the subsequent strain will, through strain hardening, exactly balance the loss. As before $\tau_y = \sigma$ and no transients are predicted. However, if rearrangement concurrently produces soft areas for deformation, strain hardening can proceed without loss of dislocations. Thus τ_y can increase above σ and the free area decrease causing a continuously decreasing $\dot{\varepsilon}$. When τ_y reaches its steady state value, recovery and strain hardening will be balanced and the strain rate will be constant.

A normal transient can be predicted by the recovery-rearrangement process unlike the simple recovery theories. It controls the creep rate in both the transient and steady state regimes consistent with the Garofalo equation analysis. At the present stage of development, the parameters of the theory cannot be related to the coefficients of the Garofalo equation. The effects of solute on the model cannot be readily assessed. Since both recovery and rearrangement are climb controlled, solute effects on diffusion would be important.

As the actual deformation is athermal in this theory strain can occur during the loading period as in the simple recovery theories. The loading strain, in this case, is

controlled by the athermal or 0°K stress-strain curve which is consistent with the similarities between the loading strain behaviour and the experimental low temperature σ-ε relationships.

The rearrangement theory is compatible with the loading strain and the primary creep results for the Pb-Bi system alloys, both the "recovery controlled" 1.3 and 8.8% Bi and the "glide controlled" 16% Bi alloys.

Non-Normal Transients

Referring to Figure 1.3, the recovery theory branch, through the rearrangement concept, is adequate to deal with the normal transients of the Class II "recovery" alloys. Since non-normal transients are associated with Class I "glide" alloys, the glide or reaction rate branch will be applied in this section.

Simple Glide Theory. The simple glide theory (Weertman, 1957) can predict an inverted transient. After the creep stress has been applied, the "locked" dislocations will begin to move as diffusion of their atmospheres is now possible. The glide rate of these grown-in dislocations is fixed by the applied stress and will not change with time. However, if the original density of these dislocations is less than that permitted at steady state, new dislocations

can be generated to increase the density and hence the strain rate. Similarly if the original density is greater than the steady state density, a decreasing strain rate transient would be anticipated.

Thus for a particular original density, increases in creep stresses should produce a transition in transient shapes from normal to inverted. This trend was found in some of the glide alloys. However, the complex sigmoidal shaped transient found in the present alloys cannot be handled by the simple theory. The combined glide-recovery theory will therefore be described in some detail and applied to the initial transients.

Combined Glide-Recovery Theory. This description of creep depends upon the division of the applied stress into two parts, an effective stress and an internal stress:

$$\sigma_c = \sigma_e + \sigma_i \tag{4.8}$$

The internal stress σ_i overcomes a back stress opposing the potential motion of the dislocation. It is usually associated with the long range elastic stress fields around immobile dislocations, i.e. the dislocation mesh network. In this context it can be associated with the processes of strain

hardening; any increase in the dislocation density will increase the internal stress. The effective stress σ_e assists the dislocation to glide against the frictional resistance to motion such as the lattice resistance (Peierls stress) or the dragging of solute atmospheres. To move an individual dislocation, the applied stress must be increased to a level to first overcome the long range stresses and then slightly higher to start the glide process.

Some of the ideas of the recovery theory have been incorporated into this new concept. In steady state creep, the internal stress is constant because of the balance between strain hardening and recovery:

$$\frac{d\sigma_i}{dt} = 0 = h\dot{\varepsilon} - r$$

or

$$\dot{\varepsilon}_s = \frac{r}{h} \tag{4.9}$$

This is identical to the Bailey-Orowan recovery equation with the exception that now r and h are formulated in terms of the internal stress instead of the total stress. The strain rate at any time is controlled by thermal activation of the glide process and depends upon the effective stress level. It can be expressed by a dislocation dynamics type of expression:

$$\dot{\varepsilon}_s = \tfrac{1}{2} b v \rho \qquad (4.10)$$

where ρ is the *average* mobile dislocation density and v is the *average* dislocation velocity, $v = v(\sigma_e)$. Equations (4.9) and (4.10) thus give two simultaneous expressions for the creep rate.

If expressions for v, ρ, r and h can be developed in terms of the internal stress, then the $\dot{\varepsilon}$ can be expressed as a function of the internal stress only (Gasca Neri *et al.*, 1970). For instance, if the deformation is controlled by a solute drag effect:

$$v = B(\sigma - \sigma_i). \qquad (4.11)$$

This is the identical equation used in the simple glide theory except the effective stress $(\sigma - \sigma_i)$ only acts to move the dislocation. Similar expressions, some theoretical some empirical, were used for r, h, and ρ and led to an equation (Gasca Neri *et al.*, 1970):

$$\dot{\varepsilon} = \dot{\varepsilon}_{\sigma,T}\left[\sigma_i(t)\right] \qquad (4.12)$$

for the creep rate. This expression can be written as:

$$S\,\frac{d\dot{\varepsilon}}{dt} = S\left(\frac{d\dot{\varepsilon}}{d\sigma_i}\right)_{\sigma,T} \cdot S\left(\frac{d\sigma_i}{dt}\right)_{\sigma,T} \tag{4.13}$$

where S denotes the sign of the derivative. By considering the sign of the two terms on the right, predictions can be made about the shape of the transient creep curve which depends upon how the internal stress changes from its initial value σ_i^0 to its steady state value σ_i^{SS}. The sign of $d\sigma_i/dt$ will be governed by the initial value of the mean internal stress σ_i^0. If $\sigma_i^0 < \sigma_i^{SS}$ then $d\sigma_i/dt > 0$. If $\sigma_i^0 > \sigma_i^{SS}$ then $d\sigma_i/dt < 0$.

An expression can be developed for the steady state value of σ_i^{SS} as a function of σ (Figure 4.15A):

$$\sigma - \sigma_i^{SS} = \text{const}\,(\sigma_i^{SS})^2 . \tag{4.14}$$

In Figure 4.15A, point A represents a metal with an initial internal stress σ_i^0 at a creep stress of σ. Since σ_i^0 lies to the left of the steady state value, the internal stress must increase during primary creep to its value at B. Thus in the area to the left of the $\sigma_i^{SS}(\sigma)$ curve, $d\sigma_i/dt$ is positive and to the right is negative.

A similar plot can be produced for $S\left(\frac{d\dot{\varepsilon}}{d\sigma_i}\right)_{\sigma,T}$ by first developing the equation:

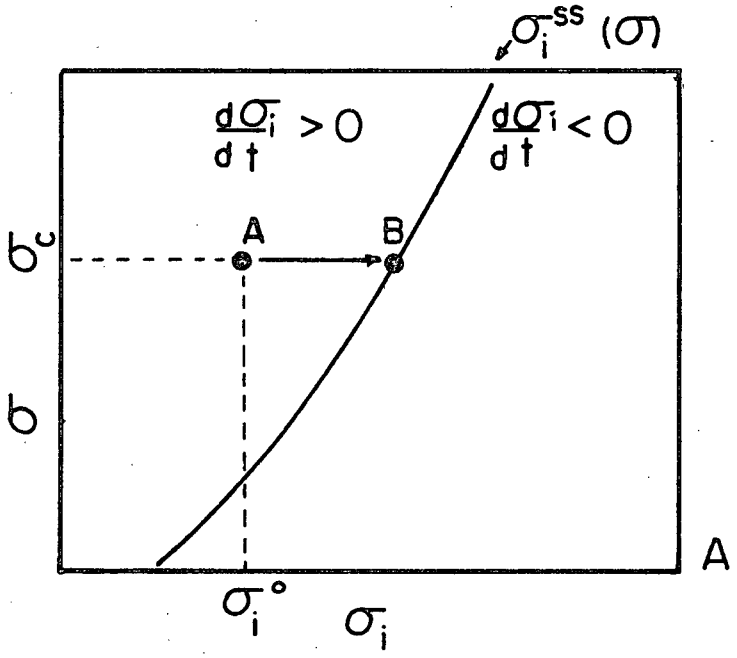

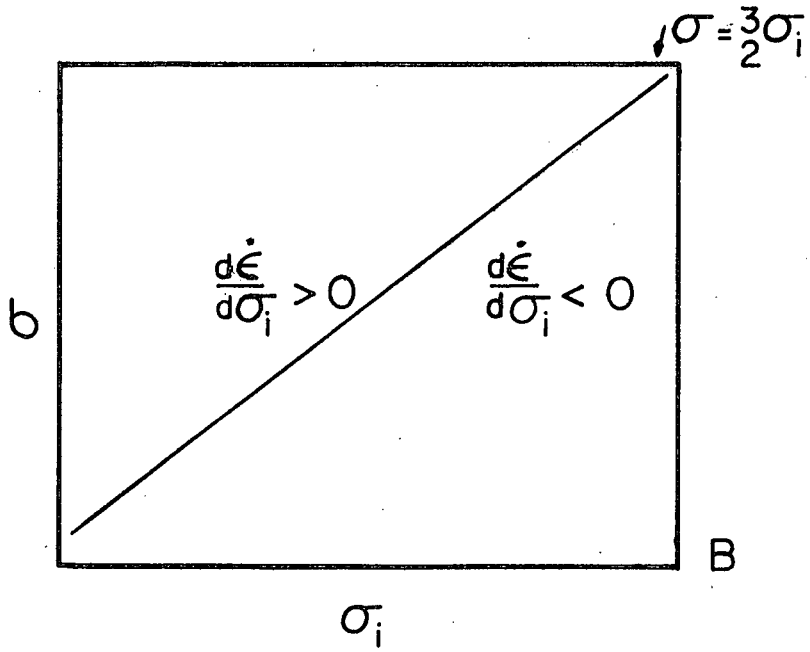

Figure 4.15. A) Changes in sign of $d\sigma_i/dt$ as a function of creep stress and internal stress.

B) Changes in sign of $d\dot{\varepsilon}/d\sigma_i$ as a function of creep stess and internal stress.

$$S \frac{d\dot{\varepsilon}}{d\sigma_i} = S\left(\sigma - \frac{3}{2}\sigma_i\right) \qquad (4.15)$$

and then graphing $\sigma = \frac{3}{2}\sigma_i$ (Figure 4.15B). Thus for a point (σ, σ_i^0) to the left of the line, $d\dot{\varepsilon}/d\sigma_i$ will be positive and to the right negative.

By combining these two figures a "mechanical history" diagram is created (Figure 4.16) which will indicate the sign of the derivative $d\dot{\varepsilon}/dt$. For instance, in the large area to the left of both curves both $d\sigma_i/dt$ and $d\dot{\varepsilon}/d\sigma_i$ are positive so that $d\dot{\varepsilon}/dt$ is positive. A continuously positive value until steady state of $d\dot{\varepsilon}/dt$ indicates an inverted type transient (Figure 4.16A). If as the internal stress changes to its steady state value the material passes through two regions in the diagram, the sigmoidal shaped transient is produced (Figure 4.16B). A material continuously in the negative region will have a normal transient curve (Figure 4.16C).

For the situation of Figure 4.16A the loading strain produced an initial internal stress value σ_i^0 which was lower than that required for steady state. Consequently σ_i and the density of both mobile and immobile dislocations must increase during creep. As strain occurs, the density of mobile dislocations will thus increase producing an increasing strain rate:

$$\dot{\varepsilon} = \tfrac{1}{2} b v \rho .$$

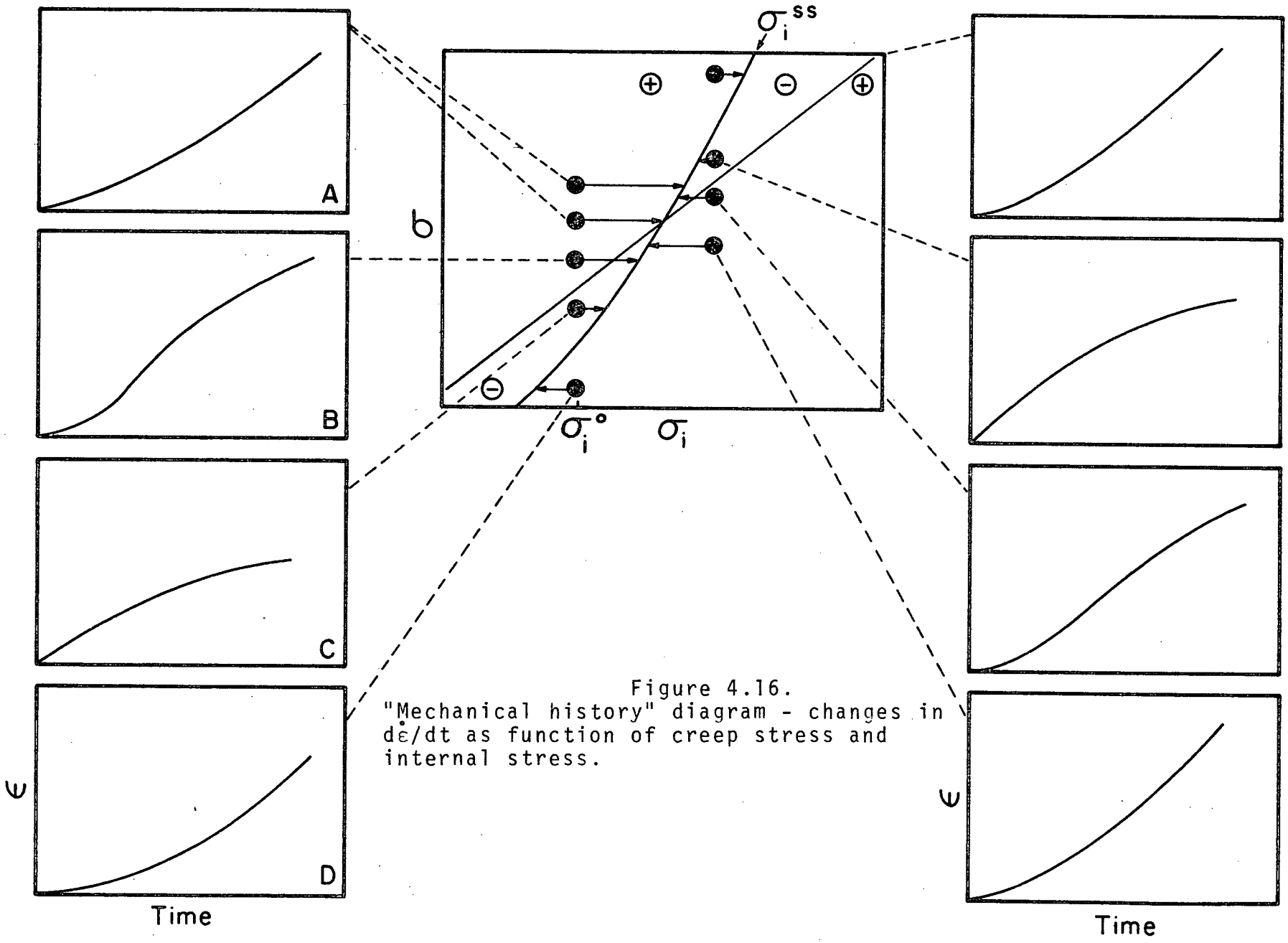

Figure 4.16.
"Mechanical history" diagram - changes in $d\dot{\varepsilon}/dt$ as function of creep stress and internal stress.

However, the average velocity of these dislocation is simultaneously decreasing since the effective stress is decreasing:

$$v = B\left(\sigma - \sigma_i\right).$$

The decrease in velocity is, however, offset by the increase in density producing a net increase in strain rate.

The physical significance of the line $\sigma = \frac{3}{2}\sigma_i$ can now be deduced. If the structure reaches that line before σ_i increases to its steady state value, the velocity decrease will no longer be offset by the density increase and the strain rate will begin to fall (Figure 4.16B).

The sequences depicted in Figure 4.16 predict the effect of applied stress on the shape of the transient curve if the mean internal stress after loading is constant. The value of σ_i^0, however will depend upon the magnitude of the loading strain which, experimentally in the present alloys, depends upon the applied stress (page 73). Thus the vertical line in Figure 4.16 at σ_i^0 should actually be sloped to the right.

It is now possible to evaluate the changes in shape of the creep transients of the In alloys (Figure 4.7 and 4.8) in relation to the mechanical history diagram.

Consider the 17% In alloy which shows (at .95 T_m) a change in transient from normal to sigmoidal with increasing

stress. At .8 T_m the transition is from normal to inverted to sigmoidal. At .7 T_m a single inverted curve was found. Normal transients were found at .6 T_m. All these trends can be explained if the initial internal stresses (after the loading strain) of the specimens had values as shown in Figure 4.17A relative to the zones of the diagram. The initial internal stress is shown as increasing with creep stress as discussed above. Thus at all stresses, the internal stress will increase during transient creep reflecting an increasing dislocation density except at .6 T_m. As stress is increased at constant temperature, the predicted transients are: normal, sigmoidal, inverted, normal.

For the 9.5% In alloy, the suggested positioning of the σ, σ_i^0 points relative to the zones is similar (Figure 4.17B). Since only one sigmoidal type curve was found in this alloy at .8 T_m and σ = 1.52 MPa, the intersection points of the σ_i^{ss} and $\frac{3}{2}\sigma_i$ lines must be close to the projected $\sigma - \sigma_i^0$ curve. Thus there is a narrow stress range where sigmoidal and inverted curves can be found. The 3.5% In alloys all had normal type transients so their σ, σ_i^0 points should all lie within one or both of the central zones (Figure 4.17C).

The sequence of these three figures seems to suggest that the σ_i^{ss} curve is shifted to the right with increased In content. The position of the σ, σ_i^0 point should be

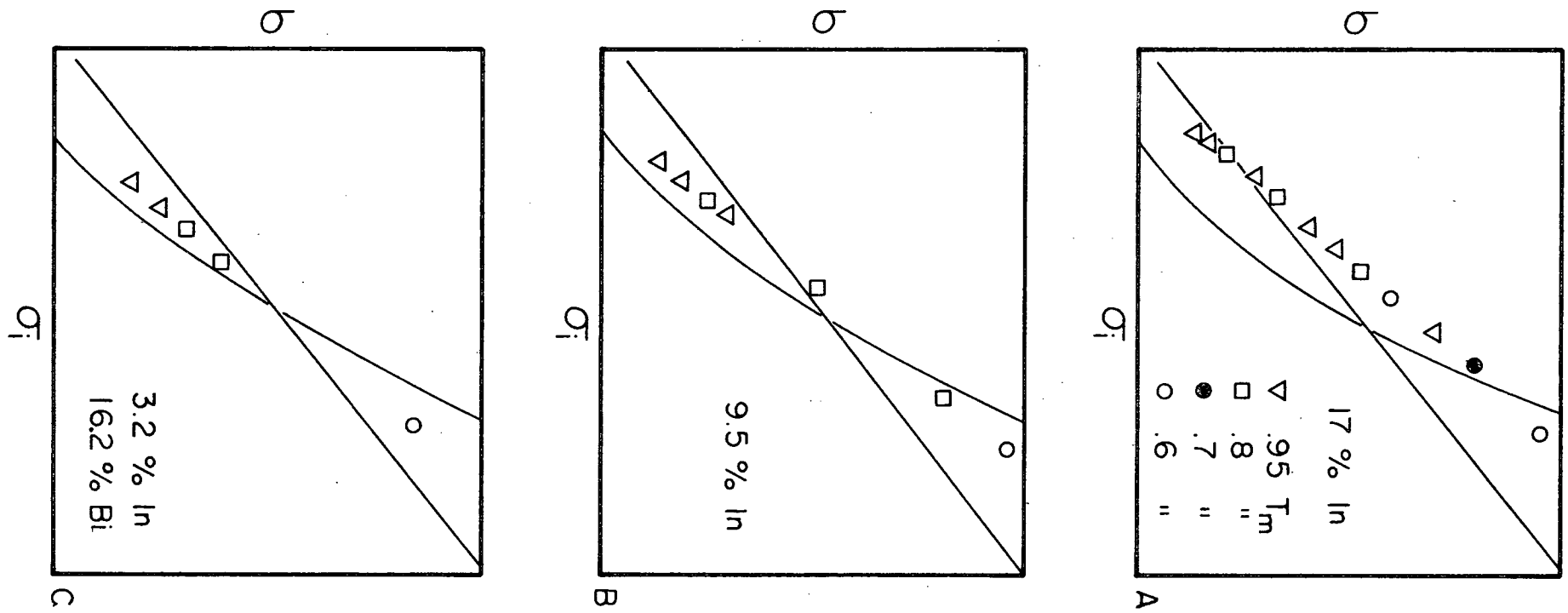

Figure 4.17. Suggested creep stress versus internal stress values in mechanical history diagram for 17, 9.5 and 3.2% In and 16% Bi alloys.

relatively invariant with alloy content since the loading strain did not vary appreciably with alloying.

The transients of the "glide controlled" 16% Bi alloy can also be explained by the mechanical history diagram if its σ, σ_i^0 are positioned as in Figure 4.17C since all transients were normal type.

The transient behaviour of the "glide" alloys can be explained satisfactorily by the combined glide-recovery model with the movement of dislocations controlled by solute atmosphere interactions. However the occurrence of plastic loading strains in these alloys is not compatible with the model. In parallel with the simple glide theory, the actual movement of the dislocation is time dependent or thermally activated, therefore no strain should occur during the fast $\dot{\sigma}$ of the initial loading.

SUMMARY

In this chapter the initial transient portion of the creep curve; the loading strain and primary creep, has been discussed. Several inconsistencies between these results and the previous classification based on the steady state region alone have been found:

1) The "glide controlled" 16% Bi alloy did not behave as expected for a Class I alloy: loading strains and normal transients prevailed at all stresses and temperatures. Classification of this alloy as "glide controlled" is questionable.

2) The other "glide" alloys, 3.2, 9.5 and 17% In, displayed some non-normal transients, as expected, but they also had large loading strains and a primary region of equivalent extent to "recovery" alloys.

The simple theories of glide and climb were not adequate to explain the transient behaviour of any of the alloys. The simple glide theory can account for neither the large loading strains nor the sigmoidal transients of the In alloys. The simple climb theories do not predict the occurrence of the normal transients common to the Bi alloys.

The refined theories were more successful in dealing with the results. The combined glide-recovery theory could qualitatively account for the transients in the "glide controlled" In alloys and the 16% Bi alloy. The large loading strains in these alloys were not consistent with this explanation, however. The rearrangement theory can also qualitatively explain the behaviour of the Class II Bi alloys.

The conclusions are outlined in the summary chart.

Table 4.1

Summary Chart

	Theory	Alloys	Stress Exponent	ε_0	Primary Creep	Athermal σ-ε	Δ_σ Transients
CLASS I -GLIDE	Simple Glide	3.2 In	✓	X	X		
		9.5 In	✓	X	X		
		17 In	✓	X	X		
		16 Bi	✓	X	X		
	Glide-Recovery	3.2 In		X	✓		
		9.5 In		X	✓		
		17 In		X	✓		
		16 Bi		X	✓		
CLASS II -RECOVERY	Simple Climb	1.3 Bi	✓	✓	X		
		8.8 Bi	✓	✓	X		
		16 Bi	X	✓	X		
	Rearrange-ment	13. Bi	✓	✓	✓		
		8.8 Bi	✓	✓	✓		
		16 Bi	✓	✓	✓		

Chapter 5

STRESS CHANGES

This chapter will be concerned with the strain effects produced by increases or decreases in the creep stress $\pm\Delta\sigma$ after steady state is established. The strain-time response can be divided into: 1) strains produced simultaneously with the stress change and 2) transient strains prior to the restoration of steady state. The initial transients, studied in Chapter 4, are just a special case of such a stress change; the $\dot{\varepsilon}_s$ before the change equals zero and the stress is increased from zero to σ_c. However, the results of stress changes in this chapter will be more indicative of the structures and mechanisms of high temperature deformation unlike the initial transients which reflect the response of fully annealed structures.

The stress increases, if performed rapidly enough, can produce an "athermal" strain response which contains minimal time dependent strain. The strain rate during such a rapid test depends only upon the rate of stress increase ($\dot{\sigma}$).

The four theories already discussed make different predictions about these athermal strain responses as well as the transient shapes after stress increases or decreases. For instance, the glide or reaction rate theories predict no plastic athermal strain until the stress increase exceeds a threshold stress associated with, for example, the breakaway of the dislocations from their atmospheres. On the other hand, in alloys controlled by recovery mechansims, some plastic athermal strain will be anticipated for any stress increase. Further, simple glide theories predict an increasing $\dot{\varepsilon}$ transient after the stress increase but simple climb theories do not predict transients of any shape.

Both the results and discussion portions of this chapter will be subdivided into 1) the athermal strain tests and 2) the transients after increases or decreases in stress.

RESULTS

Athermal Strain Tests

Stress increases were performed in two ways; rapid or "instantaneous" increases effected by removing quickly small counterweights, and slow or "continuous" increases done by a flow of glass beads directly into the load pan. A series of instantaneous increases were performed on the same sample using different values of the stress increase $\Delta\sigma$.

The added stress was applied only long enough to record the strain response. To allow the structure to equilibrate back to its steady state configuration a certain amount of creep was allowed before a new $\Delta\sigma$ was applied. The measured athermal strain $\Delta\varepsilon$ was found to be independent of such a strain history within the accuracy of the measurement (Figure 5.1).

Because of the high stress rates achieved in the rapid increases all strain responses were measured by the storage oscilloscope (Figure 5.2). A typical trace consisted of three regions:

1) a nearly horizontal portion indicative of the steady-state strain rate,

2) the "athermal" region of high strain rate during which the stress was increasing, and finally

3) a decreasing strain rate transient region after the additional stress was fully applied.

In this final portion small amplitude oscillations were usually evident probably caused by a slight acceleration overload from parts of the creep machine. The end of the athermal region was defined by an approximate extrapolation through these oscillations (Figure 5.3).

The elastic strain ($\Delta\varepsilon_e$) included in the athermal strain was estimated by performing stress increases at an applied stress well below the usual creep stresses. Such

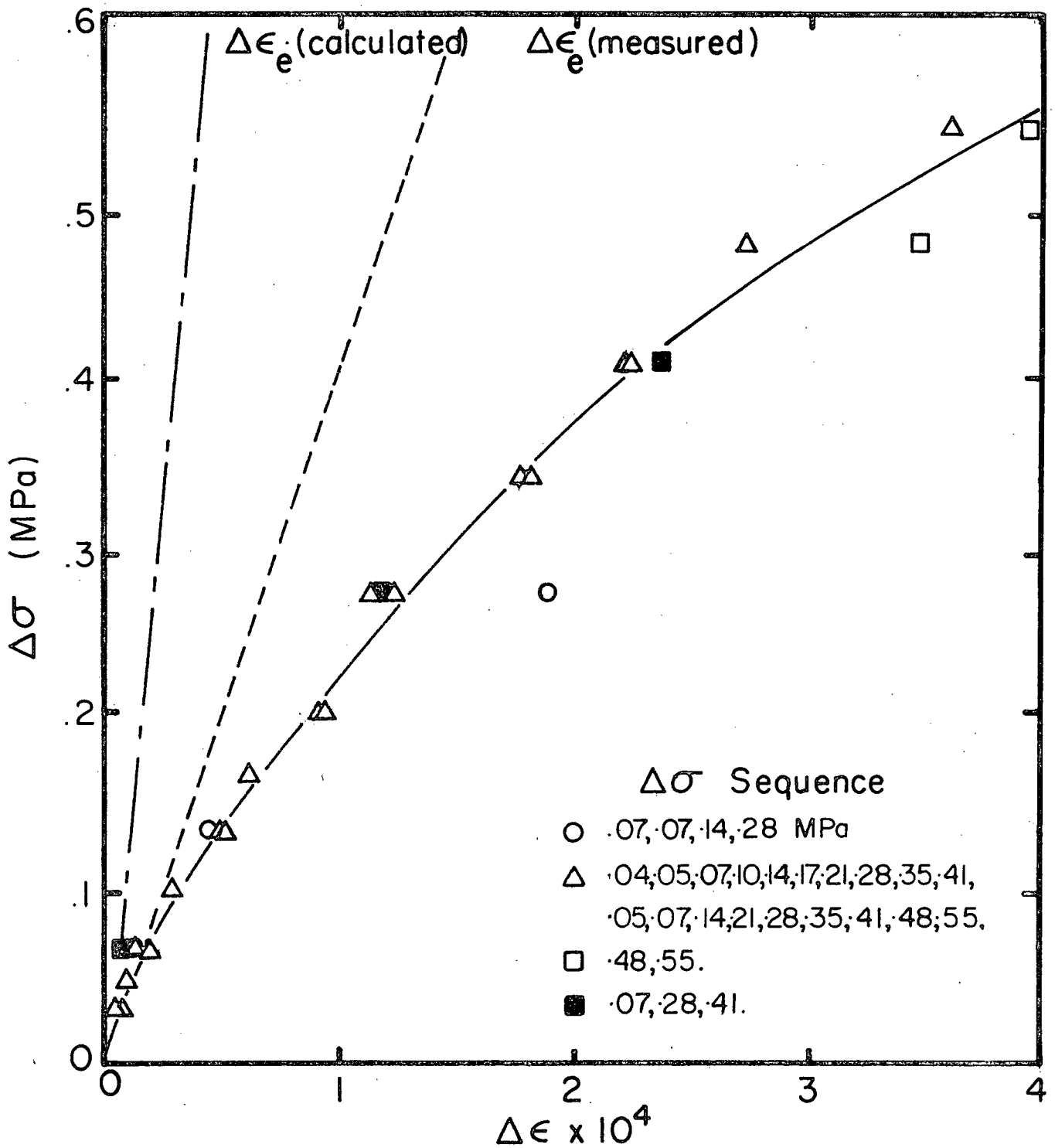

Figure 5.1. Rapid stress increase versus athermal strain for 17% In alloy at .6 T_m and σ_c = 10.35 MPa with different stress increase sequences.

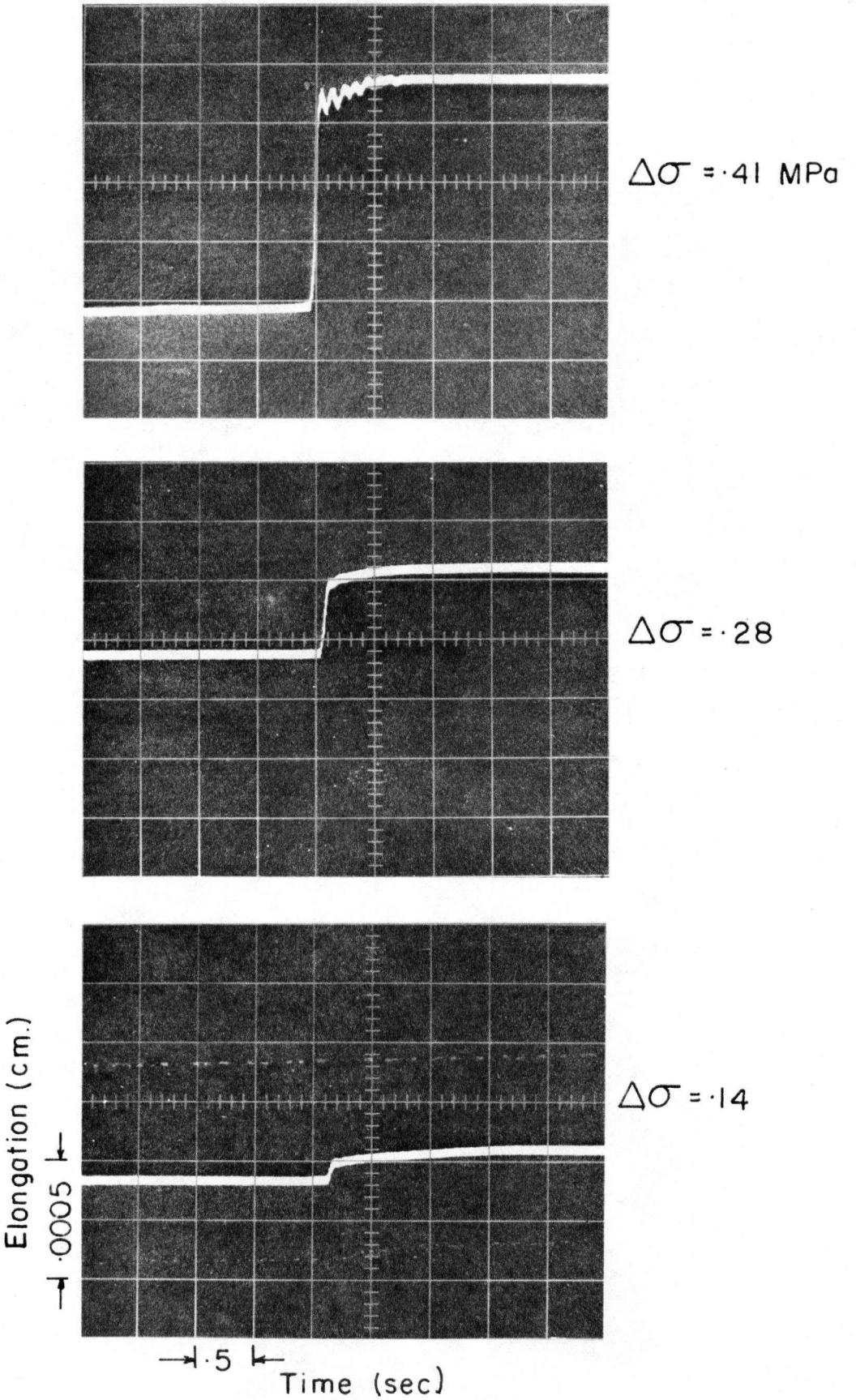

Figure 5.2. Typical strain-time responses for rapid stress increases.

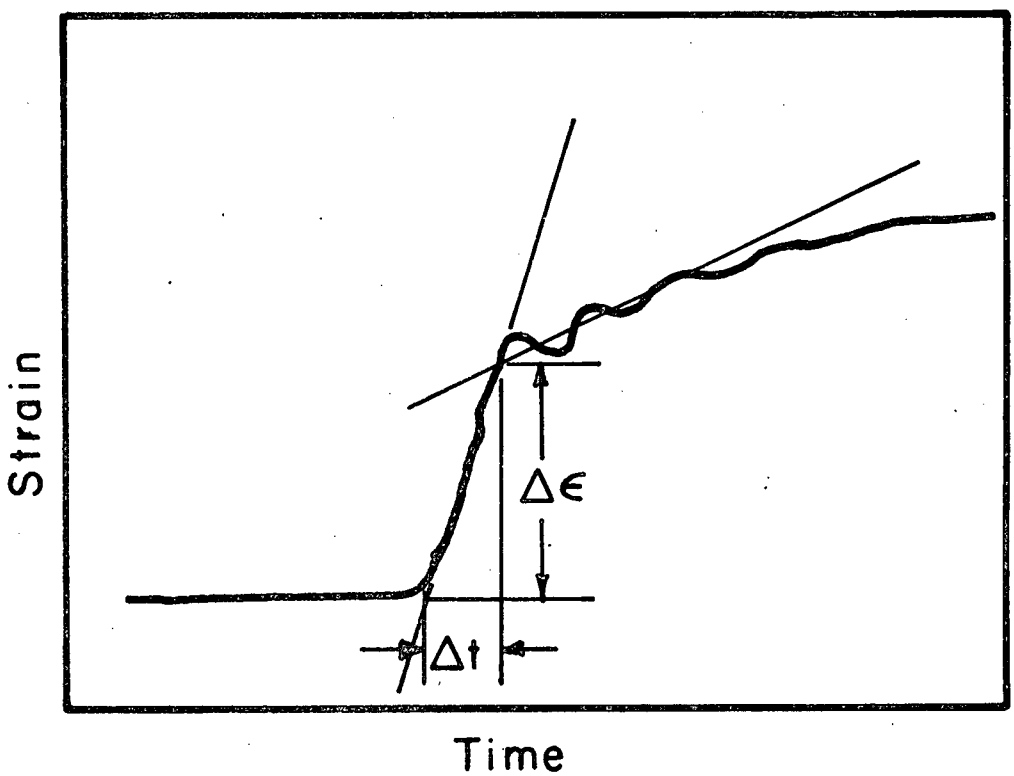

Figure 5.3. Method of athermal strain measurement from strain-time curves for rapid stress increases.

elastic measurements can be done only at low temperature, since the creep stress at high temperautres was too close to the minimum stress dictated by the machine design. These measured elastic strains contained a significant contribution from machine deflections (Figure 5.1). The use of these low temperature elastic measurements for comparison with the high temperature plastic results is thus justified, since this machine component of the total elastic strain will not change with temperature.

The plastic 'athermal' strain could also contain some time-dependent strain $\Delta\varepsilon_{pt}$ even at these very high stress rates. An estimate of $\Delta\varepsilon_{pt}$ can be made by averaging the strain rates before and just after the stress increases and multiplying by Δt, the time of the stress pulse (Clark and Alden, 1972). Such calculations for the present data revealed that $\Delta\varepsilon_{pt}$ was a small fraction of the total $\Delta\varepsilon$ ($< 3\%$). Accordingly, it has been ignored in all presentations of the data.

The continuous stress increase tests gave results consistent with the rapid increment tests. The magnitudes of the strain responses were very close (Figures 5.4 and 5.5) despite the difference in the time span of the stress increase (15 seconds as opposed to .05 seconds for $\Delta\sigma$ of 1.04 MPa). This result emphasizes the unimportance of time dependent strain during the rapid increases. The continuous

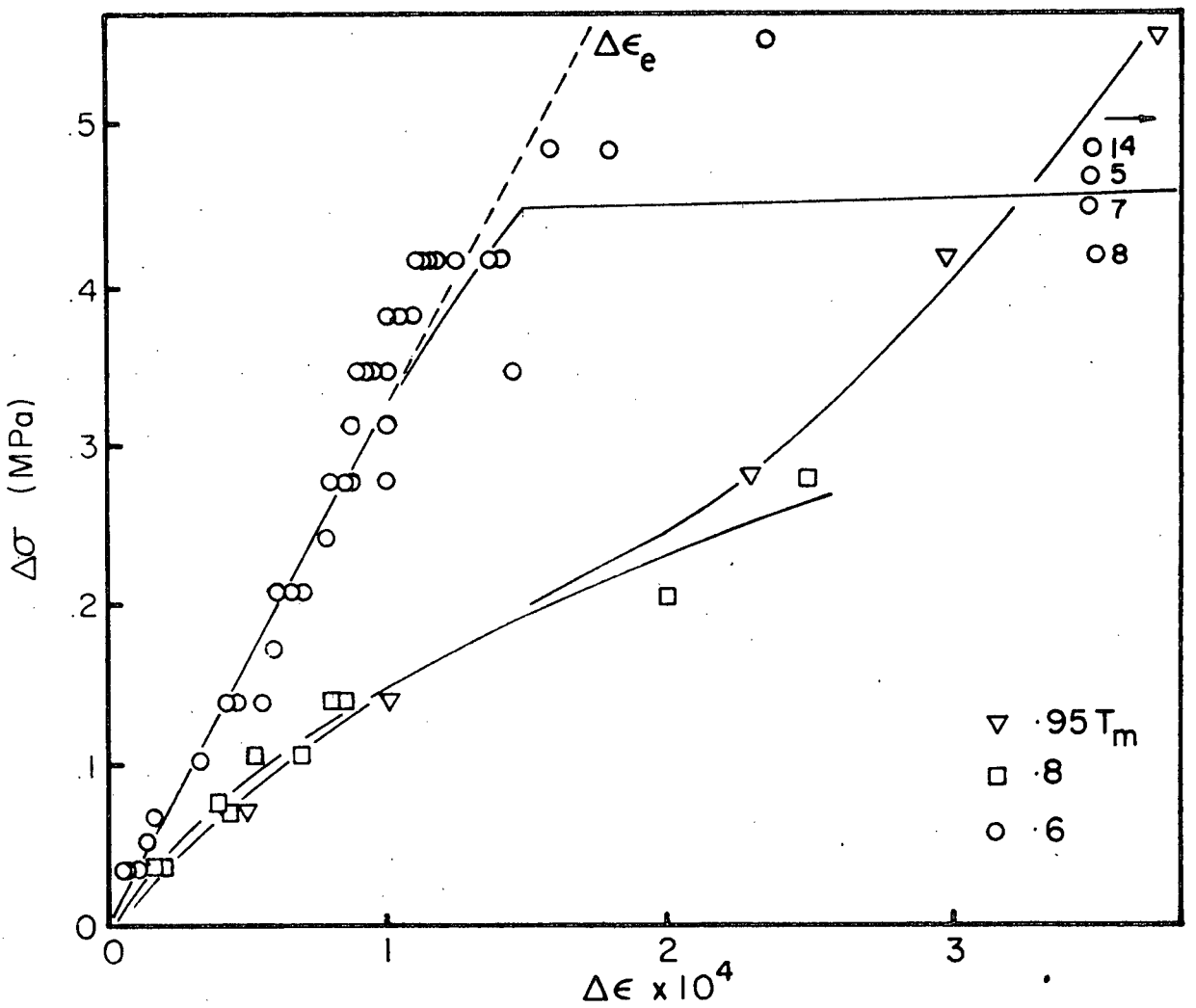

Figure 5.4. Rapid stress increase versus athermal strain for 16% Bi alloy.

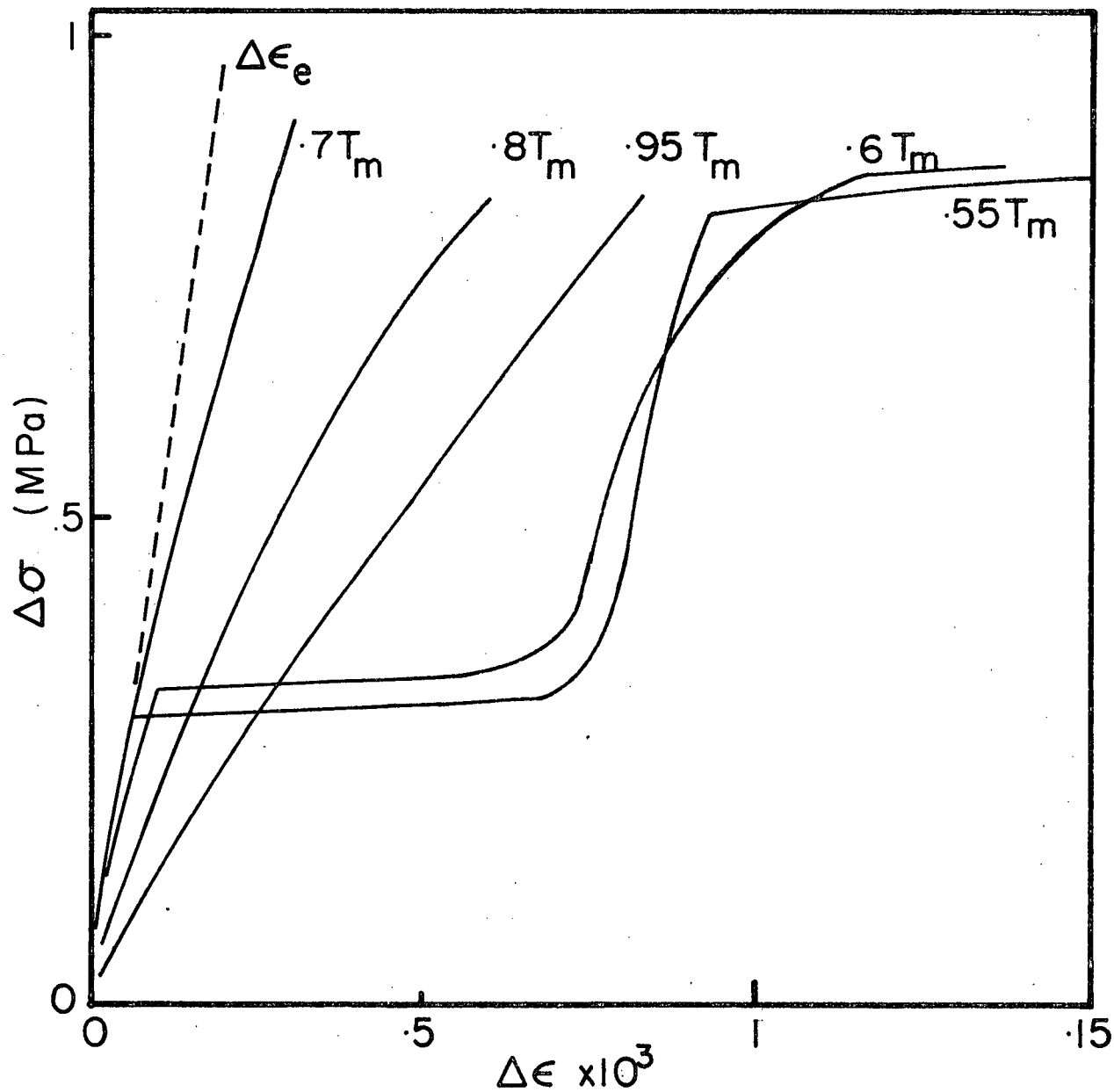

Figure 5.5. Continuous stress increase versus strain for 16% Bi alloy.

increases were supplementary to the rapid increases for confirmation of trends with stress or temperature.

Magnitude of Stress Increase. Some plastic athermal strain nearly always occurred even at very low values of $^{\Delta}\sigma$ (Figures 5.4 and 5.5) with either the rapid or continuous tests. There was very little evidence for the existence of a threshold stress (except for temperatures $\leq$ .6 T_m); the slope of the $^{\Delta}\sigma$ versus $^{\Delta}\varepsilon$ curve decreased continuously.

Temperature. Both rapid and continuous stress increase tests were done for all alloys at temperatures from .5 to .95 T_m and $^{\Delta}\sigma$ values between 0 and 1.04 MPa (Figure 5.6 and 5.7 — only the rapid increase tests are shown). To facilitate study of the trends in these data, the athermal strain at $^{\Delta}\sigma$ of .69 MPa was extracted from the figures and plotted versus temperature (Figures 5.8 A,B,C). The athermal strain versus temperature curve is u-shaped for all alloys, with a minimum strain response at approximately .7 T_m. There was little difference in the strain response between the alloy systems.

Sometimes the strain response was irregular, particularly in the continuous tests at low temperature. The material would exhibit very distinct bursts of strain as the stress increased despite the rate of stress increase being constant. Two good examples were found in the 16% Bi alloy

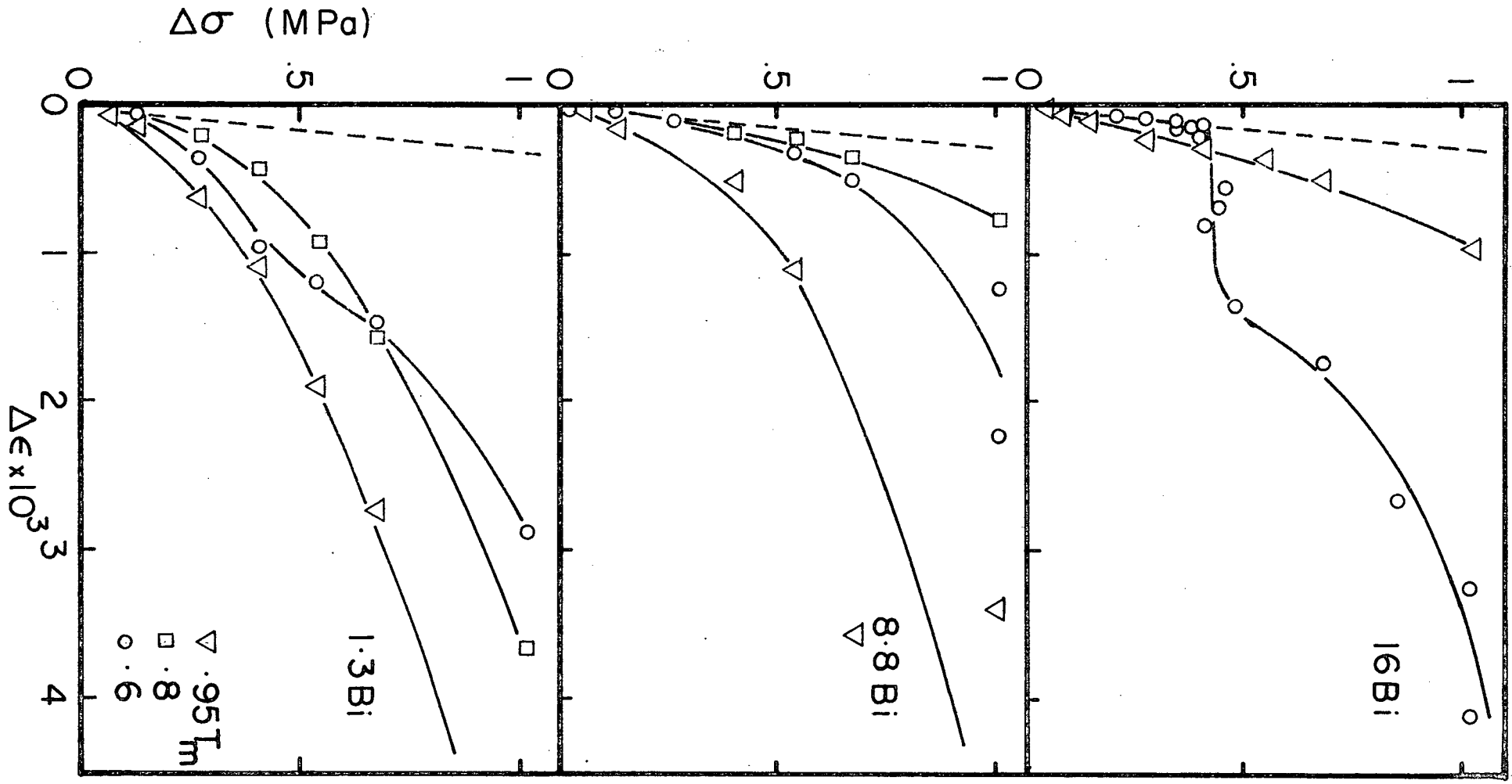

Figure 5.6. Rapid stress increase versus athermal strain for Pb-Bi alloys.

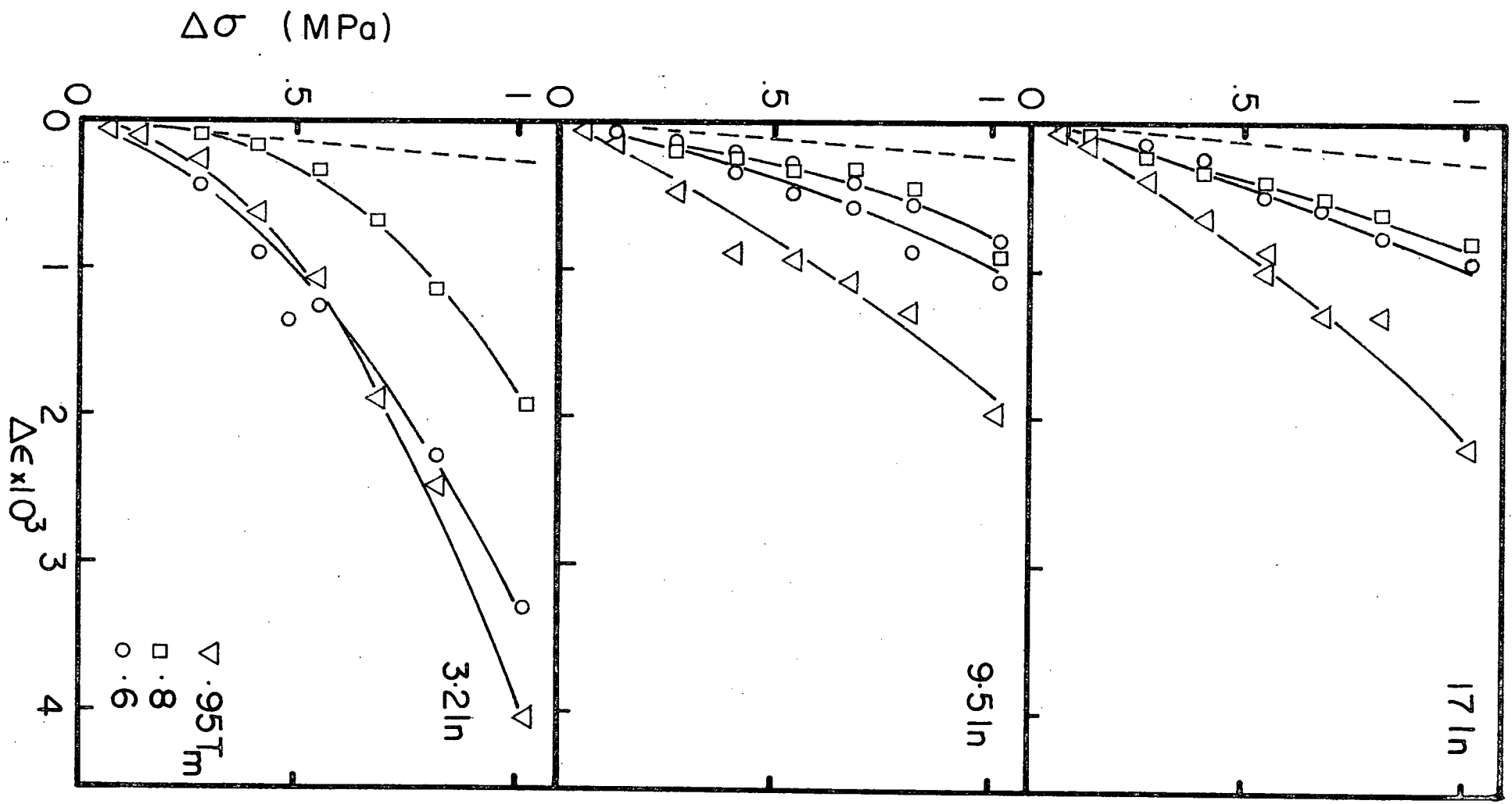

Figure 5.7. Rapid stress increase versus athermal strain for Pb-In alloys.

at .6 and .55 T_m (Figure 5.5). In both these curves there were two such strain bursts associated with two different "threshold" stresses.

The initial threshold stress decreased slightly with temperature. The "sharpness" of the strain response also increased at lower temperatures. The effect appeared over a fairly narrow range of temperature (Figure 5.9); for the Bi alloy it became evident between .67 and .65 T_m a range of about 10°C. This irregular effect was detected in all alloys (except the 3.2% In)

Solute Content. There was little difference in the athermal strain response between the two alloy systems (Figure 5.10) at equivalent temperature and stress conditions. An increase in the solute content produced a decrease in the athermal strain for the Bi system. The strain response in the In system was relatively insensitive to solute content.

Transients after Stress Increases

A decreasing strain rate transient region of very short duration (< 1 sec) was noted after rapid stress increases (Figure 5.2). This section shall be concerned with the transients subsequent to this brief initial period.

Since the two alloy systems behaved quite differently in response to these stress changes, each system will

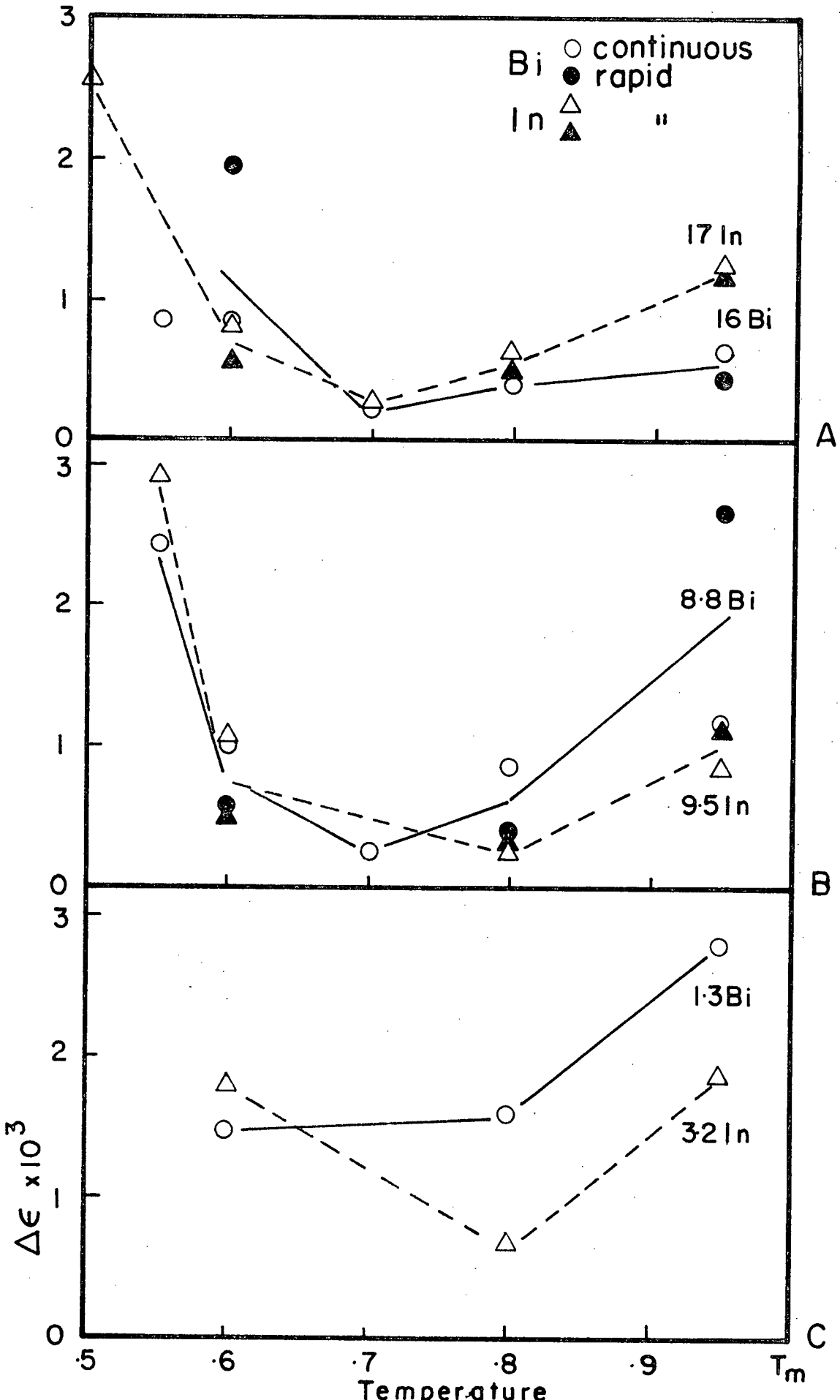

Figure 5.8. Athermal strain for $\Delta\sigma$ = .69MPa versus relative temperature for all alloys.

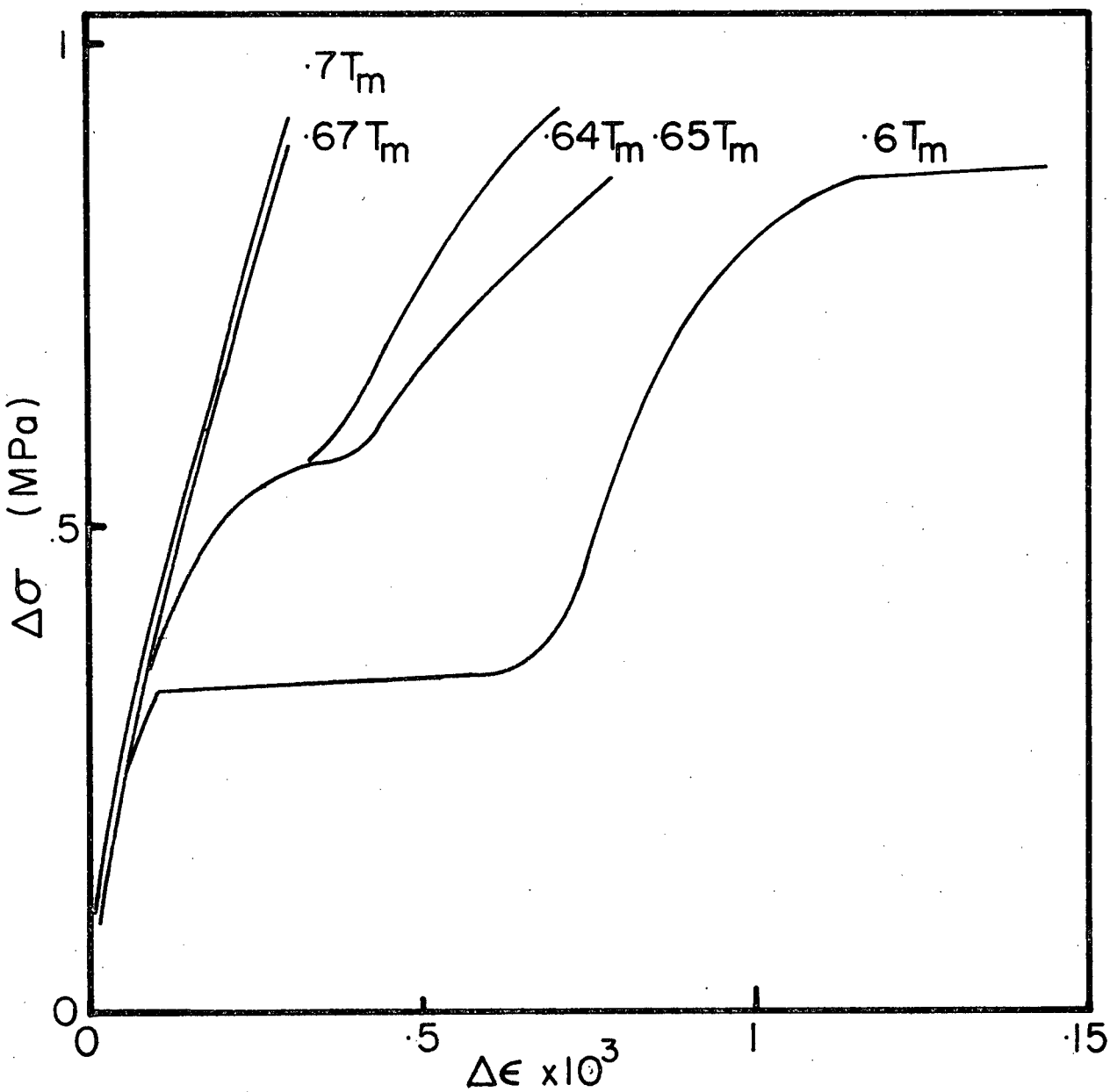

Figure 5.9. Continuous stress increase versus athermal strain for 16% Bi alloy.

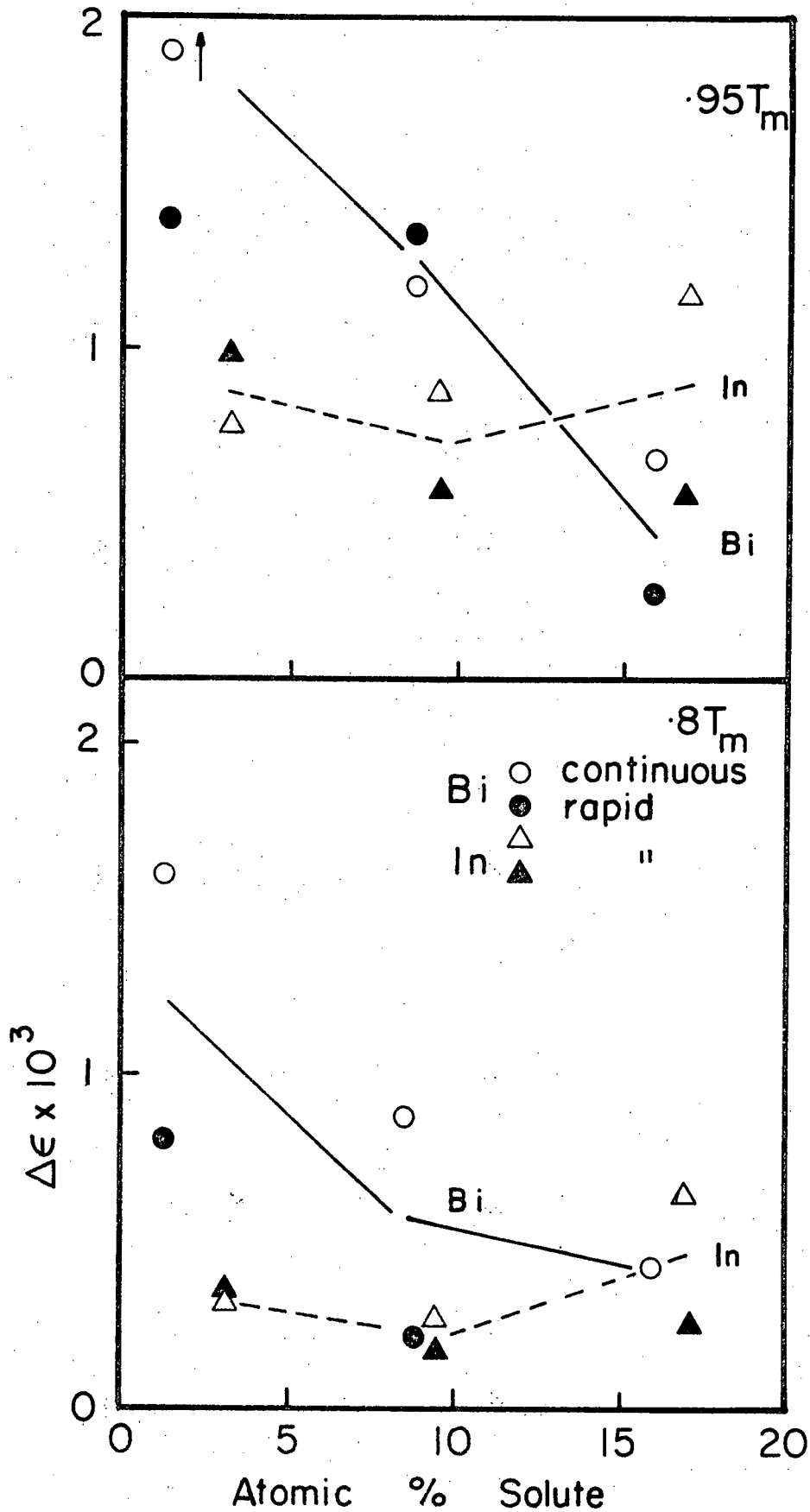

Figure 5.10. Athermal strain for $\Delta\sigma$ = .69 MPa versus solute content at two temperatures.

be considered separately. Examples of the transients will be shown to illustrate the effects of 1) creep stress, 2) the stress change $\Delta\sigma$, 3) temperature, 4) solute content.

Pb-Bi System. The three Bi alloys always displayed a decreasing rate transient. Increasing the magnitude of $\Delta\sigma$ at fixed stress and temperature did not change the nature of the transient but did produce a more pronounced and longer transient region before steady state was re-established (Figure 5.11A).

At fixed temperature and $\Delta\sigma$ the shape of the transient did not change with the magnitude of the creep stress (Figure 5.11B). Temperature also had little effect on the decreasing strain rate nature of the transient (Figure 5.11C) but lower temperatures did increase the duration of the transient region. The Bi content also had little influence on the direction of the strain rate change (Figure 5.12).

Pb-In System. The transient behaviour of the In alloys was affected by the four variables:

i) Stress Change $\Delta\sigma$. For small stress changes, the new steady state strain rate was established almost immediately. As the magnitude of $\Delta\sigma$ was increased, at fixed initial stress and temperature, inverted or increasing strain

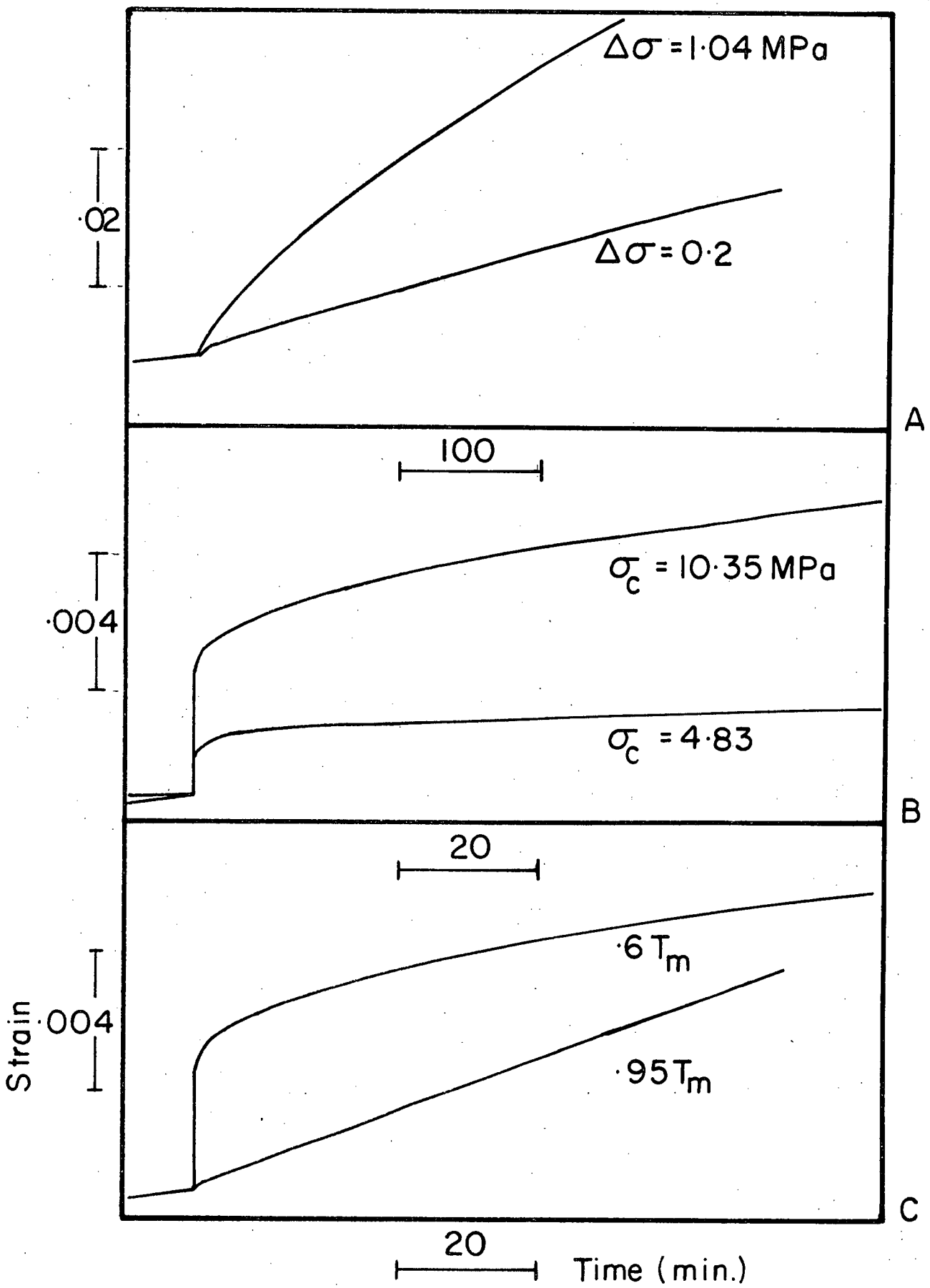

Figure 5.11. Stress increase transients for Bi alloys
A) Effect of stress increase (8.8% Bi, .8 T_m)
B) Effect of creep stress (16% Bi, .6 T_m, $\Delta\sigma \simeq 10\%$)
C) Effect of temperature (16% Bi, $\Delta\sigma$ = 10% or 20%).

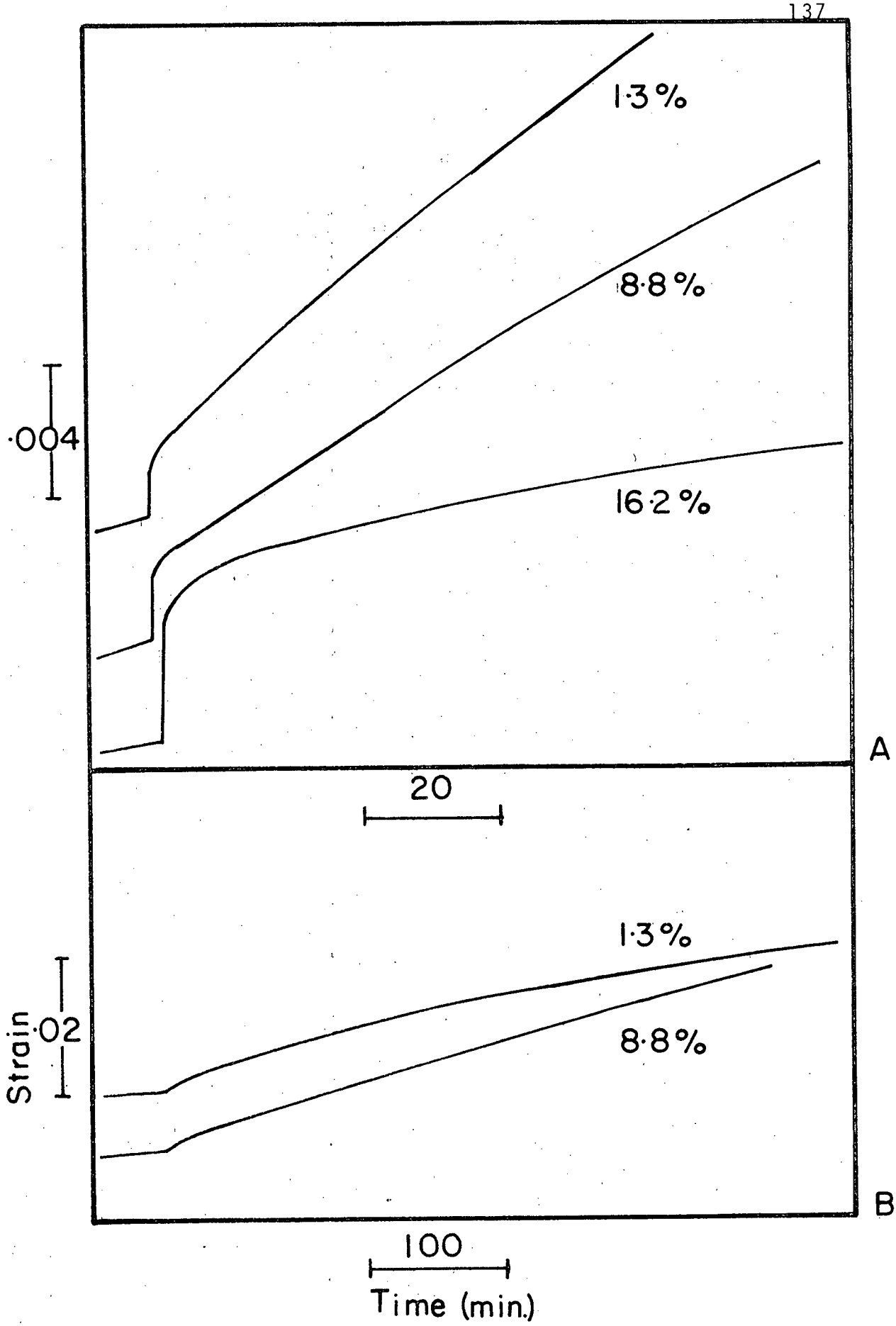

Figure 5.12. Stress increase transients for Bi alloys
A) Effect of solute content at .6 T_m, $\Delta\sigma$ = 10%
B) Effect of solute content at .8 T_m, $\Delta\sigma$ = 10%.

rate transients began to appear (Figure 5.13A). At the larger stress changes, the difference between the initial creep rate after the change and the new steady state rate was more pronounced.

ii) Stress. The inverted transients were not universal. At some stresses and temperatures, normal transients were found, i.e. at .8 T_m and low stress (Figure 5.13B).

iii) Temperature. At the low temperature (.6 T_m) normal transients were found for all stresses and stress changes (Figure 5.14). The inverted transient was most pronounced in the middle temperature range (.8 T_m) but was less obvious at .95 T_m.

iv) Solute Content. Alloy content also influenced the inverted to normal transition. The dilute alloy (3.2% In) produced only normal transients at all temperatures and stresses studied. The 9.5 and 17% In alloys in the higher temperature region experienced the inverted transients (Figure 5.15).

Transients after Stress Decreases

Decreases in stress were accomplished by adding by hand small counterweights to the short arm side of the lever system. Upon reduction of the stress an immediate decrease in specimen length occurred, followed by a region of

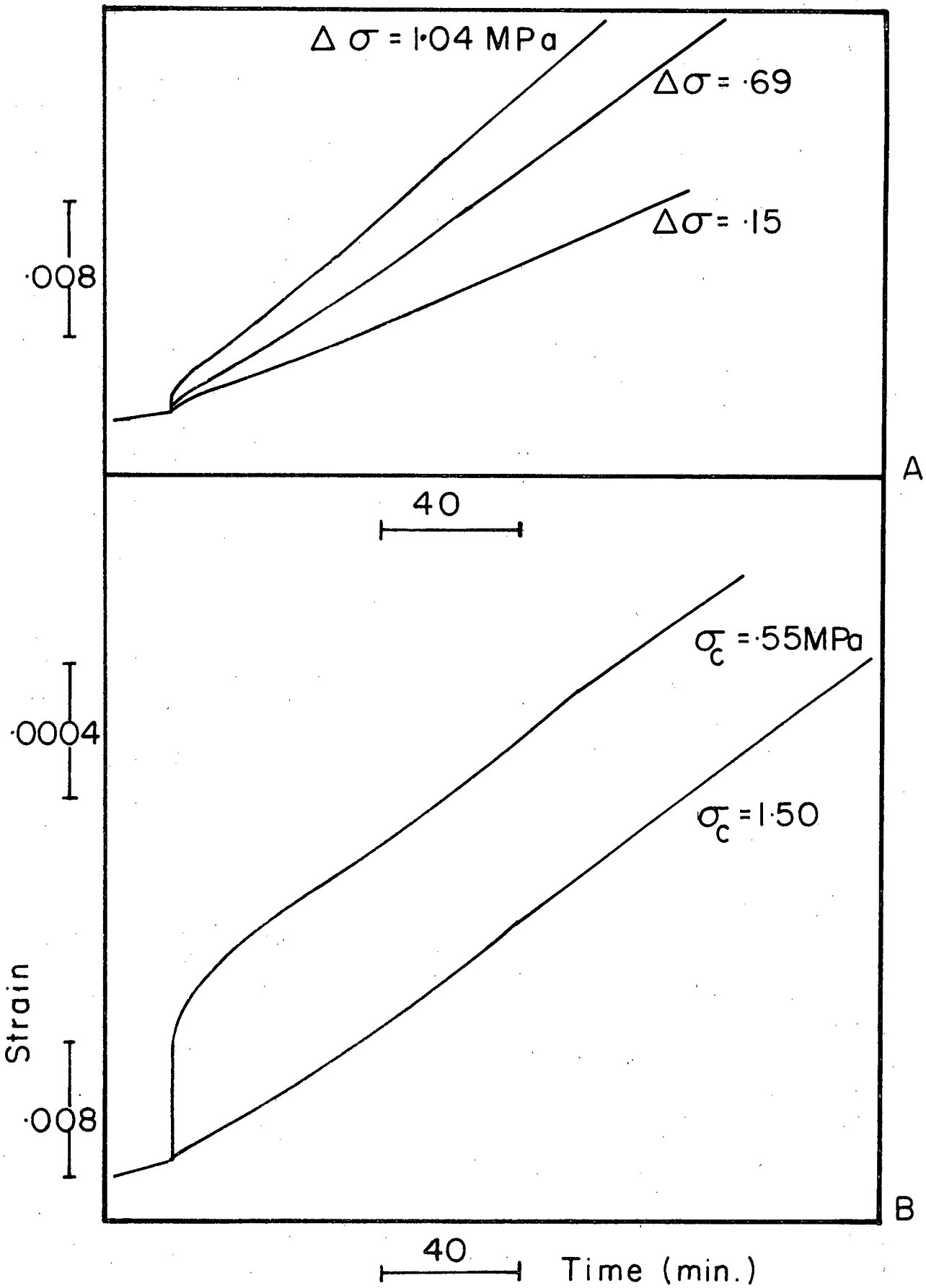

Figure 5.13. Stress increase transients for In alloys
A) Effect of stress increase (17% In, .8 T_m, σ_c = 1.5 MPa
B) Effect of creep stress (17% In, .8 T_m, $\Delta\sigma \simeq 50\%$).

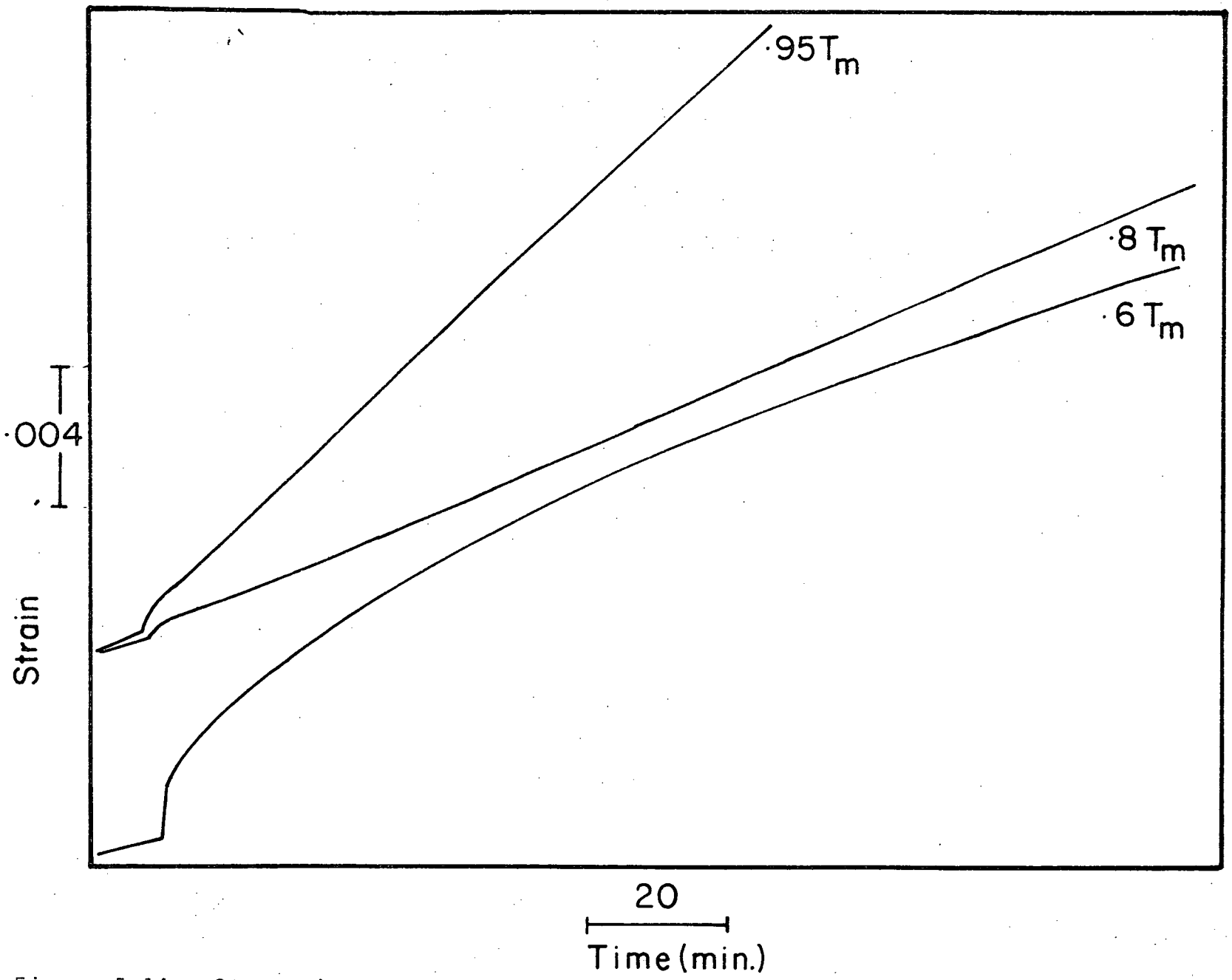

Figure 5.14. Stress increase transients for In alloys. Effect of temperature (17% In, $\Delta\sigma$ = 10 or 20%).

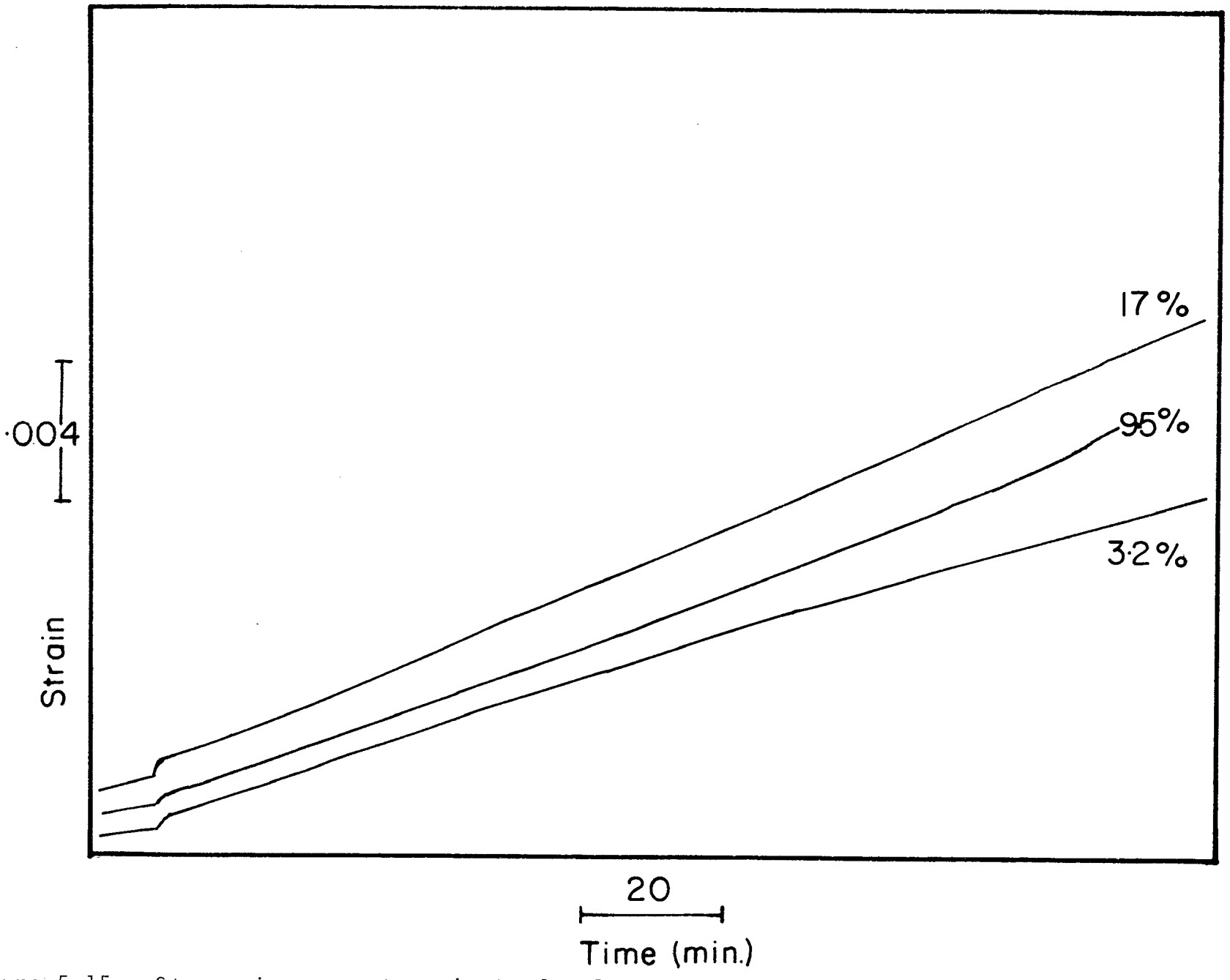

Figure 5.15. Stress increase transients for In alloys. Effect of solute content (.8 T_m, Δ_σ = 10%).

zero strain rate until measurable forward creep recommenced (Figure 5.16). The delay time $^{\Delta}t$ gave a measure of the zero strain rate portion of the curve. Two aspects of the stress decrease curves were studied: the delay time and the shape of transient after the delay time. Measurements were confined almost exclusively to the high solute, 17% In and 16% Bi alloys.

Delay Times. Considerable scatter was experienced in the delay time measurements (Figure 5.17); however some trends were detectable:

1) Increasing $(-^{\Delta}\sigma)$ produced longer delay times.

2) At .6 T_m the 16.2% Bi alloy had longer delay times than the 17% In alloy.

3) At .95 T_m the delay times were identical in the two alloys.

Transient Shape. Differences in the shape of the stress decrease transients were discovered between the 16.2% Bi and 17% In alloys (Figure 5.18), the Bi alloy having a continually increasing strain rate transient and the In showing a decreasing rate. For the Bi alloy, increasing the size of $-^{\Delta}\sigma$ produced more definitely shaped transients (Figure 5.19A). The small stress decrease actually produced a composite type curve: an increasing rate transient for a brief time followed

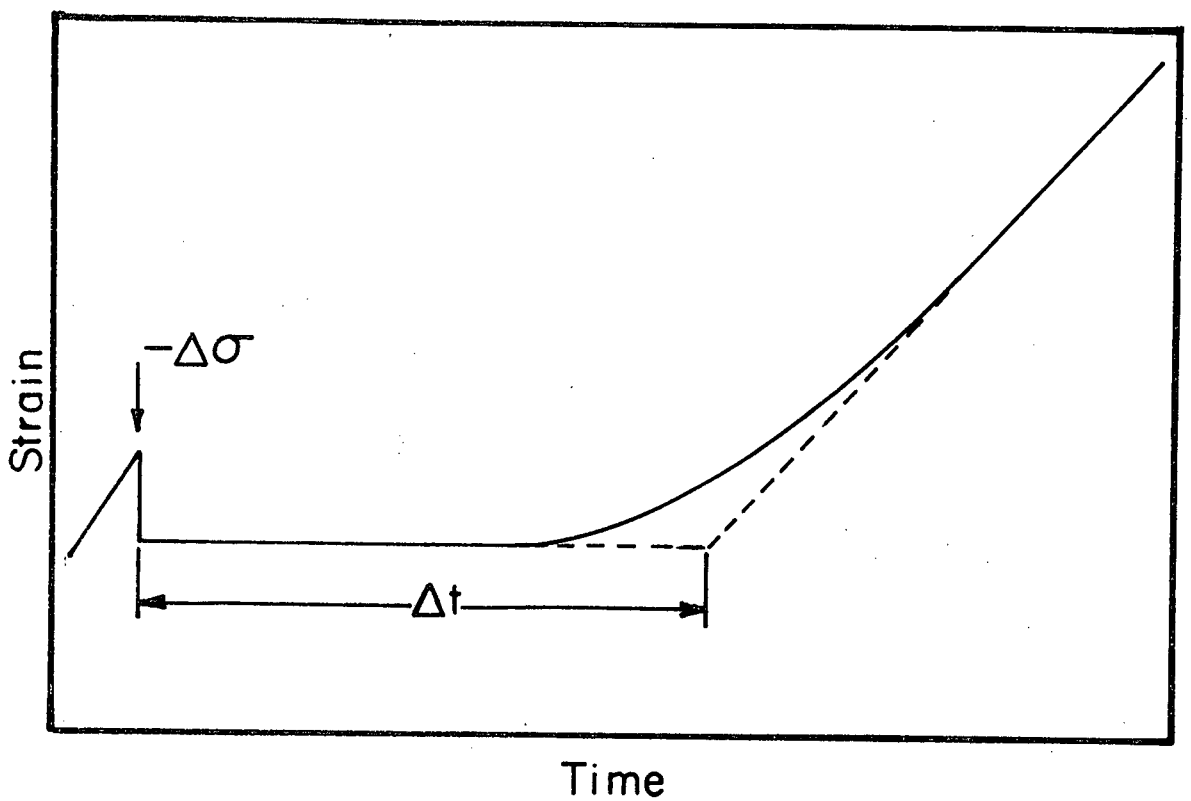

Figure 5.16. Method of measuring delay times ($^{\Delta}t$) for stress decreases.

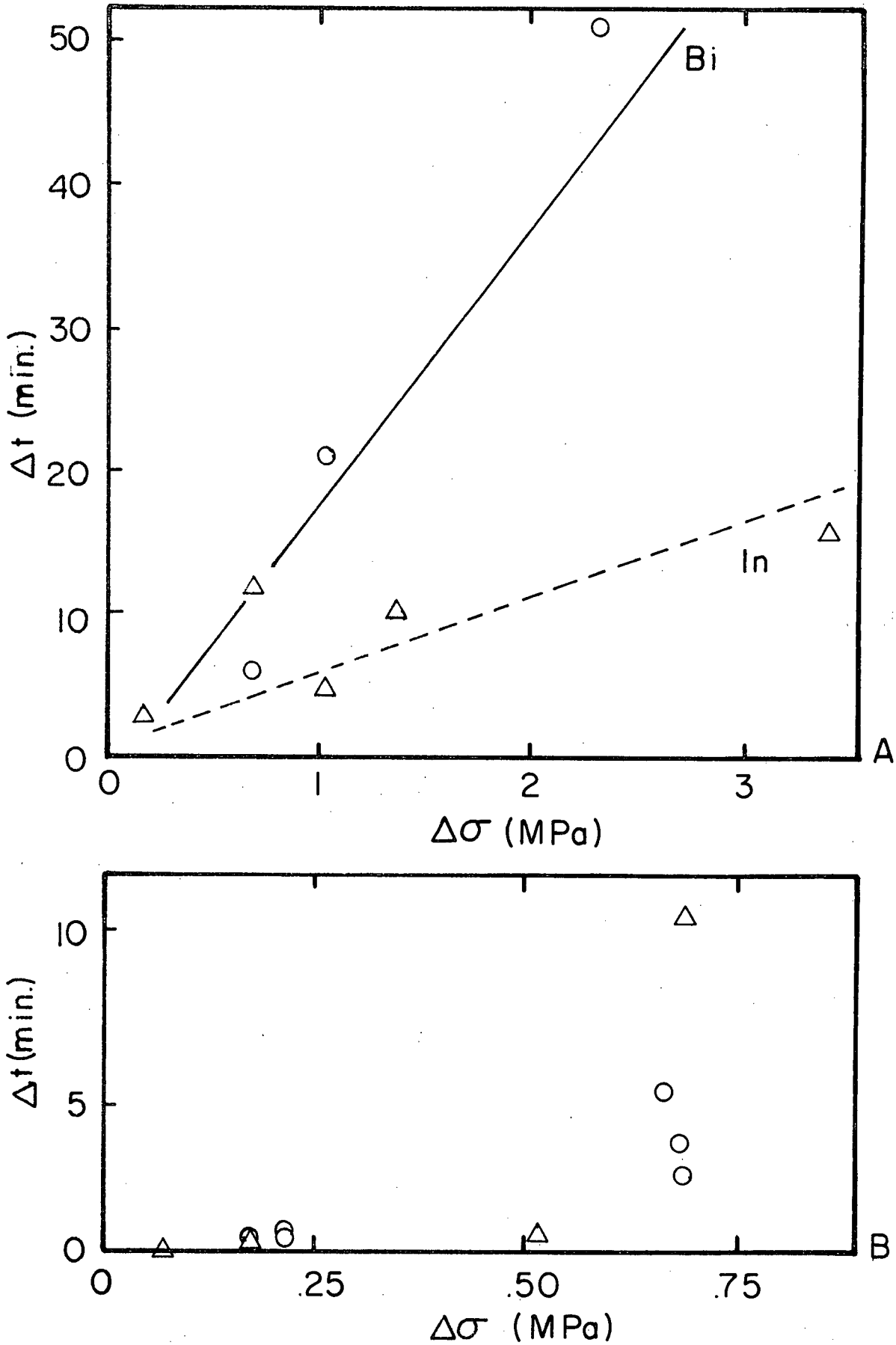

Figure 5.17. Delay time versus stress decrease for 16% Bi and 17% In alloys.
A) .6 T_m, σ_c = 10.35 MPa
B) .95 T_m, σ_c = 1.04 MPa for In

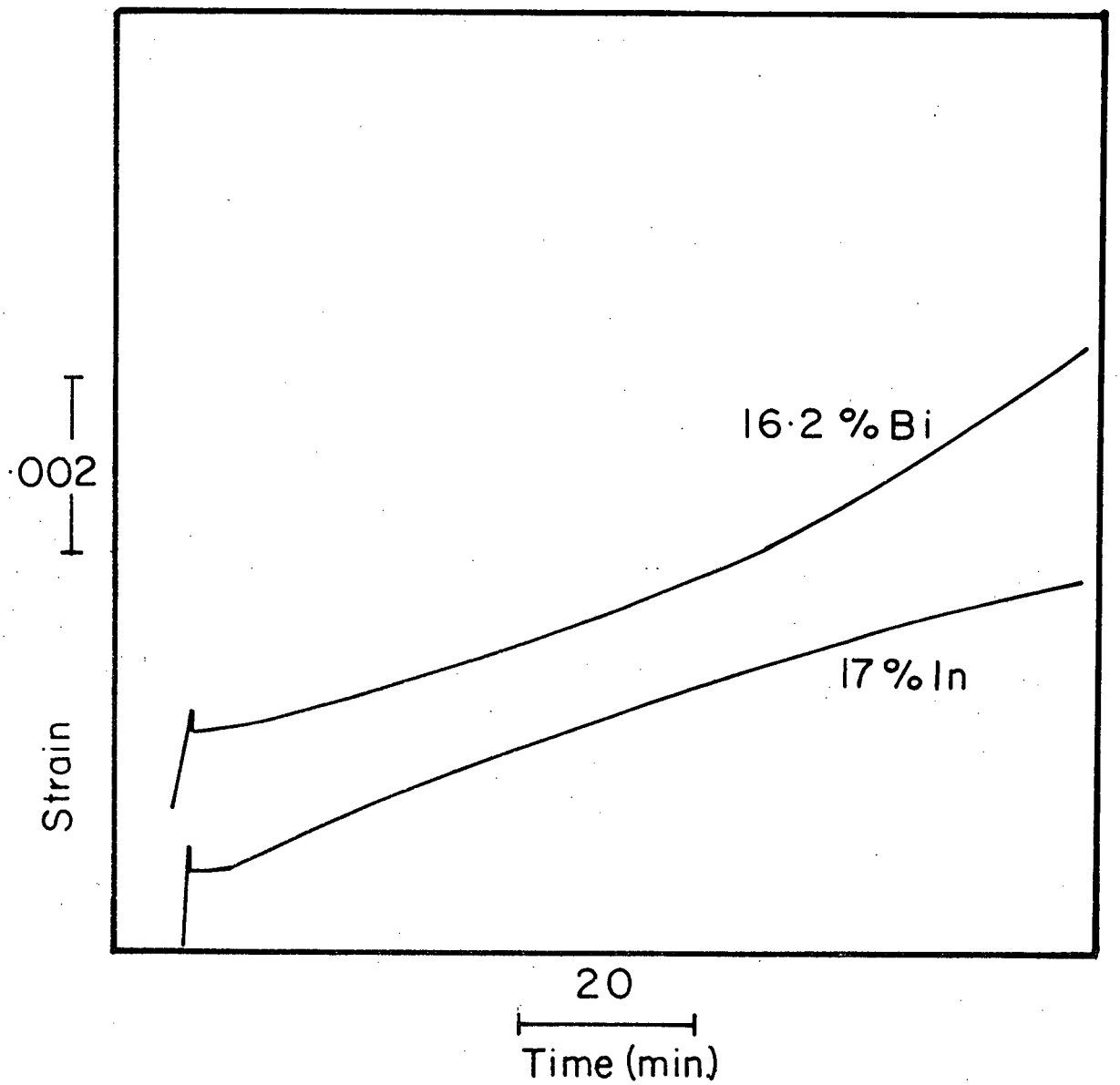

Figure 5.18. Stress decrease transients for 16% Bi and 17% In alloys (.95 T_m, $\Delta\sigma$ = -.69 MPa)

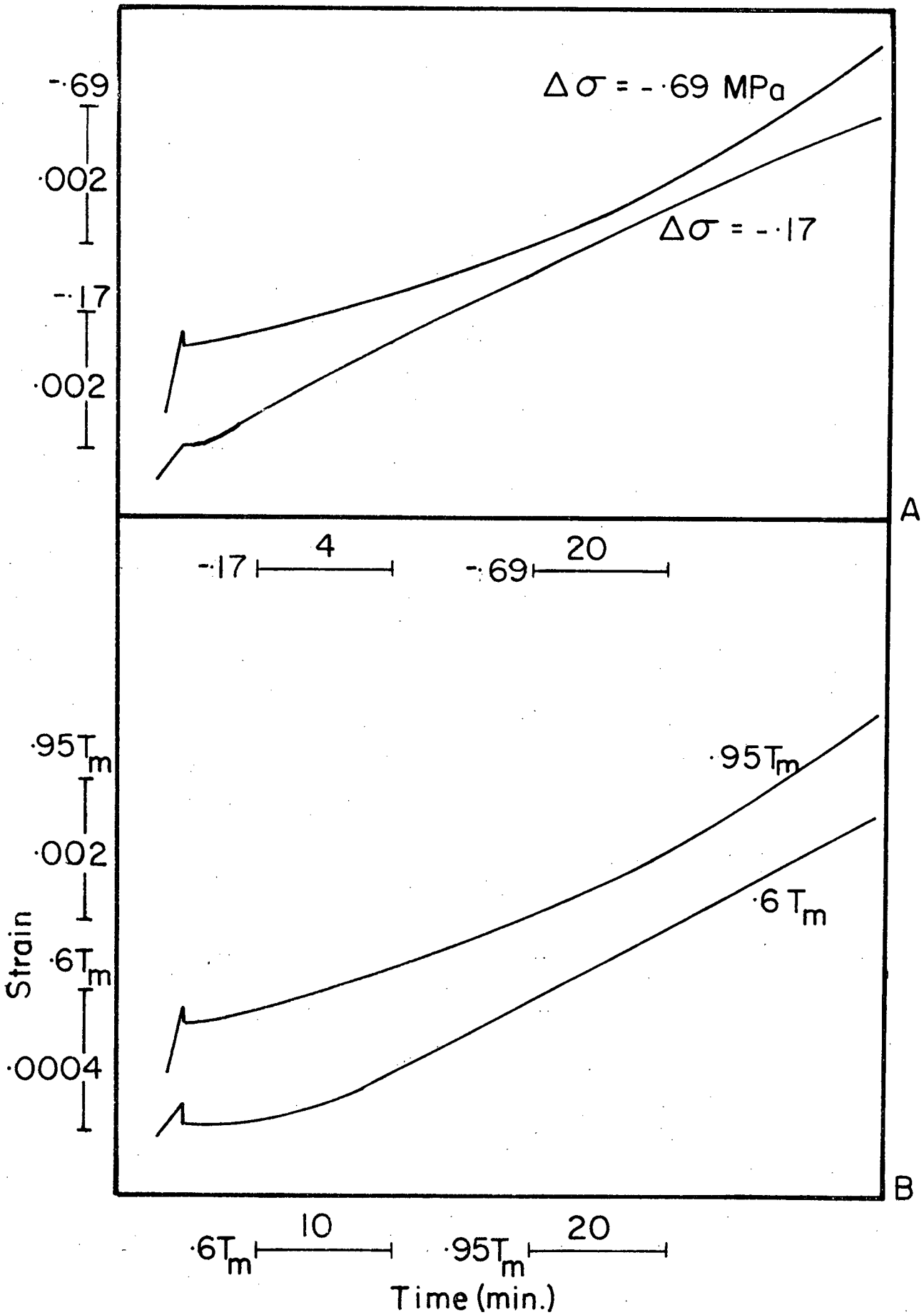

Figure 5.19. Stress decrease transients for 16% Bi alloy.
A) Effect of stress decrease (.95 T_m)
B) Effect of temperature ($\Delta\sigma$ = -.69 MPa).

by a gradual decrease in rate. Temperature did not change the shape of the transient (Figure 5.19B).

For the In alloy small stress decreases resulted in almost no transient but an immediate change to the new steady state rate (Figure 5.20A); larger decreases produced the inverted transient. The curve shape changed with temperature; the increasing rate transient occurred at low temperature, but the decreasing rate transient prevailed at higher temperatures (Figure 5.20B).

Summary

The pertinent results of this chapter are:

1. Plastic "athermal" strain occurred concurrently with the stress increases for all levels of + Δ_σ.

2. The magnitude of these athermal strain responses did not vary between the Pb-Bi and Pb-In alloys when tested under equivalent conditions.

3. The transient shapes after both increases and decreases in stress were different between the two systems under some conditions. These differences are illustrated schematically in Figure 5.21.

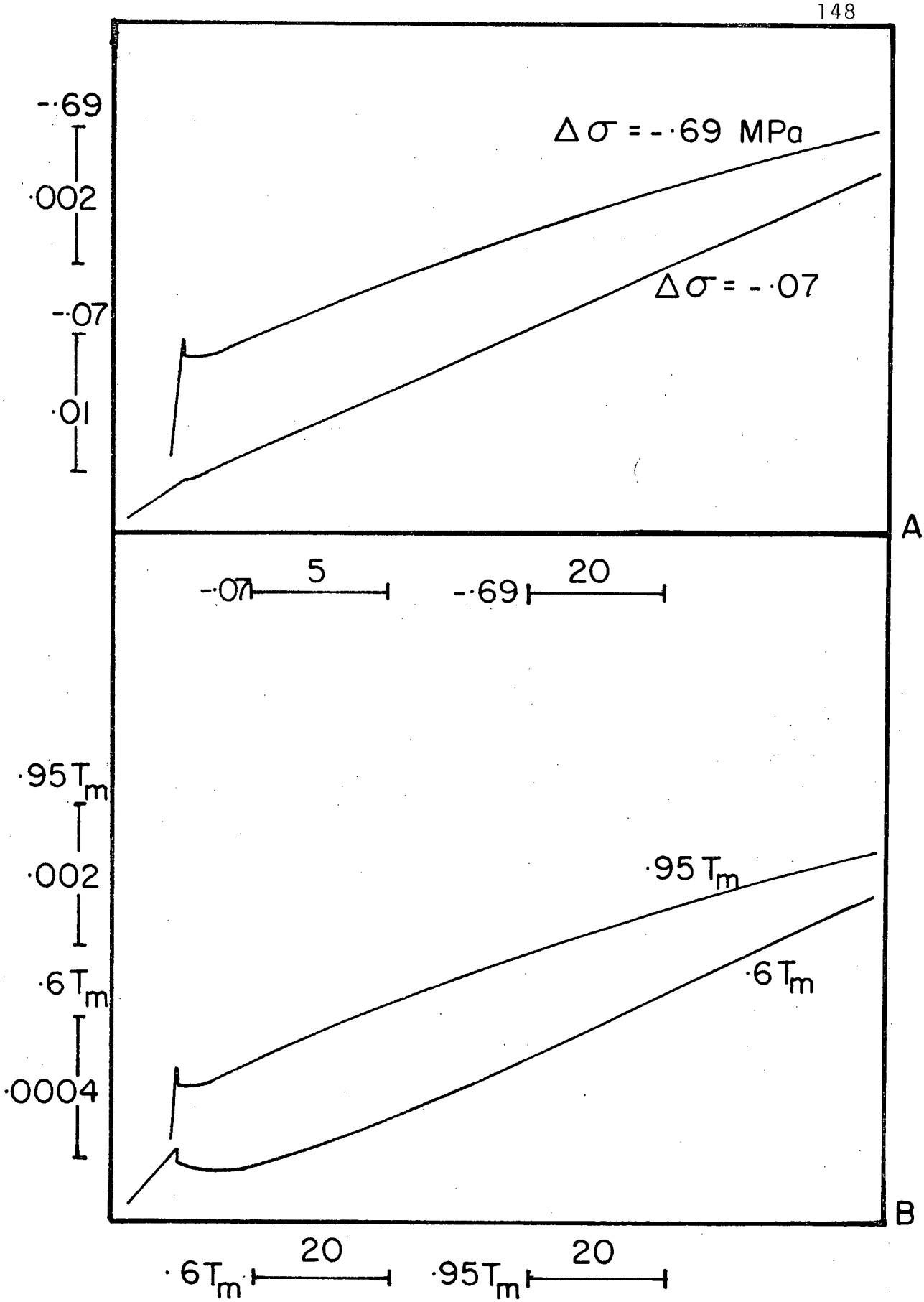

Figure 5.20. Stress decrease transients for 17% In alloy.
A) Effect of stress decrease (.95 T_m).
B) Effect of temperature ($\Delta\sigma$ = -.69 MPa).

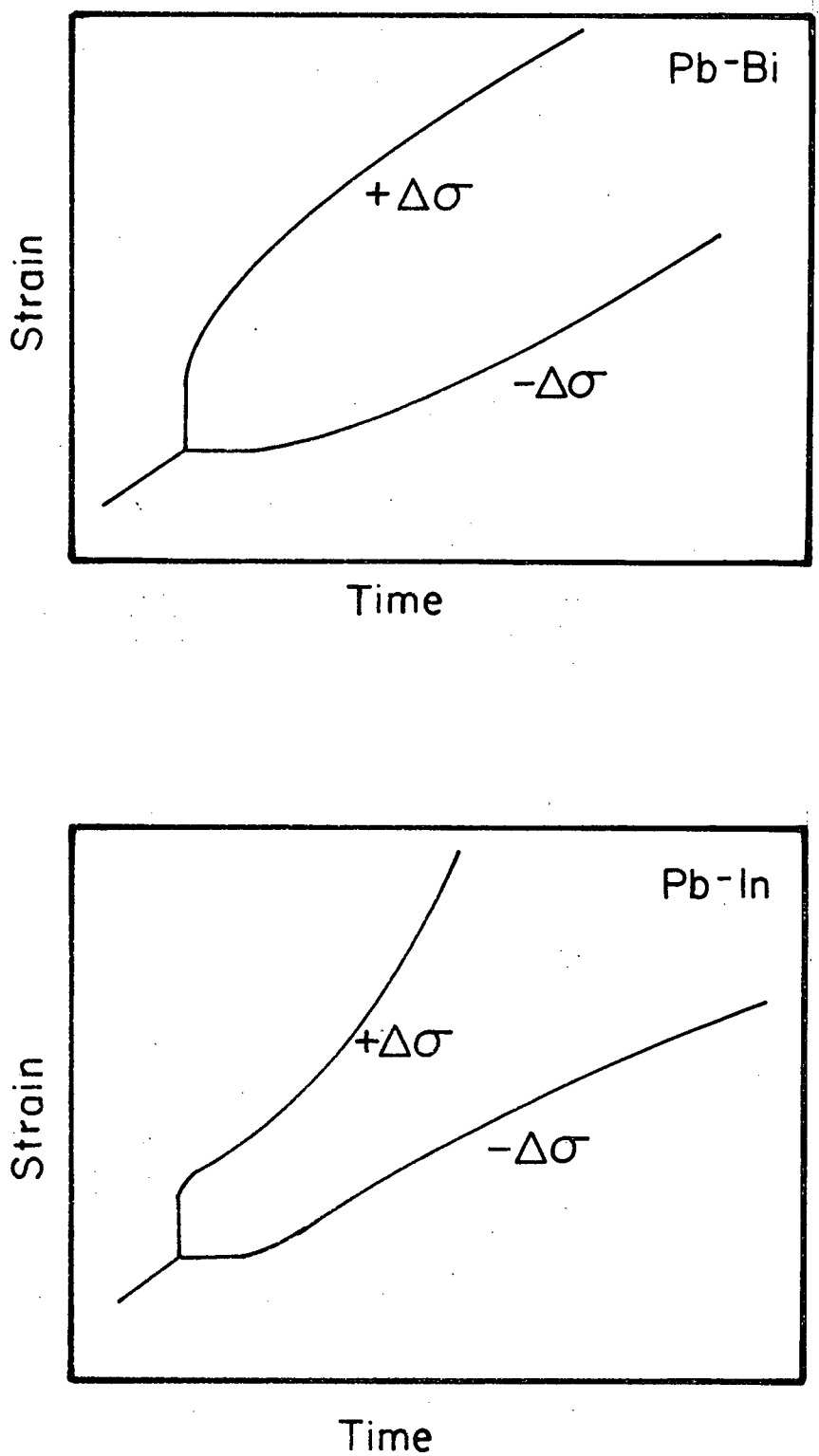

Figure 5.21. General stress change transients in Pb-Bi and Pb-In alloys.

DISCUSSION

Athermal Strain Tests

It has been shown that, during the application of the stress in rapid increase tests, time dependent strain was unimportant. The measured strain can be considered athermal: i.e. no thermally activated processes are contributing to the deformation. The curve defined by a number of these $^{\Delta}\sigma$, $^{\Delta}\varepsilon$ points (Figure 5.6 and 5.7) is equivalent to a continuous stress-strain curve at very high $\dot{\sigma}$ or at 0°K. The stress origin (at $^{\Delta}\sigma = 0$) corresponds to the creep stress and also represents the elastic limit stress for the structure before the stress change (Alden, to be published). The predictions of the theories concerning such a time-independent σ-ε curve will be considered. The recovery theories (Figure 1.3) will be treated first.

In the Weertman pile-up model, a rapid increase of stress upsets the stress balance on the source permitting generation and movement of dislocations. The amount of strain produced by these new dislocations will be restricted by the existing pile-ups. The strain hardening coefficient ($h = d\sigma/d\varepsilon$) is associated with the position and number of the pile-ups. Since $h \alpha 1/\sigma^{3/2}$ (Appendix 4) the slope of the athermal σ-ε curve should continually decrease (Figure 5.22).

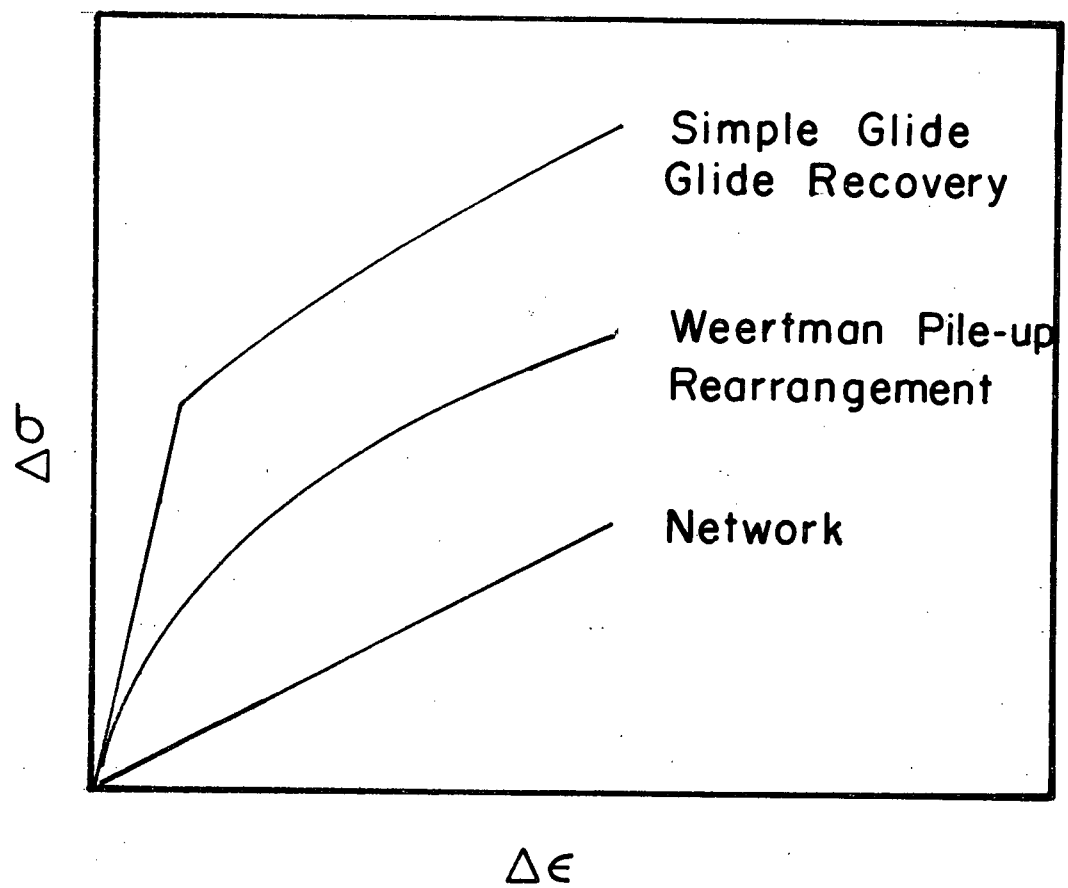

Figure 5.22. Theoretical predictions of rapid stress increase - athermal strain curves.

In the network recovery model, the high temperature structure consists of a distribution of interconnected dislocation links. The links which intersect the slip plane act as dislocation obstacles with the links of closest spacing being the strongest. At the creep stress the longest link will be just strong enough to prevent movement of dislocations. Any increase in stress will thus release a certain number of dislocations past these longer links causing strain. Thermal activation is not necessary for strain, but affects the growth of the network only. The strain produced will be linear with $^{\Delta}\sigma$ if h is constant (Evans, 1973) (Figure 5.22). This constancy of the hardening coefficient is a consequence of the area accessible to a released dislocation being governed only by the average mesh spacing (see Chapter 4, p. 100).

In the rearrangement theory, plastic athermal strain can occur for any positive $^{\Delta}\sigma$ since there will always be some "soft areas" where strain can initiate. This is similar to the network recovery theory. The strain response will not be linear with $^{\Delta}\sigma$ however, since the free area will increase with stress, unlike the simple network recovery theory. The slope of the $^{\Delta}\sigma$-$^{\Delta}\varepsilon$ curve is (from equation 4.7):

$$\frac{d\sigma}{d\varepsilon} = \frac{\theta y}{A_r} \qquad (5.1)$$

where $A_r = \exp -\left(\frac{\tau_y - \sigma}{\tau_v}\right)$ (Clark and Alden, 1975), the relative free area.

At the creep stress in steady state, τ_y is greater than σ and A_r is less than unity. For small $\Delta\sigma$, A_r will remain small and the slope will be high. As larger $\Delta\sigma$'s are used, σ approaches τ_y, A_r increases and $d\sigma/d\varepsilon$ is reduced (Figure 5.22)

In the simple glide model (Weertman, 1957) thermal activation controls the actual movement of the dislocations through diffusion of the solute atmospheres. Small rapid increases in stress will cause an "instantaneous" increase in velocity but no strain during the increase. If the stress is raised high enough to tear the dislocations from their atmospheres, strain can be produced. The theory predicts a threshold stress in the athermal stress-strain curve, the magnitude of the threshold representing the energy added by thermal activation to the creep process. After the threshold stress has been exceeded, the dislocations will no longer be controlled by the solute interaction. Presumably they will then behave in a similar fashion as the climb model forming pile-ups. The slope of the $\Delta\sigma$-$\Delta\varepsilon$ curve after the threshold should then be identical to the Weertman pile-up theory (Figure 5.22).

In the internal stress or glide-recovery model, again the actual movement of the dislocations is governed by thermal activation, the only difference being that the effective stress acts on the dislocation and its atmosphere rather than the total applied stress. The theory also predicts a threshold stress. Once the threshold is exceeded further deformation depends upon changes in the internal stress due to strain hardening. Since h is expected to vary as $1/\sigma_i$ (Gasca-Neri *et al.*, 1970) the slope of the $^{\Delta}\sigma$-$^{\Delta}\varepsilon$ should continually decrease (Figure 5.22).

Comparison of the predictions of all the theories about the athermal stress-strain curves (Figure 5.22) with the experimental results (Figures 5.6 and 5.7) is now possible. The simple glide and the glide-recovery theory are discredited by the lack of a threshold stress in the high temperature curves. Thresholds did appear in the lower temperature continuous tests (Figure 5.5 and 5.9) associated with the irregular σ-ε curves.

The sporadic nature of these curves is suggestive of the Portevin-Le Chatelier effect found in alloys during normal tensile testing (Brindley and Worthington, 1970). This effect is manifested as serrated regions in the σ-ε curves. Each serration could correspond to a strain burst in the curves of Figures 5.5 and 5.9. At constant strain rate the

serrations appear as the temperature is decreased. The usual explanation involves pinning and unpinning of dislocations from solute atmospheres. As the stress is increased dislocations are unpinned and the stress falls (or a strain burst occurs). As deformation continues the motion of dislocations creates additional vacancies which increase the diffusion rate of the solute. The increased diffusion rates enable the solute atmospheres to repin the dislocations. The occurrence of the phenomenon requires that the diffusion rates of the solute and the velocity of the dislocation are nearly equal at the temperature concerned. At higher temperatures the diffusion rates are fast enough for the solute to keep up with the dislocation. This implies that the solute atmospheres are not controlling the deformation at the higher temperatures. Thus if the irregular curves are indicative of the Portevin-Le Chatelier effect the concept of solute atmosphere control at high temperature is not meaningful. The glide and glide-recovery theories are therefore not supported by the low temperature thresholds.

The network theory does not predict the nonlinearity of the experimental curves. Both the pile-up model and the

rearrangement theories do predict curves of the correct shape. However, the degree of curvature of the curves is a difficulty for the pile-up theory. Experimentally $d\sigma/d\varepsilon$ changed from approximately E/10 close to the origin to E/200 for large $^{\Delta}\sigma$. The pile-up theory can only predict a range of E/7 to E/20 for these conditions (Appendix 4). The rearrangement theory, on the other hand, can predict large variations in $d\sigma/d\varepsilon$. For small stress increases Ar is small and $d\sigma/d\varepsilon$ is of the order of the elastic modulus. At higher $^{\Delta}\sigma$ Ar approaches unity and $d\sigma/d\varepsilon$ approaches θy which is equivalent to low temperature work hardening coefficients (E/300 or E/400).

To summarize this discussion of the athermal σ-ε curves, only the rearrangement theory is capable of explaining the results for any of the alloys, both "glide" and "recovery" controlled. In the summary chart only agreement with the Class II Bi alloys has been indicated.

Transients after Stress Changes

Delay Times. It has been proposed (Lloyd and McElroy, 1974; Bayce *et al.*, 1960) that the transient after a stress decrease is the result of two simultaneous processes; the forward creep curve at the reduced stress and the anelastic relaxation curve (Figure 5.23). If this idea is correct then the measured delay times have little significance

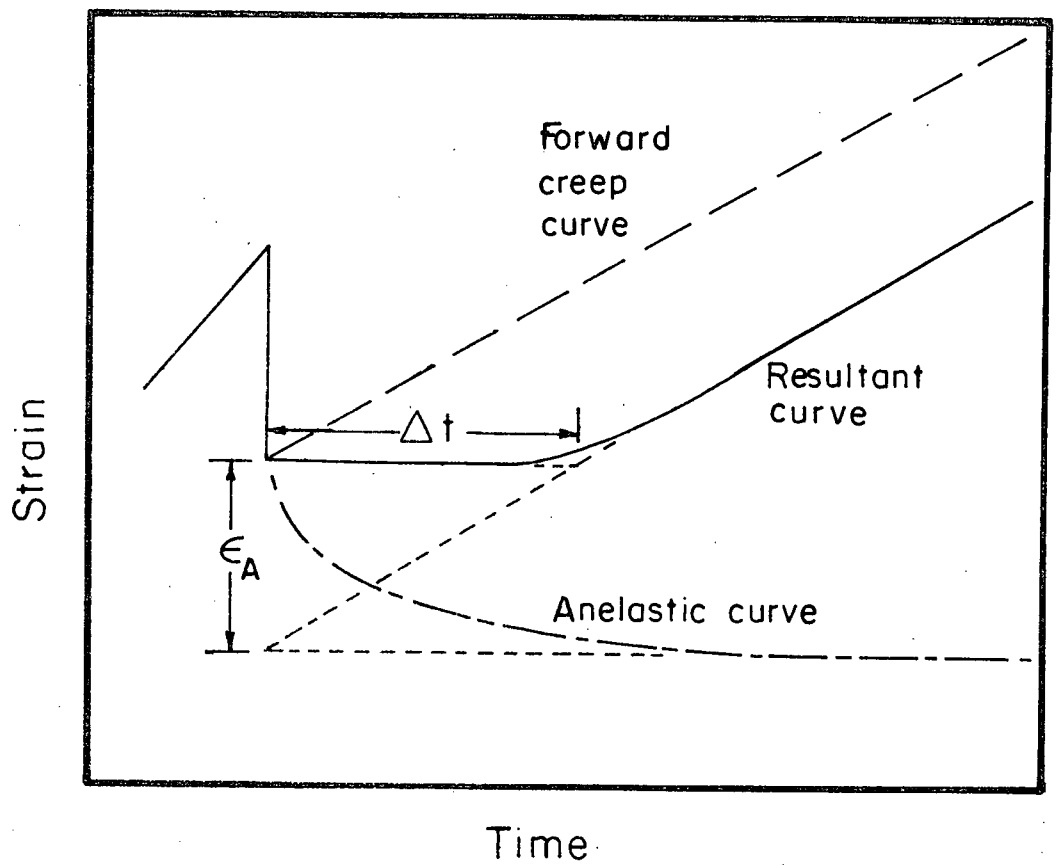

Figure 5.23. Theoretical explanation for delay times upon a stress decrease.

as regards the creep process. Instead, they are a complicated function of both the creep and the anelastic relaxation processes. The delay time, however, can be related to the two processes (Lloyd and McElroy, 1974). If the forward creep is assumed to take place at a constant rate over the time span in question, then:

$$\dot{\varepsilon} = \frac{\varepsilon_A}{\Delta_t} \tag{5.2}$$

where ε_A is the amount of the anelastic strain for the stress reduction $^{\Delta}\sigma$ (Figure 5.23). To estimate ε_A the following procedure was used. The anelastic strain for complete unloading from the creep stress ($^{\Delta}\sigma = \sigma_c$) was measured. The forward creep rate under these conditions would be zero. Then assuming that a linear relationship exists between $^{\Delta}\sigma$ and ε_A, the anelastic strain for other $^{\Delta}\sigma$ ($^{\Delta}\sigma < \sigma_c$) can be obtained. The delay time $^{\Delta}t$ could then be calculated from equation (5.1). Such measurements were done for the creep conditions and alloys of Figure 5.17

The calculated $^{\Delta}t$ could then be compared to the measured values (Table 5.1). The important observation from such a comparison is that the magnitude of the measured delay times can be accounted for by the measured anelastic contraction. Consequently the zero strain rate region in the stress decrease tests cannot be considered valid support for theories that predict delay times.

Table 5.1

Comparison of Measured and Calculated Delay Times for 16% Bi and 17% In Alloys

Alloy	Δ_σ MPa	Δ_t Calculated (min)	Δ_t Measured (min)
17% In	.07	.052	0
.95 T_m	.17	.29	.16
	.52	2.5	.47
	.69	31.	10.7
17% In	.17	.16	3.0
.6 T_m	.69	1.5	12.0
	1.04	2.5	4.6
	1.38	8.5	10.0
	3.45	22.0	22.0
16.2% Bi	.17	.8	.25
.95 T_m	.22	1.1 1.5	.55 .60
	.67	35	5.6
	.69	19	2.65
16.2% Bi	.69	1.3	5.8
.6 T_m	1.04	19.	21.
	2.41	108.	51.

Transient Shapes. The predictions of the four theories about the shapes of the creep curves after stress changes will be summarized.

The network recovery theory predicts no transients after either stress increases or decreases. Stress increases will result in instantaneous refinement of the network and increased recovery and strain hardening rates. These new values of r and h are characteristic of the new steady state value and are achieved immediately (Figure 5.24A). Upon decreasing the stress, a delay time should occur since the applied stress is too small to move dislocations through the network until it coarsens to its new steady state value (Figure 5.24A). The Weertman pile-up model, since it is also a simple recovery theory, makes identical predictions to the network theory. In the rearrangement theory, the instantaneous stress increase has the effect of increasing the relative free area function (see page 103) so that more of the slip plane is accessible to the dislocations. The strain rate after the increase is thus higher than prior to the increase. This strain rate will gradually decrease as the rearrangement process reduces the free area. A continually increasing strain rate should follow a stress decrease (Figure 5.24B). No delay time is anticipated in contrast to the recovery theories. A positive forward strain rate always remains after a stress decrease because there are always some soft areas to produce strain (A_r does not fall to zero).

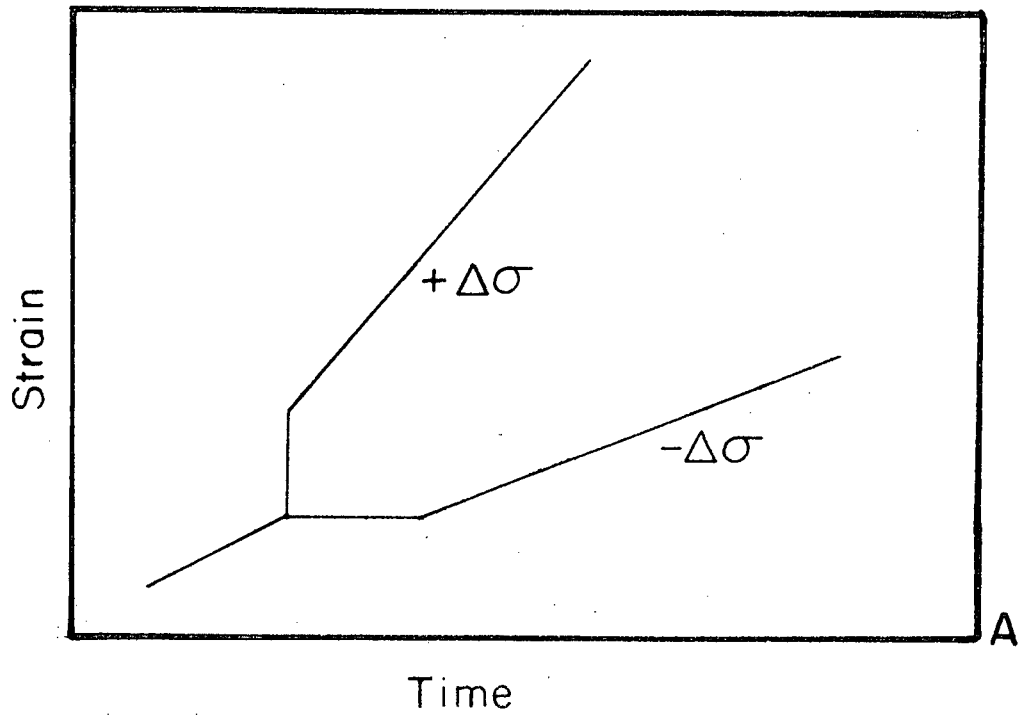

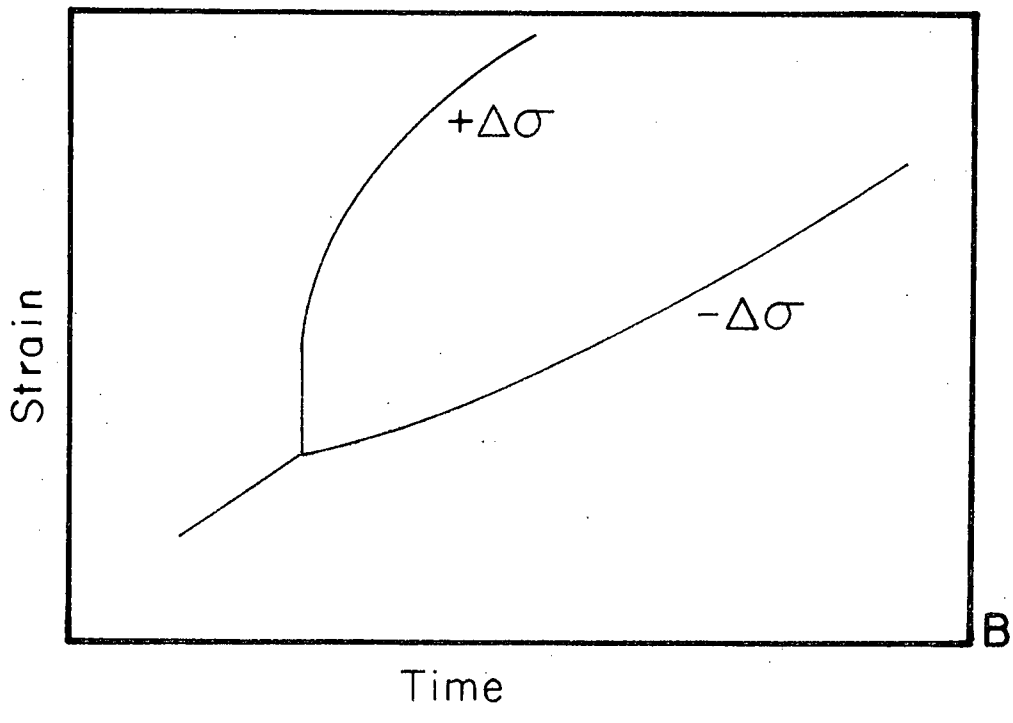

Figure 5.24. Theoretical stress change transients of:
A) Network and pile-up theories.
B) Rearrangement theory.

The rearrangement theory accurately predicts the experimental transients found in all the Pb-Bi alloys (see Figure 5.21), whereas the simple recovery theories do not. The possibility of anelastic processes can explain the apparent zero strain region without contradicting the rearrangement theory predictions.

To explain the transients in the In alloys, the glide and combined glide-recovery theories are again more appropriate. In the simple glide theory an instantaneous change in stress will result in an instantaneous change in strain rate because of the viscous nature of the dislocation movement. However, the higher value of the stress (for positive $\Delta\sigma$) permits more dislocations between the source and the climb positions. As the dislocation density increases, so will the strain rate (Figure 5.25). On stress decreases the opposite will be true, as the dislocation density and the strain rate decrease gradually. The theory does not predict a delay time. The simple glide theory can explain the general shape of the transient curves (Figure 5.21), but these inverted shapes were not universal: some stress and temperature conditions produced "normal" transients (see page 138).

The combined glide-recovery theory can predict these complex changes of transient shape with stress and temperature. The deformation maps used in Chapter 4 are used to discuss the stress change transients. Since the stress changes were done after steady state was achieved,

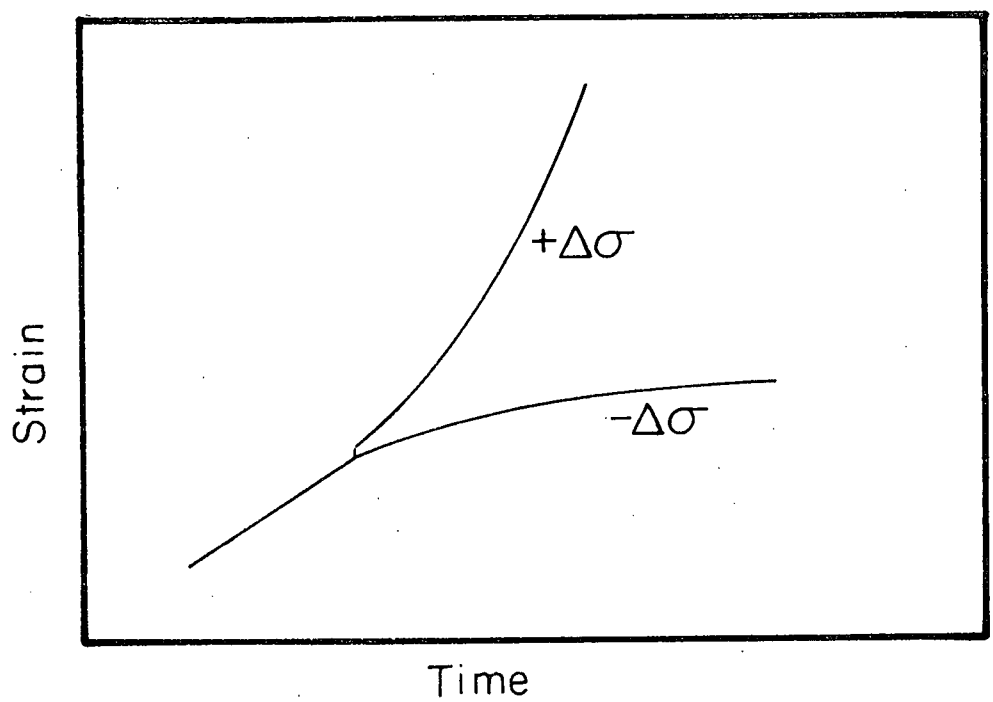

Figure 5.25. Theoretical stress change transients of simple glide theory.

the value of the internal stress will be given by the $\sigma_i^{ss}(\sigma)$ curve (Figure 5.26). Two positions for the (σ_i, σ) point are possible (Figure 5.26, Point A; Figure 5.27, Point B). Any changes in the creep stress will require readjustment of the internal stress to new values. Depending upon the magnitude of the $^{\Delta}\sigma$, the material structure can pass through various regions of the deformation maps with subsequent changes in the curvature of the transient creep. For a steady state point in the lower part of the map (Figure 5.26, Point A), stress increases produce a transient sequence with increasing $^{\Delta}\sigma$ of normal ($\dot{\varepsilon}$ decreasing), sigmoidal and inverted ($\dot{\varepsilon}$ increasing) shapes. Stress decreases from this position can produce only an increasing strain rate. The effect is reversed for a point in the upper section (Figure 5.27, Point B). The stress decrease transients vary in shape with $^{\Delta}\sigma$ but the stress increase transients do not ($\dot{\varepsilon}$ always increases).

From a consideration of the primary creep transients (Chapter 4), the (σ_c, σ_i) position of the In alloys was qualitatively determined (Figure 4.17). The suggested steady state positions are reproduced in Figure 5.26 for the 17% In alloy. For example, at .8 T_m and low stress, increasing $^{\Delta}\sigma$ should produce a transient shape sequence similar to point A, i.e. normal transients at low $^{\Delta}\sigma$ to inverted at high. Such a sequence was in fact discovered (see Figure 5.13A).

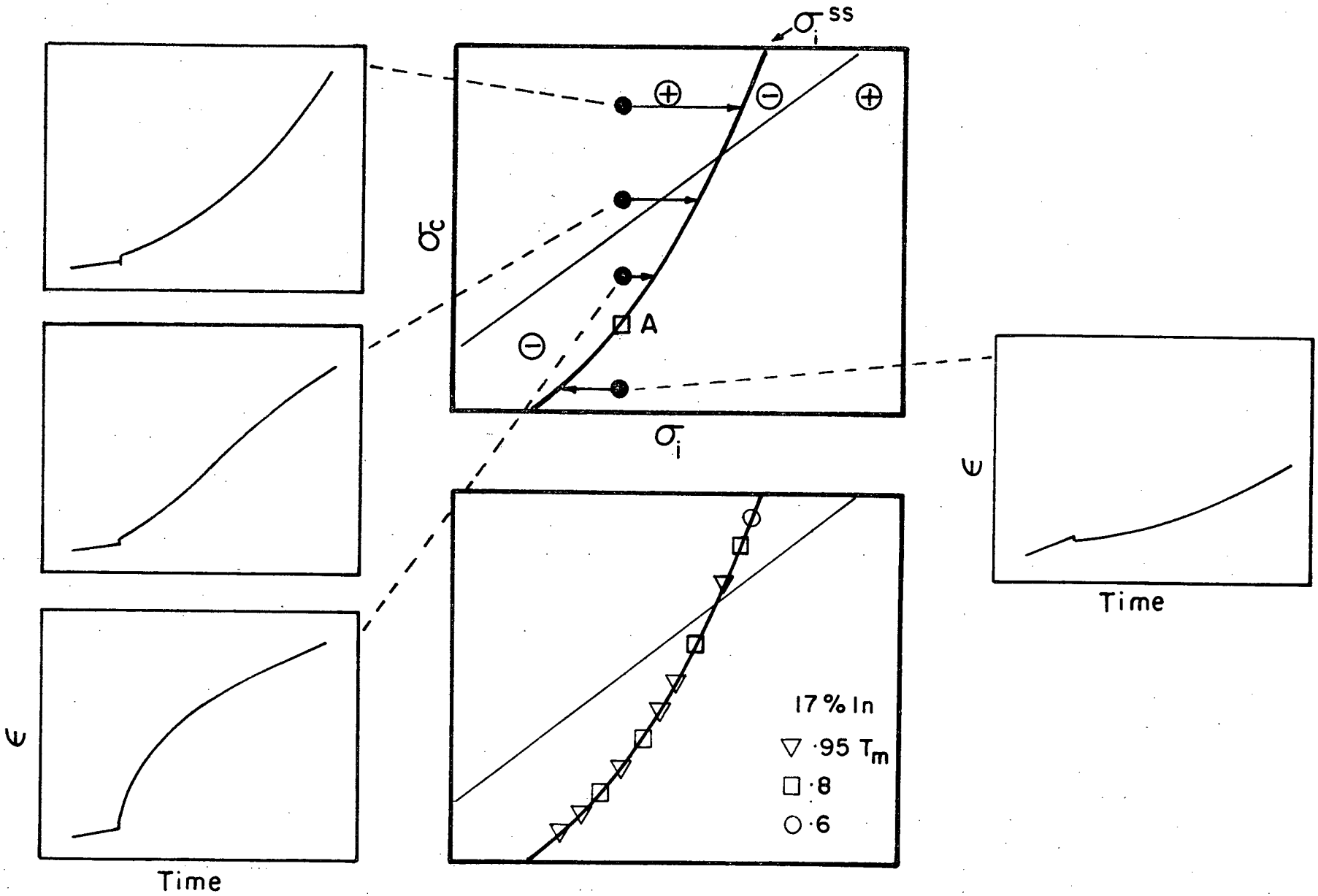

Figure 5.26. Theoretical stress change transients of combined glide-recovery theory (lower central figure represents suggested σ, σ_i^{ss} values before stress changes from Figure 5.17).

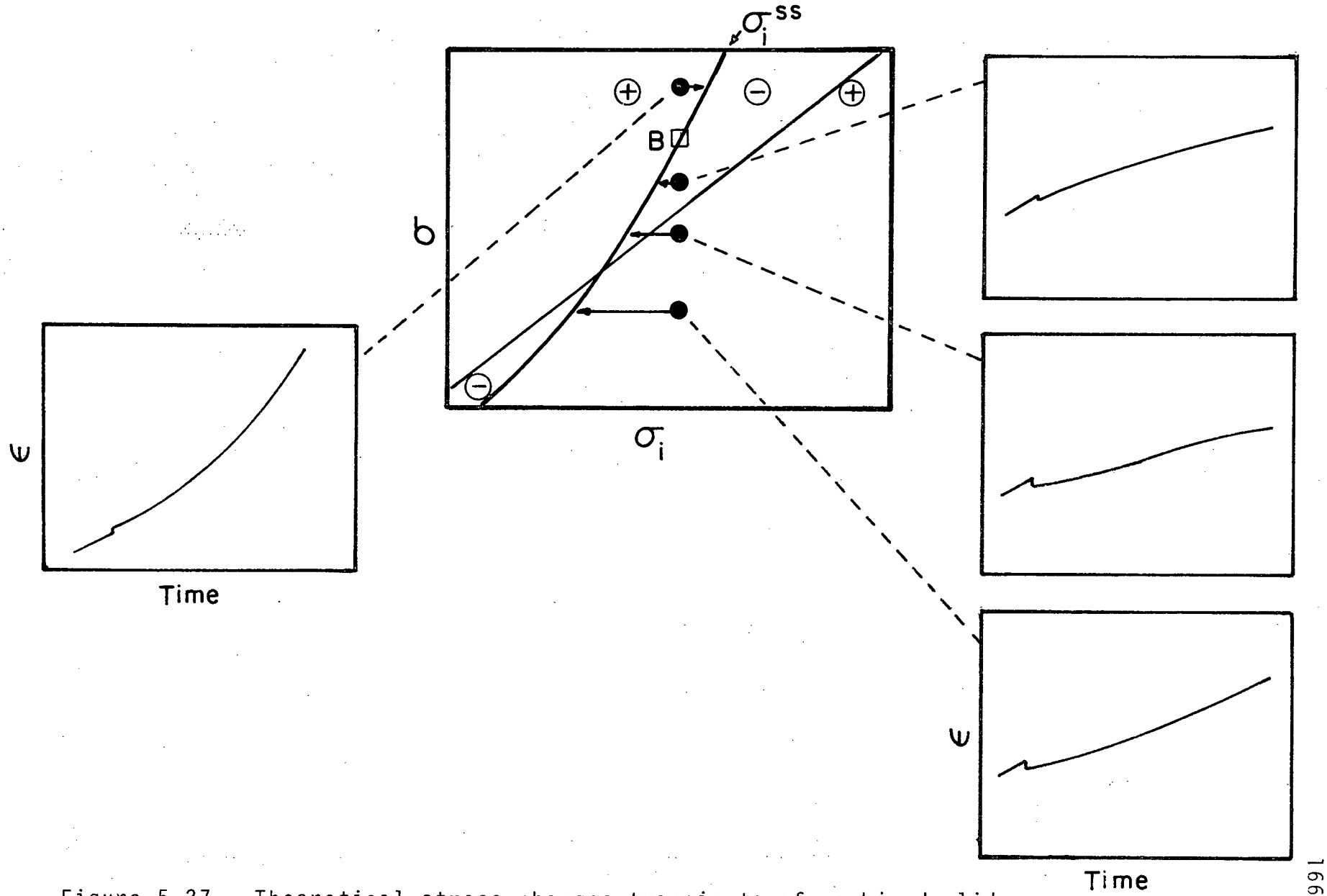

Figure 5.27. Theoretical stress changes transients of combined glide-recovery theory (continued).

The creep stress σ_c was found experimentally to influence the transient behaviour (Figure 5.13B). This effect is also consistent with Figure 5.26. At low stresses and small $\Delta\sigma$, normal transients should predominate. Higher σ_c and the same $\Delta\sigma$ should encourage the inverted behaviour.

The effect of temperature however, was not consistent with the suggested (σ_c, σ_i) positioning. The .6 T_m primary creep results necessitated placing the (σ_c, σ_i) in the upper half of the diagram corresponding to point B in Figure 5.27. Stress increases from this position should give only inverted transients. This was not the case however, as only normal transients were found (Figure 5.14). The experimental stress decrease transients are also in disagreement with the theoretical positioning. Decreasing strain rate transients were associated with the points in the lower part of the diagram (.95 T_m - Figure 5.20A). To be consistent with the stress increase transients and the primary transients, increasing $\dot{\varepsilon}$ transients should have been found in this range (Figure 5.27).

Thus the glide-recovery theory is not entirely successful in dealing with the stress change transients in the In alloy, but does afford a reasonable explanation of some of the phenomena.

Finally the 16% Bi alloy, when considered as "glide controlled," was positioned in steady state identically to

the 17% In alloy in Figure 5.26 (see page 115). In this case inverted stress change transients should have occurred at high stress and low temperatures in this alloy. Normal transients were always found in this alloy. Its classification as a "glide controlled" alloy is not supported.

Summary

The summary chart can now be completed. The rearrangement theory was adequate for the stress change transients and the athermal σ-ε tests in all the Bi alloys (last column). The combined glide-recovery theory also provided explanations for most of the transient results in the In alloys. The shapes of the athermal σ-ε curves in these alloys cannot be resolved by the glide theories.

Table 5.2

Summary Chart

	Theory	Alloys	Stress Exponent	ε_0	Primary Creep	Athermal σ-ε	Stress Change Transients
I	Simple Glide	3.2 In	✓	X	X	X	X
		9.5 In	✓	X	X	X	X
		17 In	✓	X	X	X	X
		16 Bi	✓	X	X	X	X
	Combined Glide-Recovery	3.2 In		X	✓	X	✓
		9.5 In		X	✓	X	✓
		17 In		X	✓	X	✓
		16 Bi		X	✓	X	X
II	Simple Climb	1.3 Bi	✓	✓	X	X	X
		8.8 Bi	✓	✓	X	X	X
		16 Bi	X	✓	X	X	X
	Rearrange-ment	1.3 Bi		✓	✓	✓	✓
		8.8 Bi		✓	✓	✓	✓
		16 Bi		✓	✓	✓	✓

Chapter 6

SUMMARY

The division of solid solution alloys into two classes on the basis of high temperature creep properties is justified by some of the results of the present study. The two alloy systems Pb-In and Pb-Bi did behave differently in some respects; the principle dissimilarities were in the shapes of the transient curves in the primary creep region and after changes in the creep stress in the steady state ragion. The customary criterion for distinguishing the classes, the steady state stress exponent, was found to be unreliable.

The concept of different mechanisms, glide and recovery, controlling the creep rates in the two classes was supported in part by this study. The usual approach employing the simple glide and climb theories for assessing these mechanisms did not prove adequate. The simple theories were incapable of characterizing the loading strains, the athermal σ-ε measurements and the transient shapes.

The refined theories, the combined glide-recovery theory and the rearrangement theory, were more successful.

The combined glide-recovery theory could predict qualitatively most of the transient shape results in the Class I, 3.2, 9.5 and 17% In alloys but failed to account for both the loading strain and athermal σ-ε measurements. This theory is not an entirely satisfactory explanation of the Class I alloys. The rearrangement theory adequately explained all of the measured properties in the Class II, 1.3, 8.8 and 16% Bi alloys. Additional development of the theory is required before a complete account of the influence of solute content on creep is possible.

REFERENCES CITED

Ahlquist, C.N., Gasca-Neri, R., and Nix, W.D., 1970, Acta Met., 18, 664.

Alden, T.H., 1972, Phil. Mag., 25, 785.

Alden, T.H., to be published.

Ashby, M.F., 1972, Acta Met., 20, 887.

Bailey, R.W., 1926, J. Inst. Metals, 35, 27.

Barrett, C.R., and Nix, W.D., 1965, Acta Met., 13, 1247.

Bayce, A.E., Ludemann, W.D., Shephard, L.A., and Dorn, J.E., 1960, Trans. ASM., 52, 451.

Bird, C., Moore Lee, C., and Streat, J., 1974, *UBC Curve* (The University of British Columbia Computing Centre).

Bird, J.E., Mukherjee, A.K., and Dorn, J.E., 1969, *Correlations Between High-Temperature Creep Behaviour and Structure* (prepared for The International Conf. on Quantitative Relation between Properties and Microstructure, Haifa, Israel, July 27-Aug. 1, 1969).

Bolling G.F., Massalski, T.B. and McHarque, C.J., 1961, Phil. Mag., 6, 491.

Bonesteel, R.M. and Sherby, O.D., 1966, Acta Met., 14, 385.

Borch, N.R., Shepherd, L.A. and Dorn, J.E., 1960, Trans. ASM., 52, 494.

Brindley, B.J. and Worthington, P.J., 1970, Met. Reviews, 15, 101.

Brown, N. and Lenton, D.R., 1969, Acta Met., 17, 669.

Cannon, W.R. and Sherby, O.D., 1970, Met. Trans. 1, 1030.

Cardinal, L.C. and Hart, S.D., 1968, Unpublished Data (cited by Weertman, J., 1968, Trans. ASM, 61, 681).

Clark, M.A., 1971 (M.A.Sc. Thesis, The University of British Columbia).

Clark, M.A. and Alden, T.H., 1975, *Rate Processes in Plastic Deformation*, edited by J.C.M. Li and A.K. Mukherjee (Metals Park, Ohio, ASM), p. 656.

Conway, J.B. and Mullikan, M.J., 1966, Trans. AIME, 236, 946.

Cottrell, A.H. and Aytekin, V., 1950, J. Inst. Metals, 77, 389.

Cottrell, A.H. and Jaswon, M.A., 1949, Proc. R. Soc. A199, 104.

Cottrell, A.H. and Stokes, R.J., 1955, Proc. R. Soc. A233, 17.

Davies, C.K.L., Davies, P.W. and Wilshire, B., 1965, Phil. Mag., 12, 827.

Davies, P.W. and Dennison, J.P., 1961-62, J. Inst. Metals, 90, 53.

Evans, H.E., 1973, Phil. Mag., 28, 227.

Evans, W.J. and Wilshire, B., 1968, Trans. AIME, 242, 2514.

Evans, W.J. and Wilshire, B., 1970, Metal Science Journal, 4, 89.

Feltham, P., 1956, Proc. Phys. Soc., 69B, 1173.

Feltham, P., 1968, Phys. Stat. Sol., 30, 135.

Feltham, P. and Copley, G.J., 1960, Phil. Mag., 5, 649.

Fox, G.W., 1971 (M.A.Sc. Thesis, The University of British Columbia).

Fuchs, A. and Ilschner, B., 1969, Acta Met., 17, 701.

Garofalo, F., 1965, *Fundamentals of Creep and Creep-Rupture in Metals* (New York, MacMillan).

Garofalo, F., Domis, W., Richmond, O. and Von Gremmingen, F., 1963, *Joint International Conference on Creep* (London, The Institute of Mech. Eng.), p. 1.

Gasca-Neri, R., Ahlquist, C.N., and Nix, W.D., 1970, Acta Met., 18, 655.

Gifkins, R.C., 1974, J. Australian Inst. of Metals, 19, 149.

Hazlett, T.H. and Parker, E.R., 1954, Trans. ASM, 46, 701.

Hedworth, J. and Pollard, G., 1971, Metal Sci. Journal, 5, 41.

Herring, C., 1950, J. Applied Physics, 21, 437.

Hilliard, J.E., 1964, Metal Progress, May, 99.

Honeycombe, R.W.K., 1968, *Plastic Deformation of Metals* (Great Britain, Edward Arnold Ltd.).

Hren, J., 1962 (Doctoral Thesis, Stanford University).

Johnston, W.R., Barrett, C.R., and Nix, W.D., 1972, Met. Trans., 3, 963.

Jones, B.L. and Sellars, C.M., 1970, Metal Sci. Jour., 4, 96.

Karashima, S., Motomiya, T., and Oikawa, H., 1968, Tech. Reports, Tohoku Univ., 33, 193.

Karashima, S., Oikawa, H. and Watanabe, T., 1968, Trans. AIME, 242, 1703.

Kauzman, W., 1941, Trans. AIME, 143, 57.

King, H.W., 1966, J. Mat. Sci., 1, 79.

Kocks, U.F., 1966, Phil. Mag., 13, 541.

Kucera, J. and Stransky, K., 1969, Can. Met. Quart., 8, 91.

Laks, H., Wiseman, C.D., Sherby, O.D. and Dorn, J.E., 1957, J. Applied Mech. ASME, 24, 207.

Lawley, A., Coll, J.A., and Cahn, R.W., 1960, Trans. AIME, 218, 166.

Linga Murty, K., Mohamed, F.A., and Dorn, J.E., 1972, Acta Met., 20, 1009.

Lloyd, G.J. and McElroy, R.J., 1974, Acta Met., 22, 339.

Lytton, J.L., 1962 (Doctoral Thesis, Stanford University).

Matlock, D.K. and Nix, W.D., 1974, Met. Trans., 5, 1401.

Mclean, D., 1968, Trans. AIME, 242, 1193.

Millar, J.W., 1969, Phys. Rev., 181, 1095.

Mohamed, F.A. and Langdon, T.G., 1974, Acta Met., 22, 779.

Monma, K., Sato, H. and Oikawa, H., 1964a, Japanese Inst. of Metals J., 28, 304.

Monma, K., Sato, H. and Oikawa, H., 1964b, Japanese Inst. of Metals J., 28, 258.

Monma, K., Sato, H. and Oikawa, H., 1964c, Japanese Inst. of Metals J., 28, 253.

Oikawa, H. and Karashima, S., 1974, Met. Trans. 5, 1179.

Oikawa, H., Kariya, J. and Karashima, S., 1974, Metal Science J., 8, 106.

Oikawa, H., Maeda, M. and Karshima, S., 1972, Scripta Met., 6, 339.

Orowan, E., 1946-47, J. West Scot. Iron and Steel Inst., 54, 45.

Pahutová, M., Čadek, J. and Rys, P., 1969, Acta Met., 17, 745.

Pahutová, M., Hostinsky, T., Čadek, J. and Rys, P., 1969, Phil. Mag., 20, 975.

Richards, C.W., 1961, *Engineering Materials Science* (Chapman and Hall, London).

Rose, M.E., 1953, Phys. Rev., 91, 610.

Rossard, C. and Blain, P., 1958, IRSID, A, 174.

Russell, B., Ham, R.K., Silcock, J.M. and Willoughby, G., 1968, Metal Sci. J., 2, 201.

Sellars, C.M. and Quarrell, A.G., 1961-62, J. Inst. Metals, 90, 329.

Sidey, D. and Wilshire, B., 1969, Metal Sci. J., 3, 56.

Sherby, O.D., Anderson, R.A. and Dorn, J.E., 1951, Trans. AIME, 191, 643.

Sherby, O.D. and Burke, P.M., 1967, Prog. Mat. Sci., 13, 325.

Sherby, O.D. and Simnad, M.T., 1961, Trans. ASM, 54, 227.

Vandervoort, R.R. and Barmore, W.L., 1968, *Proc. Sixth Plansee Seminar* (Reutle-Tyrol Austria, June).

Webster, G.A., Cox, A.P.D. and Dorn, J.E., 1969, Metal Sci. J., 3, 221.

Weertman, J., 1955, J. of Applied Phys., 26, 1213.

Weertman, J., 1957a, J. of Applied Phys., 28, 362.

Weertman, J., 1957b, J. of Applied Phys., 28, 1185.

Weertman, J., 1960, Trans. AIME, 218, 207.

Weertman, J., 1968, Trans. ASM, 61, 680.

Wiseman, C.D., Sherby, O.D. and Dorn, J.E., 1957, Trans AIME, 209, 57.

Zener, C. and Holloman, J.H., 1944, J. of Applied Phys., 15, 22.

APPENDIX 1

ANALYSIS OF INITIAL LOADING CURVE

When the pan support is raised, the bottom grip assembly does not contact the machine base (Figure 2.1) and the load on the specimen is zero. To start a test the support is moved downward at constant rate ($\dot{\ell}_{TOT}$). When the bottom grip contacts the base, loading of the specimen commences. The maximum value of the load (P_c) is realized when the support releases the load pan. During the time the load is increasing from 0 to P, the creep machine is analogous to a constant crosshead speed tensile machine. Such a machine may be represented by two springs in series (Figure A1.1) (Richards, 1961).

The specimen elongation ℓ_s represents the deflection measured by the transducer after P = 0 and therefore includes some grip and pull rod elongation. Before P = 0 the transducer measures movement of both the specimen and the complete machine ($\ell_{TOT} = \ell_m + \ell_s$) (Figure A1.2).

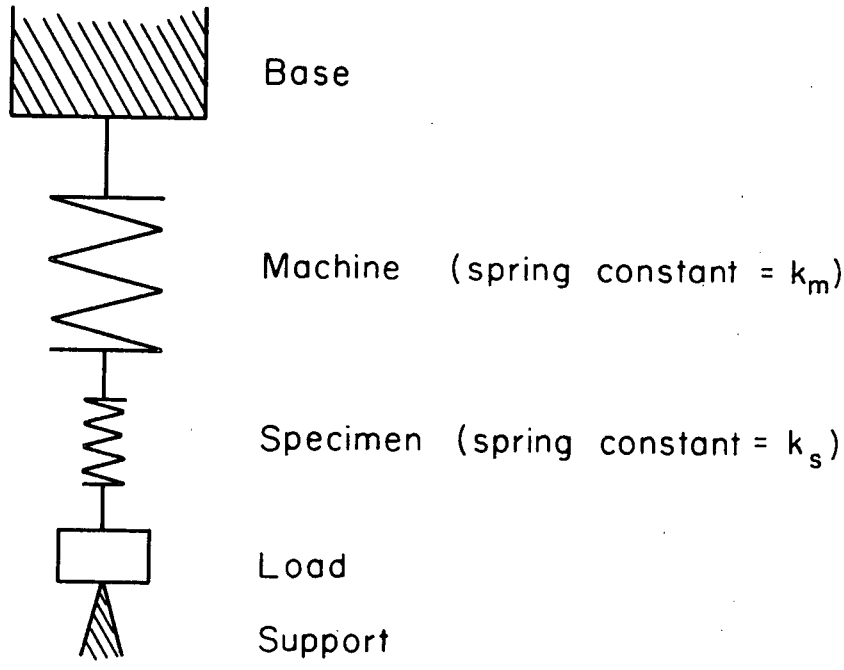

Figure A1.1. Mechanical analogue of creep machine.

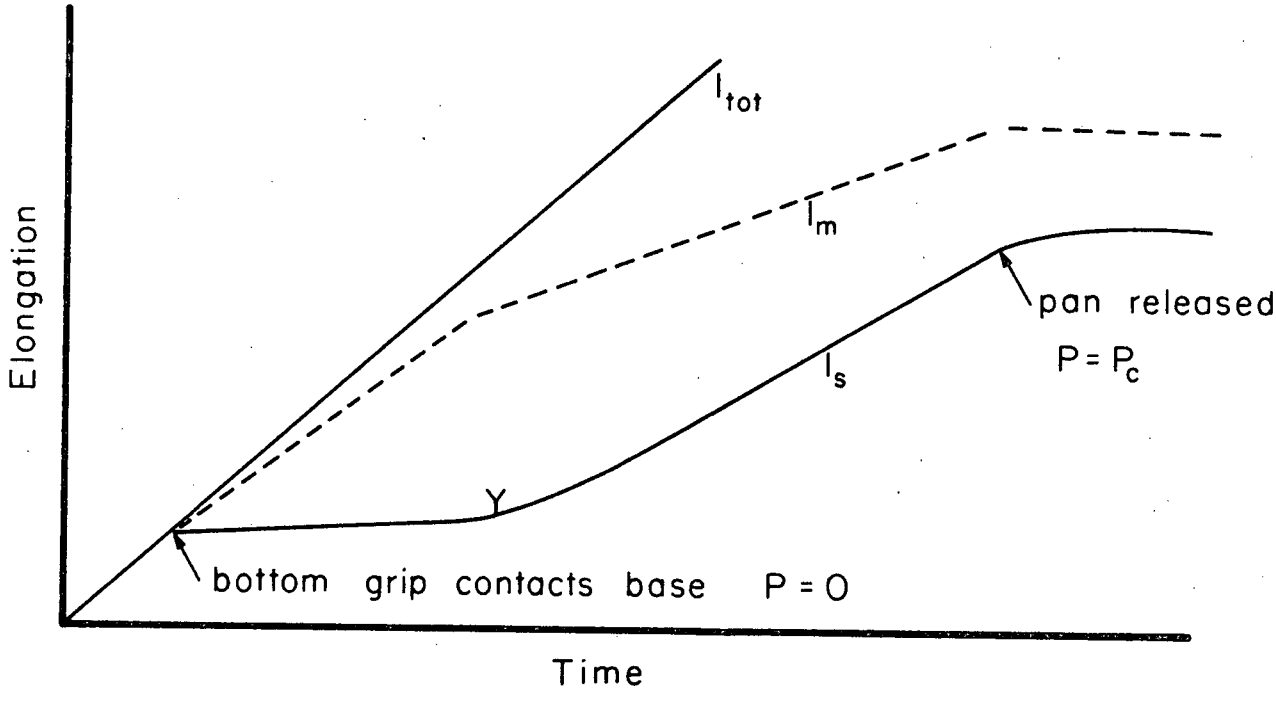

Figure A1.2. Strain -time curve during initial loading.

After loading begins:

$$\ell_{TOT} = \ell_s + \ell_m$$

$$\dot{\ell}_{TOT} = \dot{\ell}_s + \dot{\ell}_m = \text{constant} .$$

At any point between P = 0 and P = P_c:

$$P = k_m \ell_m = k_s \ell_s = k \ell_{TOT}$$

where k is an equivalent spring constant

or $\dot{P} = k_m \dot{\ell}_m = k_s \dot{\ell}_s = k \dot{\ell}_{TOT}$.

Since $\dot{\ell}_{TOT} = \text{constant}$

$$\dot{P} = \text{constant} = k_s \dot{\ell}_s .$$

Before the specimen yield point Y and ignoring the grip and pull rod extension:

$$k_s = \frac{AE}{\ell_0}$$

where A is the specimen area

ℓ_0 is the original length

E is Young's modulus,

The elastic stress rate on the specimen is:

$$\dot{\sigma} = \frac{\dot{P}}{A} = \frac{E\ \dot{\ell}_s}{\ell_0}$$

and can be determined by measurement of $\dot{\ell}_s$.

APPENDIX 2

COMPUTER PROGRAM FOR CREEP CURVE

The computer program converts the elongation-time chart record to true strain-time, calculates an approximate strain rate from the slope between adjacent points and plots strain and strain rate as a function of time. The readings are taken directly from the 0-100 chart paper and a variable scale factor included to convert to length measurements. Factors are also included to account for the shifts required to keep the recorder pen on scale. The time of stress changes is also plotted.

Definitions of the variable names are:

ELNOT = initial gauge length

DELTAO = chart reading at zero strain x scale factor at start of test

NCRISI = number of changes of scale or shifts of pen

SUMSH = total amount of shift

NMEAS(I) = number of points between changes

FSCALE(I) = scale factor

SHIFT(I) = amount of pen shift in chart divisions

TIM(J) = time in minutes

CHART(J) = chart reading at time = TIM(J)

STRAI(J) = total strain at time = TIM(J)

CSTRAN(J) = creep strain (total strain - loading strain) at time = TIM(J)

CSTRAI(1) = loading strain

TIM(1) = zero time

RATE(K) = strain rate

KCRIT = value of K when stress is changed

```
C       CREEP CURVE CALCULATION
        DIMENSION FSCALE(15),SHIFT(15),TIM(200),CHART(200),CSTRAN(200),
       +STRAI(200),STRAIN(200),CSTRAI(200),TIME(200),RATE(200),TITLE(20)
        COMMON/DEBUG/FLAG
        LOGICAL FLAG
        FLAG=.TRUE.
        READ(5,1)NTESTS
1       FORMAT(I3)
        DO 60 N=1,NTESTS
        READ(5,2)(TITLE(I),I=1,20)
2       FORMAT(20A4)
        READ(5,3) ELNOT,DELTAO,NCRISI,KCRIT
3       FORMAT(F8.5,F9.6,2I3)
        SUMSH=0
        K=0
        DO 10 I=1,NCRISI
        READ(5,4) NMEASU,FSCALE(I),SHIFT(I)
4       FORMAT(I4,F8.5,F8.3)
        FSCALE(I)=FSCALE(I)/100
        SUMSH=SUMSH+SHIFT(I)*FSCALE(I)
        READ(5,5)(TIM(J),CHART(J),J=1,NMEASU)
5       FORMAT(4(F10.2,F10.3))
        DO 30 J=1,NMEASU
        STRAI(J)=ALOG(1+(CHART(J)*FSCALE(I)-DELTAO+SUMSH)/ELNOT)
        IF(I.EQ.1.AND.J.EQ.1) STRAI1=STRAI(1)
        CSTRAN(J)=STRAI(J)-STRAI1
        K=K+1
        STRAIN(K)=STRAI(J)
        CSTRAI(K)=CSTRAN(J)
        TIME(K)=TIM(J)
30      CONTINUE
10      CONTINUE
        L=K-1
        DO 40 K=2,L
        RATE(K)=(CSTRAI(K+1)-CSTRAI(K-1))/(TIME(K+1)-TIME(K-1))
        IF(K.NE.KCRIT) GO TO 40
        RATE(K-1)=RATE(K)
        RATE(K-2)=RATE(K-3)
40      CONTINUE
        RATE(1)=RATE(2)
        RATE(L+1)=RATE(L)
        K=K+1
        WRITE(6,6) TITLE,STRAI1,K
6       FORMAT(1H1,1X,16HCREEP CURVE FOR //1X,20A4,///1X,16H LOADING STR
       1N=,F8.5,19HNO OF DATA POINTS= ,I3///1X,45H  TIME     CREEP STRAIN
       2TOTAL STRAIN     RATE/1X,6H   MIN,35X,7HMIN**-1//)
        WRITE(6,7)(TIME(NK),CSTRAI(NK),STRAIN(NK),RATE(NK),NK=2,K)
7       FORMAT(1X,0PF8.2,4X,0PF8.5,6X,0PF8.5,4X,1PE9.2)
        CALL PLOT (0.0,0.0,-3)
        CALL SCALE(TIME,K,20.,XMIN,DX,1)
        CALL SCALE(CSTRAI,K,10.,YMIN,DY,1)
        CALL SCALE(RATE,K,10.,ZMIN,DZ,1)
        CALL AXIS(0.,0.,9H TIME MIN,-9,20.,0.,XMIN,DX)
        CALL AXIS(0.,0.,8H STRAIN ,8,10.,90.,YMIN,DY)
        CALL LINE(TIME,CSTRAI,K,1)
```

```
      XO=TIME(K)-.4
      YO=CSTRAI(K)+.1
      CALL SYMBOL(XO,YO,.07,6HSTRAIN,0.,6)
      CALL AXIS(20.,0.,20H STRAIN RATE MIN**-1,-20,10.,90.,ZMIN,DZ)
      CALL LINE(TIME,RATE,K,1)
      ZO=RATE(K)+.5
      CALL SYMBOL(XO,ZO,.07,11HSTRAIN RATE,0.,11)
      CALL SYMBOL(1.,10.,.14,TITLE,0.,80)
      CALL SYMBOL(18.5,10.,.14,TITLE,0.,11)
      XI=TIME(KCRIT-2)
      YI=CSTRAI(KCRIT-2)-.3
      ZI=RATE(KCRIT-2)-.3
      CALL SYMBOL(XI,YI,.28,6,0.,-1)
      CALL SYMBOL(XI,YI,.28,6,0.,-1)
      CALL PLOT(22.0,0.0,-3)
60    CONTINUE
      CALL PLOTND
      STOP
      END
```

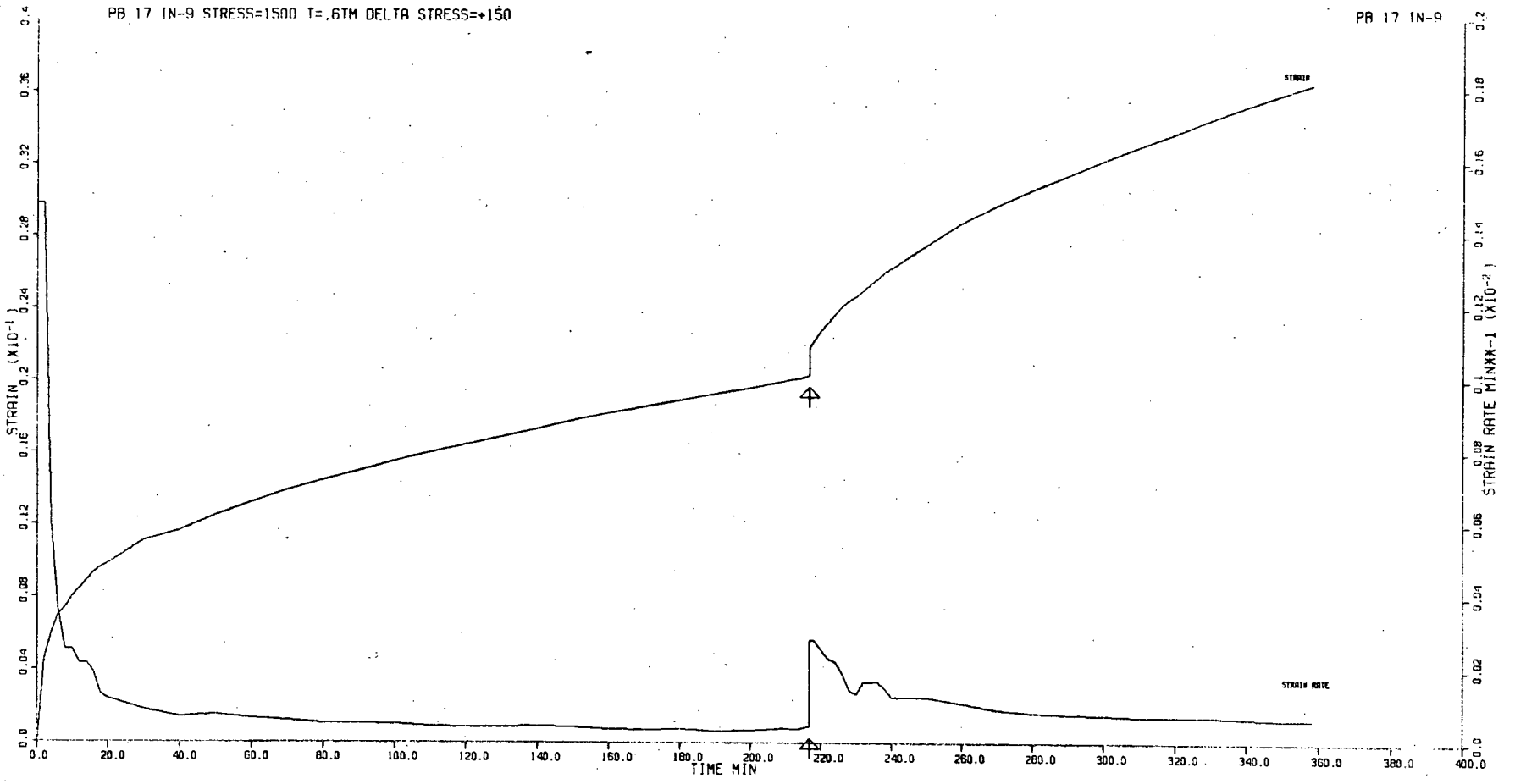

Figure A2.1. Example of computer output.

APPENDIX 3

FIRST ORDER KINETICS ANALYSIS

If the strain rate during the primary transient obeys the principles of first order kinetics, the parameters of the Garofalo equation ($\varepsilon = \left(\frac{\dot{\varepsilon}_i - \dot{\varepsilon}_s}{m}\right)\left(1 - \exp -mt\right) + \dot{\varepsilon}_s t$ should behave in certain ways (Mukherjee, Bird, and Dorn 1969). The present results are evaluated for four such characteristics:

1. First-order kinetics implies that the same process controls the transient and steady state rates, therefore the initial and steady state creep rates should have the same temperature and stress dependencies or:

$$\dot{\varepsilon}_i = A\ \dot{\varepsilon}_s \qquad \text{(A3.1)}$$

This relationship has been found in pure metals and some alloys (Evans and Wilshire, 1968; Webster, Cox and Dorn, 1969; Sidey and Wilshire 1969; Garofalo *et al.*, 1963; Evans, and Wilshire, 1970).

In the present alloys $\dot{\varepsilon}_i$ was calculated using the relationship :

$$\dot{\varepsilon}_i = m\ \varepsilon_T + \dot{\varepsilon}_s \qquad \text{(A3.2)}$$

and the measured values of m, ε_T and $\dot{\varepsilon}_s$. For the 16% Bi alloy it was found that $\dot{\varepsilon}_i \simeq 2.8\ \dot{\varepsilon}_s$ (Figure A3.1) temperature range .8 to .95 T_m. Insufficient results did not permit establishment of the relationship for other alloys.

2. The rate constant m should also have the same stress and temperature dependence as the steady state strain rate, therefore :

$$m = B\ \dot{\varepsilon}_s \qquad \text{(A3.3)}$$

This prediction was validated in pure metals and in stainless steel (Evans and Wilshire, 1968; Garofalo *et al.*, 1963). In the present study use of a fairly narrow stress range precludes accurate assessment of the relationship (Figure A3.2).

3. Because of the above relationships (Eq. A3.1, A3.2, A3.3), it follows that:

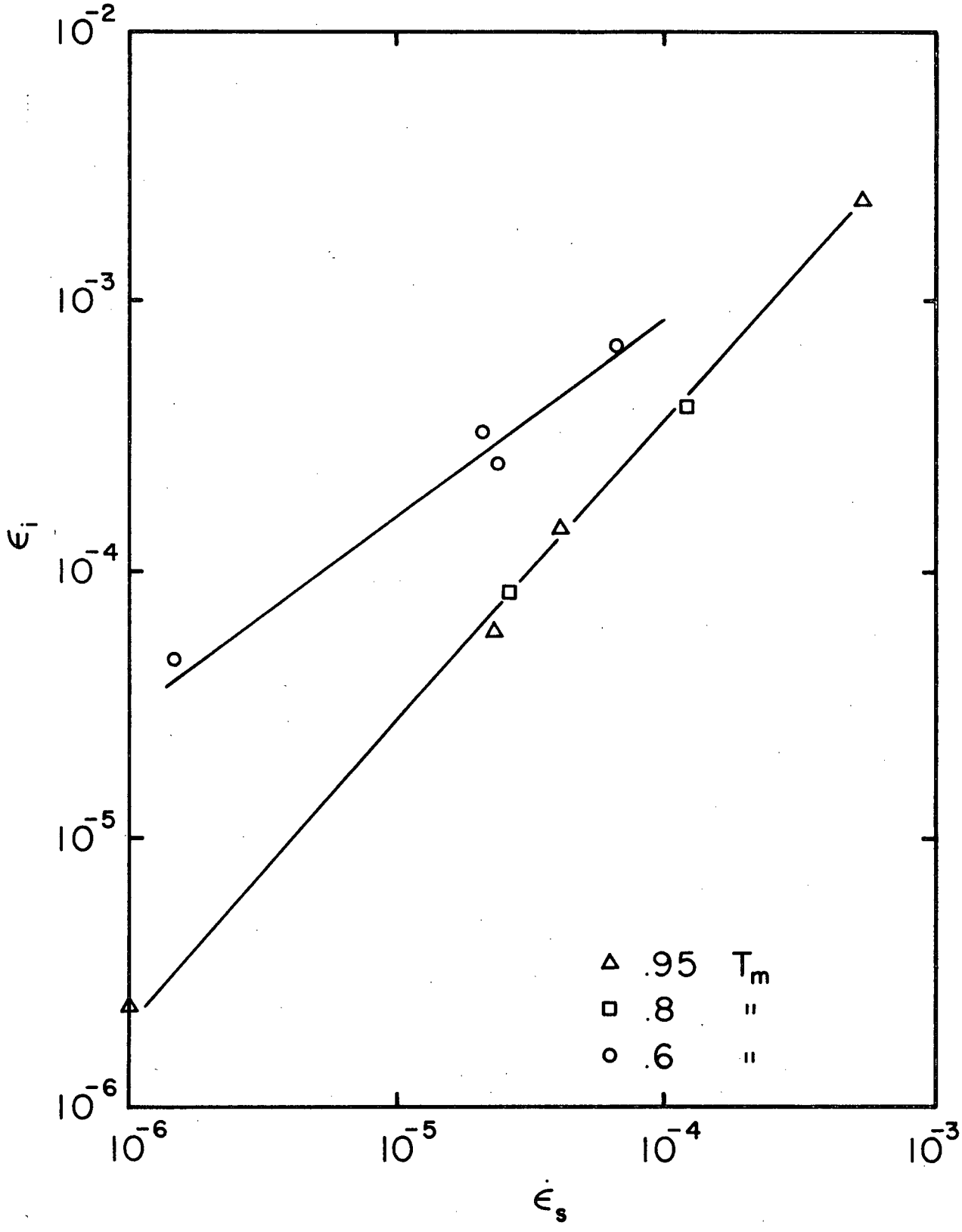

Figure A3.1. Initial creep rate versus steady state creep rate for 16% Bi alloy.

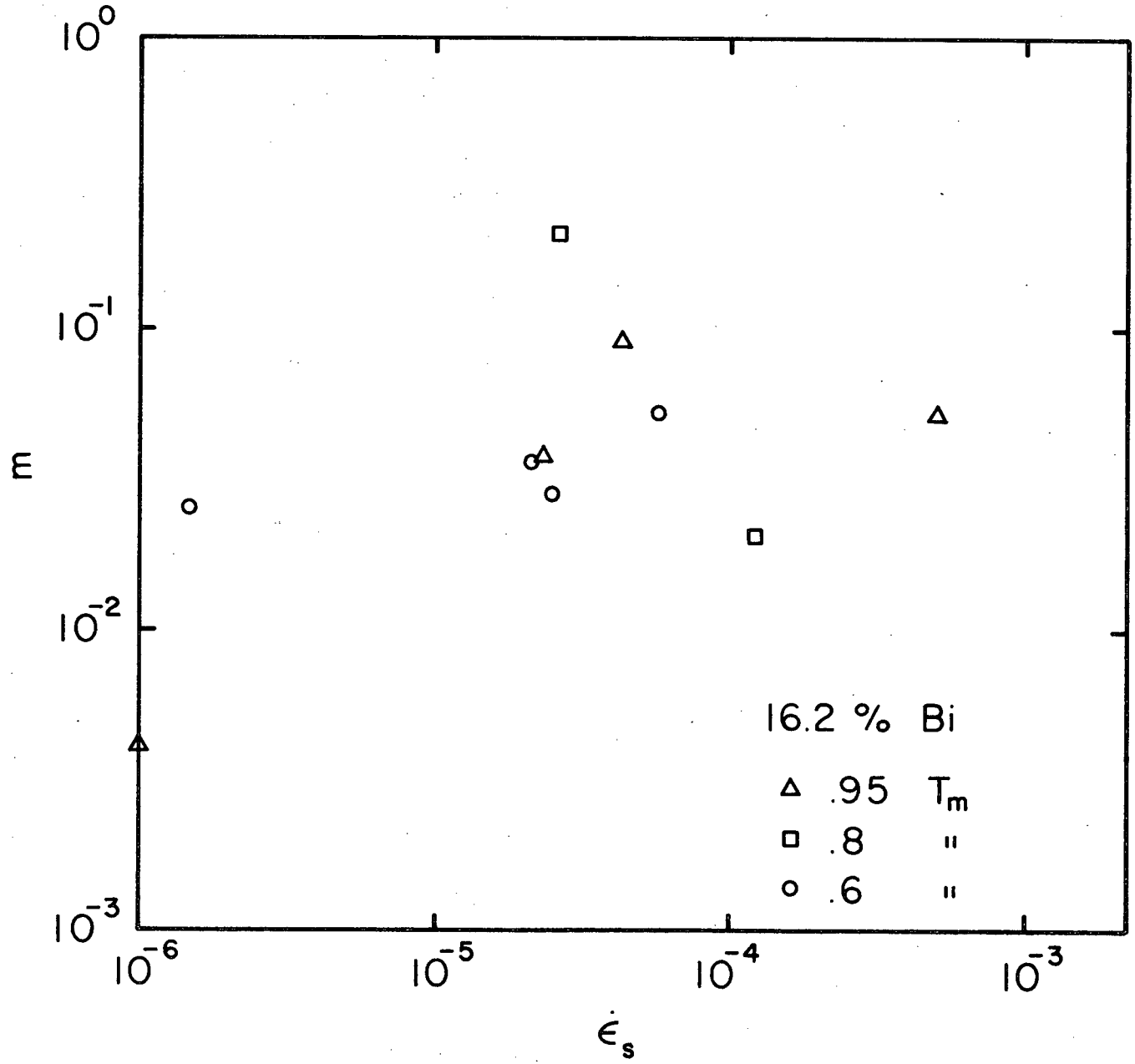

Figure A3.2. Rate constant, m versus steady state creep rate for 16% Bi alloy.

$$\varepsilon_T = \frac{A-1}{B} \qquad (A3.4)$$

Thus ε_T is a constant since A and B do not contain stress or temperature factors. However some stress dependence of ε_T has been found (Evans and Wilshire, 1968; Garofalo *et al.*, 1963). In the present Bi alloys ε_T does not vary with temperature but does change with stress and alloy content (see Figures 4.12, 4.13).

4. The initial strain rate $\dot{\varepsilon}_i$ should be independent of the loading strain ε_0 depending solely on the value of $\dot{\varepsilon}_s$. Little data have been generated to test this prediction. In the present study $\dot{\varepsilon}_i$ is independent of ε_0, as predicted (Figure A3.3).

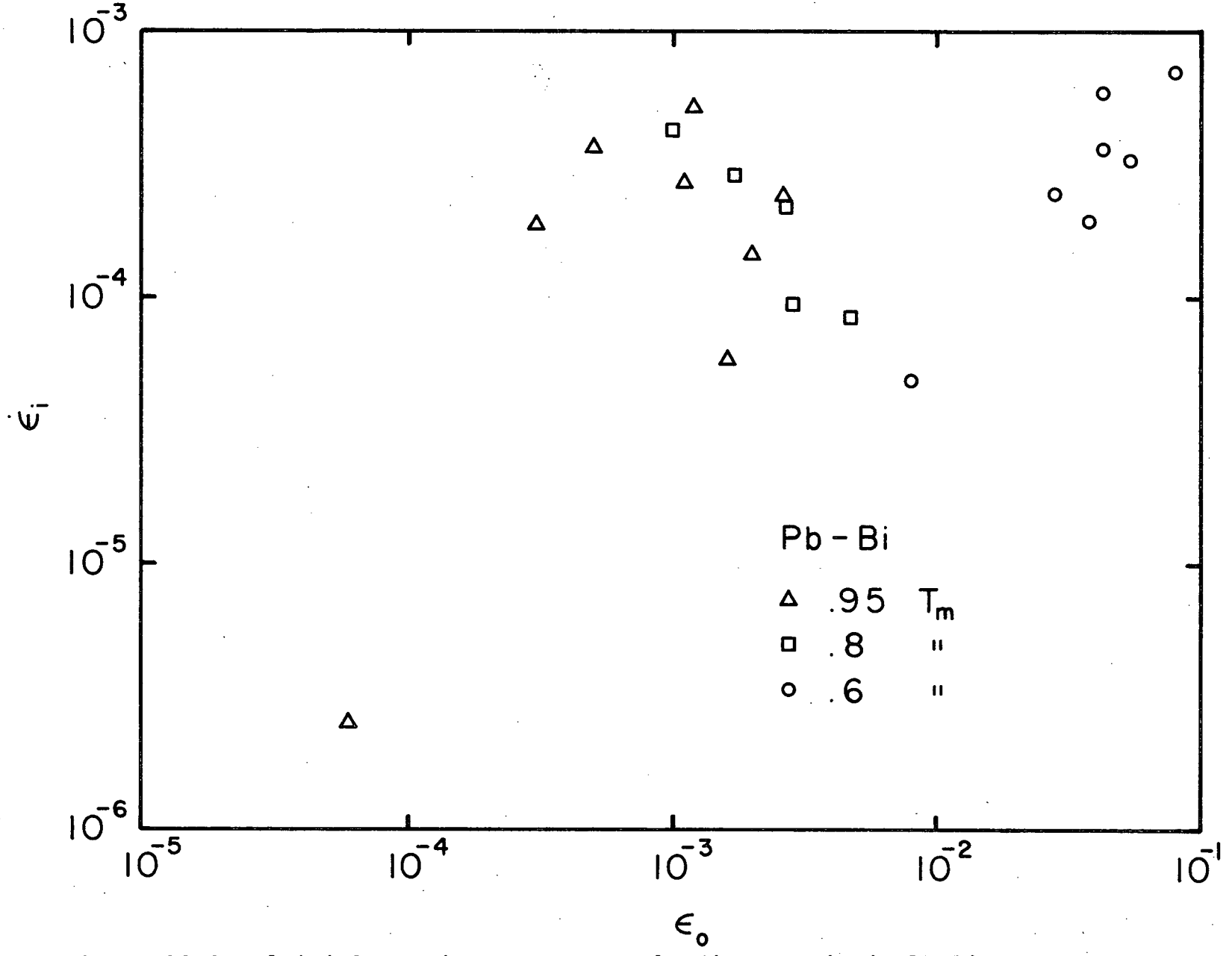

Figure A3.3. Initial strain rate versus loading strain in Pb-Bi system.

APPENDIX 4

CALCULATION OF A STRAIN HARDENING COEFFICIENT FOR THE WEERTMAN CLIMB THEORY

The model of the Weertman climb theory is one of pile-ups created by interaction with dislocations on neighbouring planes.

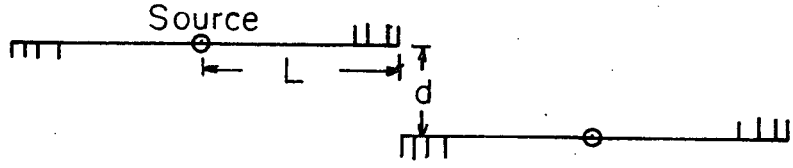

Weertman uses the following equations: The average number of dislocations in the pile-ups:

$$n = \frac{2\sigma L}{\mu b}$$

where σ is the applied stress

L is the distance between the source and the climb position

μ is the shear modulus

b is the Burger's vector.

The climb distance d also depends upon the applied stress:

$$d \simeq \frac{\mu b}{4\pi\sigma}$$

An expression for L, the slip distance is obtained by considering any one source to be blocked by three neighbouring sources:

$$L^2 = \frac{3\sigma}{2\ \mu b\ M}$$

where M is the density of Frank-Read, considered a constant in this model.

A rapid increase in the stress by $d\sigma$ will initiate a strain increment $d\varepsilon$. The magnitude of this strain is the product of density of sources times the average area swept out by each dislocation, A, multiplied by b and the number of dislocations released at each source dn:

$$d\varepsilon = MAb\ dn.$$

The area swept out is almost equivalent to the area of the leading dislocation loop; $A \simeq 4\pi L^2$. Actually, A will increase somewhat during the stress increment since the added stress will cause some of the pile-ups to move past each other. This variation in A will be small if $\Delta\sigma$ is small compared to σ_c.

From above

$$n = \frac{2\sigma L}{\mu b} = \frac{2\sigma}{\mu b} \cdot \left(\frac{3\sigma}{2\ \mu b\ M}\right)^{\frac{1}{2}}$$

$$= \frac{k'}{M^{\frac{1}{2}}}\ \sigma^{3/2}\ .$$

then $$dn = \frac{k'}{M^{\frac{1}{2}}} \cdot \frac{3}{2}\ \sigma^{\frac{1}{2}}\ d\sigma$$

also $$A = 4\pi\ L^2 = 4\pi \cdot \frac{3\sigma}{2\ \mu b\ M}$$

$$= \frac{k''}{M}\ \sigma$$

thus $$d\varepsilon = M \cdot \frac{k''}{M}\ \sigma \cdot b \cdot \frac{k'\ 3\sigma^{\frac{1}{2}}\ d\sigma}{M^{\frac{1}{2}}\ 2}$$

$$= \frac{3}{2}\ \frac{k''\ k'\ b}{M^{\frac{1}{2}}}\ \sigma^{3/2}\ d\sigma$$

thus $$h = \frac{d\sigma}{d\varepsilon} = \frac{2}{3}\ \frac{M^{\frac{1}{2}}}{k''\ k'\ b}\ \ \frac{1}{\sigma^{3/2}}\ .$$

An estimate of the magnitude of h can be made with this equation and the following values:

Temperature = 200°C

Creep stress = 1.04 MPa

$\mu = 5.76 \times 10^{10}$ dynes/cm (Cardinal and Hart, 1968)

$b = 3.5 \times 10^{-8}$ cm (Weertman, 1960)

$M^{\frac{1}{2}} = \frac{2.4}{1.9} \times 10^{7}$ cm^2 (Weertman, 1960).

In this case $h \simeq \frac{E}{7}$ where E is the Young's modulus. For the same conditions but a stress of 2.08 MPa $h \simeq \frac{E}{20}$.